The Dissertation Committee for Adam Thomas Hilterbrand Certifies that this is the approved version of the following dissertation:

Novel Routes for Cytomegalovirus Diagnosis and Treatment

Committee:

Jason W. Upton, Supervisor

Maria A. Croyle

Lauren I. Ehrlich

Jon M. Huibregtse

Christopher S. Sullivan

Novel Routes for Cytomegalovirus Diagnosis and Treatment

by

Adam Thomas Hilterbrand, B.S.

Dissertation

Presented to the Faculty of the Graduate School of

The University of Texas at Austin

in Partial Fulfillment

of the Requirements

for the Degree of

Doctor of Philosophy

The University of Texas at Austin

May 2017

Dedication

To my mother, Laura Hilterbrand, for your love and continued support in all my efforts. Your strength and perseverance through all that you have endured drives me to better myself each and every day. Without you, I would not be the man I am today.

Acknowledgements

First, I would like to extend my sincerest thanks to my mentor, Dr. Jason Upton. Thank you for giving me the encouragement and independence to explore my own ideas, even when they had little chance of working. Your support, guidance, and encouragement have molded me into the scientist I am today.

I would like to thank my lab mates, both past and present. Thank you all for your help from the numerous discussions we had regarding my project ideas. I would especially like to thank a former post-doctoral researcher, Priya. Not only was she a great friend, but when I first joined the lab, she got me up to speed on many of the molecular biology tools I used extensively during my graduate career. Lastly, thank you everyone for making each work day enjoyable.

I would also like to extend my sincerest thanks to my collaborators and committee members. As far as collaborators go, I'd especially like to thank Jeffrey Dick and Dan Boutz. I truly enjoyed doing science with you guys. In the process, we have also become good friends, which shows the power of these collaborative efforts. I hope to continue pushing the boundaries of knowledge with you in future scientific endeavors. Also, thank you to my committee for the insightful discussions and suggestions to better my thesis project. I believe it has truly made my thesis work stronger.

I also want to thank my family for being so supportive and loving. You might think 22 years of school is a long time, but I think it's been worth it. I love you all!

Finally, to my beautiful, strong, and fearless wife, Emily, I want to say I love you and thank you. Thank you for keeping me grounded and sane. Thank you for listening to me. We will do great things together. I know it.

Novel Routes for Cytomegalovirus Diagnosis and Treatment

Adam Thomas Hilterbrand, Ph.D.

The University of Texas at Austin, 2017

Supervisor: Jason W. Upton

Human cytomegalovirus (HCMV) represents a massive burden on infected individuals and healthcare systems worldwide. Though HCMV is not normally disease causing in healthy individuals, it poses a significant threat to immunocompromised people and developing fetuses, causing a broad range of diseases due to its ability to infect several organ and tissue types. Current diagnostic and treatment modalities for HCMV are extremely limited in their scope. In the United States, HCMV testing is typically only done when one presents with possible HCMV-caused symptoms, as current methods are deemed unwarranted if no symptoms are presented in a patient. Additionally, if treatment is to be given, current antiviral drugs are limited to targeting only one aspect of HCMV's replication cycle and, at times, can be rather toxic. As such, continued research and development is needed to create rapid, facile point–of-care diagnostics as well as identify new druggable targets to lessen the impact of infection. Utilizing a murine model system to study HCMV infection, we recently showed that precise detection of murine cytomegalovirus (MCMV) from the urine of infected mice was rapidly achieved through the use of a novel electrochemical immunoassay. By attaching glucose oxidase to an antibody recognizing MCMV, we readily detected MCMV at an electrode using chemistry similar to that used in modern day glucometers. Additionally, we characterized and identified a major role for a uniquely structured MCMV deubiquitinating enzyme (DUB) during infection. When the virus lacked DUB activity, levels of a virally encoded pro-inflammatory chemokine increased, leading to the mutant DUB virus' dramatic attenuation in mice. As this enzyme is incredibly important for MCMV pathogenesis and

is highly conserved between MCMV and HCMV, it may serve as a viable target for antiviral therapies. Because HCMV infections persist for the lifetime of the individual, continued success in diagnosis and treatment of HCMV will be needed as long as humans exist as a species.

Table of Contents

List of Tables

List of Figures

Chapter 1: Introduction

1.1 Human Cytomegalovirus: A Global Burden

1.1.1 Human Cytomegalovirus Prevalence, Disease, and Treatment

It seems unfathomable that despite years of tremendous scientific and technological advances, there remains a viral pathogen that infects 50-90% of the world's population with no vaccine to effectively protect against it. This pathogen, human cytomegalovirus (HCMV) constitutes a significant health risk and massive financial burden to countries worldwide. HCMV causes an estimated $1.9 billion/year in the United States alone in medical costs [1], where greater than 50% of the nation's population is infected with HCMV by the age of 40 [2]. Worldwide, HCMV seroprevalence tends to follow socioeconomic lines, with infection rates approaching 100% in developing nations [3].

HCMV belongs to the beta-herpesvirus sub-family of *Herpesviridae*. As such, it has an approximately 230kb linear dsDNA genome. Virions are organized as illustrated in Figure 1.1. Briefly, a capsid is surrounded by a cell-derived lipid bilayer envelope. Between the envelope and capsid lies the amorphous protein layer known as the tegument [4]. While generally not disease causing in immunocompetent hosts, HCMV poses a threat to developing fetuses, newborns, and immunocompromised adults. Though infection can occur at any point during a pregnancy, infections of developing fetuses occurring in the first trimester of pregnancy typically lead to more severe outcomes than those infected later. Newborns infected with HCMV prenatally are at risk for defects in

neural developmental, which can result in hearing loss, mental retardation, microcephaly, or combinations thereof [5]. At-risk adults include solid organ transplant recipients on anti-rejection medication, AIDs patients, and patients receiving chemotherapy [6]. These HCMV-infected individuals are at a greater risk of developing inflammatory conditions including retinitis [7], colitis, pneumotitis, or hepatitis [8]. Additionally, organ transplant recipients are at a greater risk of allograft loss due to HCMV infection [9]. Though vaccine development is ongoing, current vaccination efforts are in various stages of clinical trials [10] with nothing available to the public at this time. Modern treatment options for active HCMV infection utilize nucleoside analogs or HCMV DNA polymerase inhibitors including gangciclovir, valganciclovir, cidofovir, and foscarnet [11], which act by blocking DNA replication of the HCMV-encoded DNA polymerase. Perhaps not surprisingly, resistant populations of HCMV are continuously reported [12]. Only recently have phase III clinical trials for a new class of anti-HCMV drugs shown real promise in attenuation of infection [13, 14]. Continued research into treatment and diagnosis is needed to effectively combat HCMV infection. In order to develop better diagnostic measures and understand the important viral contributions that allow HCMV to successfully replicate in a live host, relevant small animal model systems are essential. It is with these small animal model systems that we can begin understanding the efficacy of novel diagnostic tools and unique viral contributions to a successful infection.

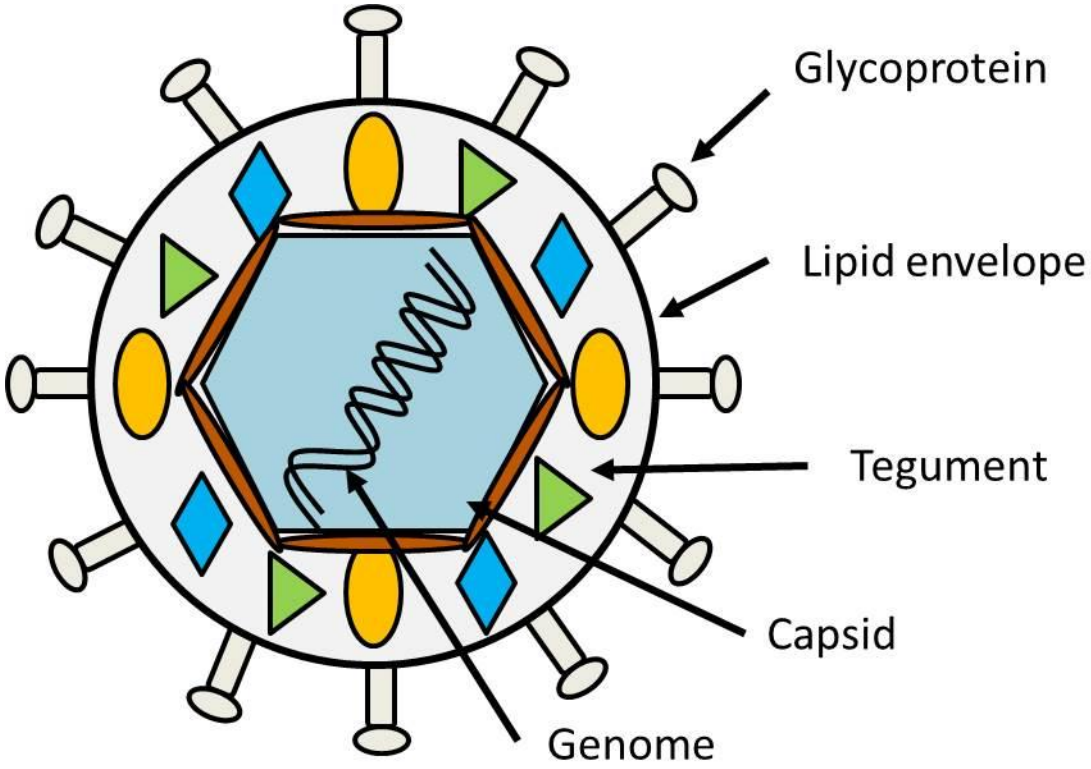

Figure 1.1: Cartoon schematic of HCMV (or MCMV) virion organization.

An icosahedral capsid, surrounding a linear dsDNA genome (~230kb), is surrounded by a lipid bilayer serving as an envelope, packaging the virion. Between the lipid envelope and capsid is an amorphous protein layer known as the tegument. The lipid bilayer is studded with numerous viral glycoproteins, each with different functions.

1.2 MODEL SYSTEMS FOR HCMV STUDY

1.2.1 Murine Cytomegalovirus (MCMV) as a model beta-herpesvirus

While studies of HCMV have yielded significant insight into the molecular mechanisms governing infection, these analyses are limited to cell culture. Unlike some *in vivo* infection systems developed to study other herpesviruses [15], the cytomegaloviruses are species specific, which prevents the use of HCMV in animal model systems [16]. In order to learn what contributions virally-encoded products make to infection in a live mammalian host, small animal model systems must be utilized. Though CMV infection models using rats and guinea pigs exist, pathogenesis etiology in these systems remains relatively understudied. Over the decades, CMV virologists have made heavy use of murine model systems. These model systems are incredibly valuable, especially with the advent of modern genetic techniques (CRISPR/Cas9) [17], in that mice are becoming more genetically tractable. This allows researchers to better understand the contributions of host proteins to CMV infection.

Murine cytomegalovirus (MCMV), like HCMV, is a beta-herpesvirus with a large, linear dsDNA genome. Additionally, MCMV shares significant similarity with HCMV in its virion structure (Figure 1.1). MCMV shares a significant amount of genetic and biological similarity with HCMV. While differences do exist between HCMV and MCMV, many of the MCMV core proteins share significant sequence and functional similarity [18]. These core proteins tend to localize to the middle of their respective genomes and are typically involved in entry, replication, and egress. Comparative analyses on the functions and roles of proteins conserved between HCMV and MCMV

have allowed researchers to define the roles of CMV proteins during infection of natural hosts. Though the MCMV model system has been instrumental in advancing our understandings of cytomegalovirus biology as a whole, there are limitations. MCMV does not serve as a good model for studying congenital infection as MCMV does not readily cross the placental barrier [19]. Additionally, route of infection and the immune status of the mouse influence the pathogenicity of MCMV [20]. Thus, when designing MCMV studies to most closely mimic HCMV infection, these limitations must be taken into consideration. So long as the proper precautions are taken in experimental design, significant and important insight can be gleaned using MCMV model systems, as illustrated in Chapter 3 of this dissertation.

1.3 CURRENT HCMV DIAGNOSTIC MEASURES

1.3.1 Current Screening Methods for HCMV

When one considers the prevalence of HCMV infection and the slew of diseases and developmental deformities it can cause, it is surprising that early screening for infection is not more common. Typically, individuals are only diagnosed when disease symptoms are present. In the case of an expecting mother, these symptoms include those resembling infectious mononucleosis with negative test results for Epstein-Barr virus or signs of hepatitis that test negative for hepatitis A, B, and C [21]. Since the greatest risk of complications to the developing infant occurs during the first trimester of pregnancy [5], testing early and often should be of great importance.

Presently used screening methods for HCMV infection involve IgG or IgM testing for exposure to the virus [22], PCR-based methods for the detection of HCMV genome present in patient blood, urine, or amniotic fluid samples, as well as culturing of possibly infected samples with permissible cells (See Table 2.1) [23]. Unfortunately, these diagnostic tests require significant sample preparation (i.e. serum isolation and DNA extraction) and importantly, are currently not implemented as point-of-care measures in the United States. Interestingly, only 9 countries (Israel, France, Belgium, Spain, Italy, Germany, Austria, Portugal, and the Netherlands) regularly screen pregnant women serologically for HCMV [24]. As these countries implement regular testing for HCMV seropositivity, cost may not prove as big of a cost barrier as previously thought. In fact, predictive models suggest that universal HCMV screening would be a cost-effective strategy, assuming passive immunization could achieve at least a 47% reduction in clinical disease [25]. These data all point us in a direction toward universal testing. As such, implementing rapid, facile methods requiring little to no sample preparation for diagnosis would be of benefit or could be used in conjunction with current diagnostic measures. Direct detection of virus, as opposed to immunoglobulin directed against HCMV antigen, would be of high priority so as to indicate whether an infection is active at the time of testing.

1.3.2 Using electrochemistry for the detection of interesting species

Electrochemistry is a field of chemistry concerned with the interrelation of electrical and chemical effects [26]. Electrochemistry is a powerful tool and is highly

amenable to the study of a number of interesting biological problems [27]. Of particular interest is the use of electrochemical methods that have been implemented heavily in the development of various biosensors [28]. A number of different molecules can be detected using electrochemical means. Perhaps the most popular and well-known utilization of electrochemical biosensors is seen with glucometers for the measurement of blood glucose concentrations [29]. Certain cancer-associated biomarkers have been detected with great sensitivity, with detection limits reaching sub-femtomolar ranges in some cases [30, 31]. Additionally, electrochemical nanobiosensors have been incredibly useful for the detection of trace amounts of various metals, harmful organic compounds, biomolecules, as well as microorganisms contained in or sitting on various foods [32]. In fact, due to their relative ease of use, portability, and cost effectiveness, the development of electrochemical detectors for species of interest is an exciting and burgeoning field [28].

1.3.3 Electrochemical Analysis Using Collision Electrochemistry

Many of the measurements scientists make during their experiments are ultimately mean values derived from a multitude of experiments over ensemble amounts of species. While these results are meaningful, they lack the resolution that would allow one to characterize and identify the contributions of individual molecules or species to the calculated mean values. Single molecule analyses, on the other hand, allow the researcher to observe the functional heterogeneity inherent in a sample, precise localization of a molecule, and kinetic properties of molecule function [33, 34]. The

science of electrochemistry provides one with a powerful set of tools to query systems traditionally measured by ensemble methods [35]. These types of experiments led to a field of stochastic electrochemistry that was first reported in 2004 by Lemay and co-workers analyzing the collision of latex beads on ultramicroelectrodes (UMEs) [36]. Since then, the field of electrochemical collisions has generated significant interest in the electrochemistry community as it allows for the discrete detection of singular particles or even molecules in solution [37]. In order to observe stochastic processes on UMEs, one must decrease the concentration such that the collision of analyte species with the UME surface is on the order of one every few seconds. Thus, inherent in these experiments are limits of quantitation at sub-picomolar levels. For example, the femtomolar detection of ions has also been reported [38, 39]. One collision technique most relevant to this dissertation and of interest due to its high reproducibility of results is termed blocking [40]. In these experiments, a reaction is driven at the electrode surface (such as the oxidation of ferrocene methanol to ferrocenium methanol). Particles that collide with an electrode and adhere irreversibly are said to "block" the flux of ferrocene methanol to the electrode surface, thereby decreasing the overall current (Figure 1.2a). This manifests as a sharp change (i.e. decrease) in current as measured by the now blocked electrode (Figure 1.2b). According to the "classic" or U.S. plotting convention for amperometry current vs. time (i-t) curves, oxidation events at the electrode are plotted in the 4^{th} quadrant in a Cartesian coordinate plane. Therefore, changes in current toward 0 are decreases in current (Figure 1.2b). The movement, or mass transfer, of particles to the surface of the electrode can be explained in a stochastic sense by considering the

frequency, *f*, with which analyte species collide with the electrode, given by the following equation:

$$f = 4DCaN_A \quad \text{(Equation 1)}$$

where D is the diffusion coefficient, estimated using the Stokes-Einstein approximation [41], C is the concentration, a is the radius of the UME, and N_A is Avagadro's Number. Thus, by studying the frequency of particle collisions and the change in current each time there is a collision at the electrode, one can learn the size range and possibly even the shape of a particle by considering its footprint.

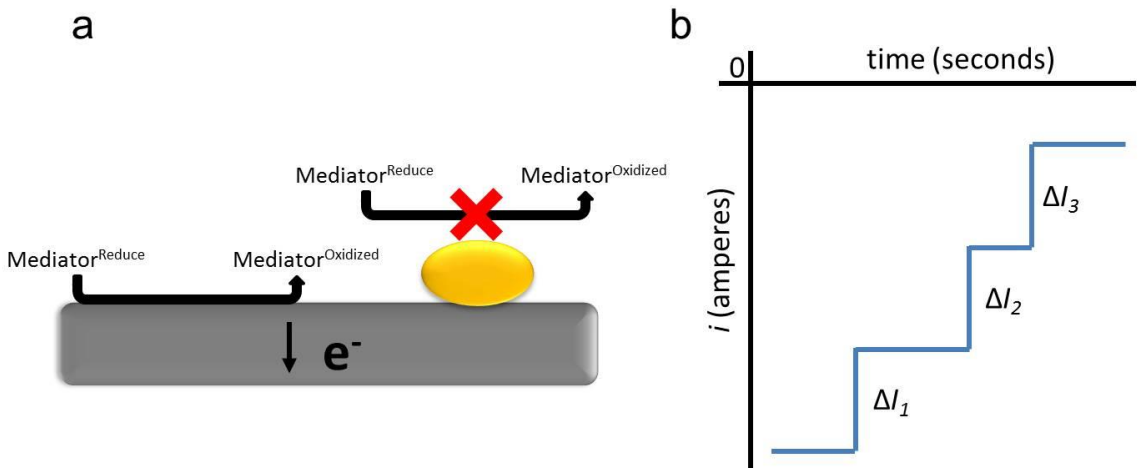

Figure 1.2: Collision and the subsequent blocking of the flux of redox active molecules at an electrode surface.

A) Without any obstruction, the oxidation of a mediator molecule (e.g. ferrocene methanol) can be carried out at an electrode surface. Upon collision and blocking of the electrode surface by some particle, the oxidation of the mediator molecule is blocked, therefor blocking the current. B) Individual blocking events are seen as stepwise decreases in current by measuring the amount of current passing through an electrode over a time course. Multiple steps indicates multiple blocking events.

While this tool is incredibly powerful and simple compared to other single molecule analyses, it is non-specific [42]. This means that anything in solution can potentially collide with the electrode and cause a change in current. However, if one can specifically label a species of interest such that a specific current change (e.g. a current increase) occurred upon the species of interest colliding with an electrode, the collision method could be used to positively identify particles in solution at the sub-picomolar level (Figure 1.3). With a detection scheme such as this, one could imagine extending these ideas to the detection of a number of different pathogens, which, in this scheme, act as the colliding particles. Chapter 2 describes work in collaboration with the laboratory of Allen J. Bard (UT Austin) in which a method to specifically detect viral particles at the 30 fM level was achieved. This method was then extended to the detection of virus in urine of infected mice [43].

While a correct diagnosis is important in order to determine the appropriate treatment regimen for a patient, resolution of the infection is essential for a patient to make a full recovery. As such, new viral targets for inhibition need to be identified in order that novel, less toxic inhibitors are developed. As previously stated, current HCMV treatment regimens only target viral DNA replication. While this is a logical strategy as DNA replication is an essential process to produce viral progeny, resistance to these drugs is increasing. In order to better treat HCMV infections, new drug targets must be identified. As host ubiquitin systems are necessary for HCMV infection, possible targets for anti-HCMV therapies may include viral proteins that manipulate the ubiquitin system. In the following section, examples of the specific ways herpesviruses interact with the

ubiquitin system are presented, emphasizing the contributions of uniquely structured viral deubiquitinating enzymes and how they may be viable targets for pharmacological intervention via future therapies.

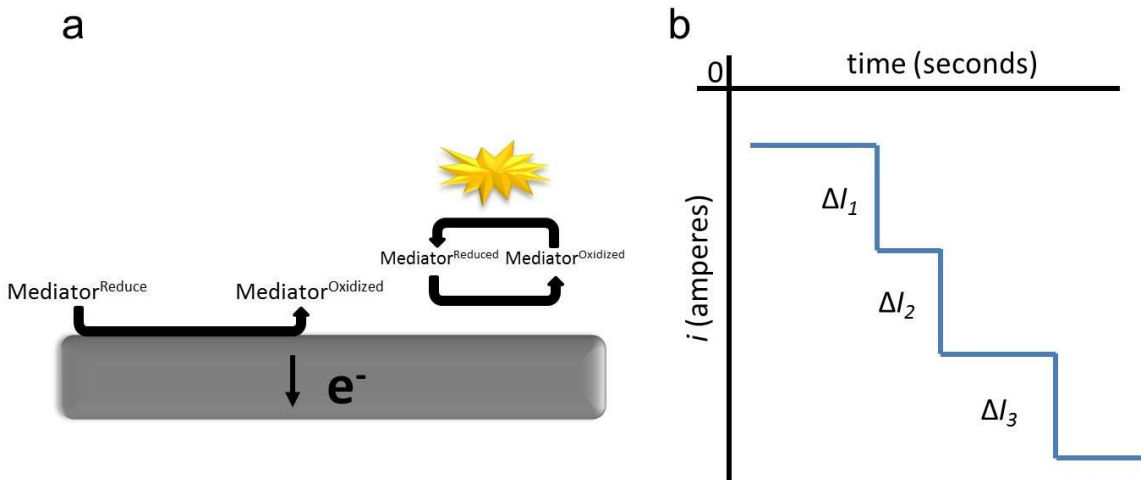

Figure 1.3: An electrochemical collision scheme demonstrating a current increase upon collision of a species of interest with an electrode.

A) A redox active species, being oxidized at an electrode, can be replenished enzymatically through the reduction of the oxidized mediator molecule upon collision at an electrode surface of species capable of doing so. B) Upon discrete collision of the reducing particle, the resulting amperometry manifests as stepwise increases in current (i.e. away from 0). Each ΔI represents a single collision event.

1.4 HERPESVIRUSES AND THE UBIQUITIN SYSTEM

1.4.1 Ubiquitin: a post-translational modification with a diverse functional range

Ubiquitin is a small ~8 kD protein that serves as a post translational modification (PTM) in cells. Its covalent attachment to target proteins depends on a cascade of E1 activating, E2 conjugating, and E3 ligating enzymes. E1 activating enzymes are charged with ubiquitin on their active site cysteine in an ATP-dependent manner. The ubiquitin molecule is then transferred to the active site cysteine residue of an E2 conjugating enzyme. This E2 enzyme then interacts with a specific E3 enzyme, which facilitates the ligation of the ubiquitin molecule onto the target protein (Figure 1.4). Substrate specificity is defined by interactions of E3 ubiquitin ligating enzymes with their targets. In the human genome, there are about 2 E1 enzymes, about 40 E2 enzymes, and around 600 E3 ligating enzymes [44]. With an estimate of around 20,000-25,000 genes in the human genome [45], these E3 ligating enzymes must possess the ability to recognize a broad range of substrates for ubiquitination

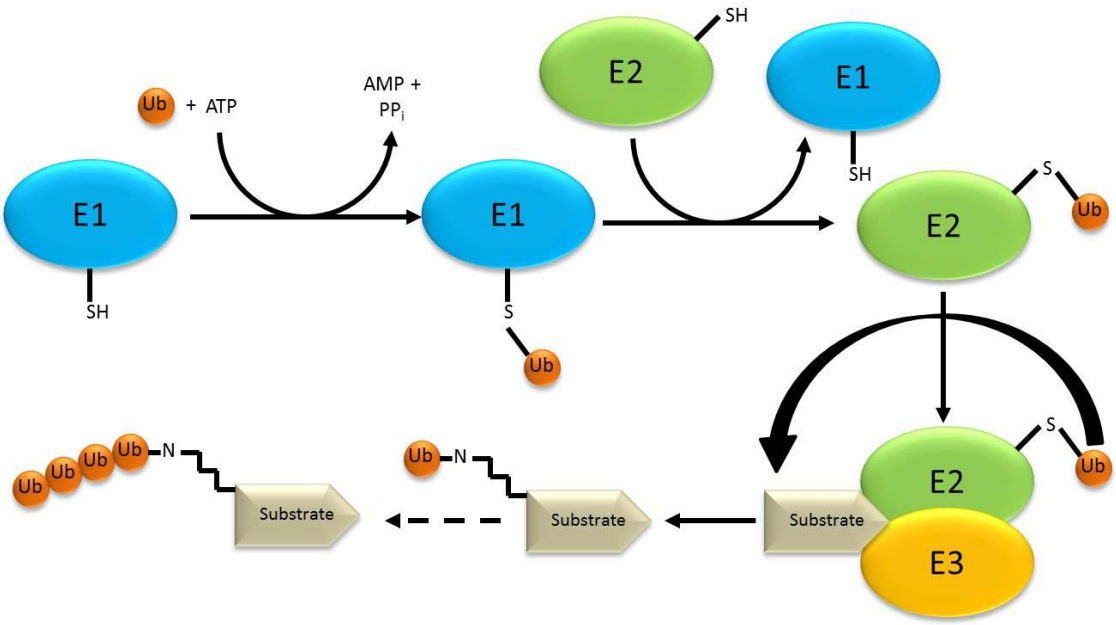

Figure 1.4: The ubiquitin cascade.

In an ATP-dependent manner, ubiquitin is attached to an E1 activating enzyme. Transfer of the ubiquitin molecule from an E1 to an E2 conjugating enzyme is performed. E2 interaction with an E3 ligating enzyme facilitates the transfer of ubiquitin to a target substrate. Multiple cycles of this can leads to a poly-ubiquitinated substrate molecule.

Though only a single protein, the function-altering potential ubiquitin possesses is quite amazing. Ubiquitin molecules are attached via the C-terminal glycine to the ε-amine group on lysine residues via an isopeptide bond. From here, ubiquitin chains can be assembled any number of different ways. Ubiquitin contains 7 internal lysine residues (K6, K11, K27, K29, K33, K48, and K63) and an N-terminal methionine which can all serve as sites upon which to build ubiquitin chains [46].

With the ability to be conjugated a number of ways, ubiquitin modifications can have significant functional heterogeneity. The most well studied ubiquitin linkages, K48 and K63, serve to modify targets proteins for destruction by the 26S proteasome and serve as a signal for the modified protein to participate in signaling pathways, respectively [46]. The other linkages, so-called "non-canonical" linkages, have been shown to have diverse roles in cells. K6 linkages have been shown to be involved in mitophagy [47-50]. K11 linkages have been shown to be heavily preferentially produced during early G1 and mitosis stages of the cell cycle [51]. This linkage plays a role similar to K48, in that it promote proteasomal degradation in some cases [52] while serving a protective role in others [53]. K27 linkages have been observed on mitochondrial trafficking protein Miro1 which slows down its own degradation and acts as a signal for mitochondrial clearance [54]. Additonally, K27 ubiquitin linkages are involved in controlling innate immune responses [55]. K29 linkages have been shown to be involved in growth and development pathways as well as affecting mRNA stability [56]. K33 linkages have been shown to be involved in post-golgi transport [57]. As clearly evidenced here, ubiquitin plays a diverse yet essential role in cells.

While ubiquitin can rapidly elicit effects on protein functionality, this must be balanced with the potential to reverse these processes when needed. To this end, deubiquitinating enzymes, or DUBs, catalyze the removal of ubiquitin linkages from proteins to effectively reverse the effects ubiquitin once had. In humans, several classes of DUBs exist. These DUBs function in a number of different cellular processes, ranging from cell cycle regulation to regulating proteasomal degradation to DNA repair [58]. Mammalian DUBs can be divided in to 5 different classes: the ubiquitin C-terminal hydrolases (UCH), the ubiquitin specific proteases (USP), the ovarian tumor (OTU) domain containing DUBs, the Josephin domain (MJD) containing DUBs, and the JAB1/MPN/Mov34 metalloenzyme (JAMM) domain containing DUBs. The first four are cysteine proteases while the last class cleaves ubiquitin via a metalloproteolytic mechanism [58]. As DUBs serve a number of different roles under normal conditions, ranging from control over protein levels to trafficking of proteins [59], their importance must not be undermined. In fact, as discussed in section 1.4.2 and in more detail in the remaining sections, herpesvirus manipulation of the ubiquitin system not only includes directing ubiquitin attachment, but catalyzing its release, suggesting herpesviruses usurp multiple aspects of the ubiquitin system.

1.4.2 Herpesvirus manipulation of the ubiquitin system

Since the processes of ubiquitin attachment and removal are critical to optimal cellular function [59], it comes as no surprise that many viruses have evolved mechanisms to hijack the ubiquitin system for their own means [60]. One could argue

that the most masterful manipulators of host ubiquitin systems belong the family *Herpesviridae* as these pathogens encode numerous proteins evolved to hijack ubiquitin pathways [61]. For example, herpes simplex type 1 virus (HSV-1) encodes an E3 ligating enzyme known as infected cell protein 0 (ICP0). ICP0 E3 ubiquitin ligating activity targets a number of different proteins involved in innate immune signaling, the DNA damage response, and intrinsic immune responses to facilitate replication [62]. Kaposi's sarcoma associated herpesvirus (KSHV) and murine gammaherpesvirus 68 (MHV68) also encode E3 ubiquitin ligating enzymes. KSHV encodes two E3's: K3 and K5. These two enzymes are responsible for facilitating the ubiquitination and subsequent degradation of many cell surface localized immunomodulatory proteins [63]. The MHV68 E3 enzyme, mK3 performs a similar function, facilitating the degradation of MHC class I presentation [64]. While their targets differ, these E3 ubiquitin ligating enzymes operate similarly in that they promote the dampening of the host immune responses to infection.

Although the HCMV genome does not encode any known E3 ligating enzymes, it does encode proteins that facilitate the ubiquitination and subsequent degradation of MHC I and II (US2 and US11). These two HCMV genes are not E3 ubiquitin ligating enzymes themselves. However, both US2 and US11 hijack the cellular endoplasmic reticulum-associated degradation (ERAD) machinery to facilitate the degradation of the peptide presenting complex, MHC class I. That is to say, they facilitate the extraction, ubiquitination, and subsequent proteasomal degradation of MCH class I [65]. Like HSV-1, KSHV, and MHV68, HCMV manipulation of the ubiquitination system modulates the

host response to infection. Though these examples only describe a few virally-encoded proteins that manipulate the ubiquitin system, they serve to illustrate that herpesviruses must utilize the host ubiquitin system in order to effectively navigate host responses to infection.

As evidenced above, not all herpesviruses encode E3 ubiquitin ligating enzymes. Interestingly, all herpesviruses from the three sub-families (alpha, beta, and gamma) do encode deubiquitinating enzymes (DUBs). This DUB activity lies in N-terminus of a conserved herpesvirus gene known as the large tegument protein (LTP) [66]. The tegument constitutes the amorphous space between the viral capsid and lipid envelope and contains a number of proteins critical for viral entry, assembly, and egress [67]. As the name suggests, these viral proteins lie within the herpesvirus tegument in close contact with the capsid. Herpesvirus LTPs have been shown to be critical in several capacities during entry, assembly, and egress. For example, the HCMV LTP UL48 may aid in genome deposition into the nucleus in cooperation with another tegument protein, UL47, upon capsid interaction with the nuclear pore complex [68]. Recent work has also shown that the HSV-1 LTP, UL36, serves as a scaffold for the assembly of other tegument protein [69]. Additionally, impressive work from the Pellett laboratory has demonstrated that the HCMV LTP, UL48, is critical for assembly compartment formation [70].

Over the past decade, much work has been conducted on the herpesvirus DUBs. Structural analyses of the MCMV DUB, M48, revealed that although herpesvirus DUBs seem to belong to the papain superfamily of proteases, they are distinctly structured and

have unique interactions with ubiquitin [71]. Even though the structure of herpesvirus DUBs appears conserved, functional studies have identified a variety of targets (Table 1.2). However, much of the work characterizing the roles of herpesvirus DUBs has been done on the alpha- and gamma-herepsviruses, with only limited work conducted with beta-herpesviruses, which will be outlined in the sections below.

1.4.3 Alpha-herpesvirus DUBs: roles during infection

Much of the initial work uncovering the functions of herpesvirus DUBs has focused on the roles that alpha-herpesvirus DUBs served during infection. The archetypal alpha-herpesvirus, HSV-1, is a significant cause of morbidity. Specifically, HSV-1 primarily causes lesions in mucosal membranes [15]. The HSV-1 DUB protein UL36, was the first described over ten years ago [66]. Protein alignment analysis subsequently revealed that other members of *Herpesviridae* appeared to encode for similar enzymes. As these DUBs did not align with any known cellular DUBs at the time, a novel class of DUBs was established, termed the herpesvirus tegument ubiquitin specific proteases (htUSPs). Single- and multi-step replication kinetics with a UL36 mutant (C40A) revealed only a modest replication defect in cell culture [72]. Though not necessary for replication *in vitro*, initial studies characterizing the role of HSV-1 UL36 deubiquitination activity during infection showed that UL36 acts on TRAF3. Deubiquitination of TRAF3 resulted in an inability of Tank-binding kinase 1 (TBK1) to bind to TRAF3 and propagate signaling. The activity of UL36 therefore ultimately results in a diminished type 1 interferon (IFN) response [72]. Recent work has also demonstrated

that HSV-1 UL36 blocks activation of NFκB following infection by deubiquitinating the NFκB antagonist, IkBa, thus preventing its degradation thereby preventing activation of the NFκB response [73].

Pseudorabies virus (PRV), another alpha-herpesvirus, also encodes a DUB (UL36) in the N-terminus of its LTP. As PRV can cause significant neurological disease in infected pigs [74], the pig industry is vested in treating and protecting livestock against infection. Similar to HSV-1, inactivation of the PRV DUB by mutagenesis of the catalytic cysteine (C26S) resulted in a modest decrease in replication in cell culture. Interestingly, mice infected with mutant DUB PRV survived twice as long as mice infected with a wildtype (WT) virus control. Additionally, mutant DUB PRV exhibited a delay in neuroinvasion not observed in mice infected with a WT virus [75]. These data indicate the PRV DUB activity is important for PRV pathogenesis. Work from Gregory Smith's laboratory independently arrived at a similar conclusion. Their work demonstrated that the PRV DUB was essential for initial neuroinvasion, but not subsequent neuron-to-neuron infection [76]. In fact, through the use of a technique known as di-glycine proteomics, Huffmaster and co-workers determined that this neuroinvasion was dependent on the auto-deubiquitination of a specific lysine residue (K442) of UL36. This deubiquitination of UL36 allowed transmission to nerve terminals and subsequent neuroinvasion [77]. While not shown to be the "switch" allowing for successful neuroinvasion by HSV-1, the positionally conserved lysine residue in HSV-1 UL36 (K636) was also found to be heavily ubiquitinated in HSV-1 mutant DUB infected cells. This conservation suggests a similar phenomenon is occurring in HSV-1.

Unlike other alpha-herpesviruses, Marek's disease virus (MDV), an alpha-herpesvirus associated with chickens, does not infect or go latent in neurons, but instead infects B- and T-cells. T-cells that are latently infected may transform, ultimately leading to T-cell lymphoma and death of the infected poultry [78]. Like other herpesviruses, MDV contains a DUB in the N-terminus of its LTP (UL36). While not necessary in cell culture, a lack of DUB activity led to a significant decrease in the incidence of lymphomas in infected chickens [79, 80]. Additionally, the researchers showed that DUB domain structure, not the catalytic cysteine, of UL36 was important for *in vitro* and *in vivo* replication [80].

1.4.4 Gamma-herpesvirus DUBs: roles during infection

Like the alpha-herpesviruses, the gamma-herpesviruses share the conserved DUB function in their respective LTPs [66]. Kaposi's sarcoma associated herpesvirus (KSHV) is a gamma-herpesvirus and is the causative agent of Kaposi's sarcoma, primary effusion lymphomas, and multicentric Castleman's disease [81, 82]. Like other herpesvirus DUBs, the DUB of KSHV, ORF64, has the ability to cleave lysine 48 (K48) and lysine 63 (K63) linked ubiquitin molecules [82]. Though silencing of the entire gene leads to a decrease in replication, it is not clear what the contribution is of ORF64 DUB activity to KSHV infection. Interestingly, in transfected cells, ORF64 appears to antagonize host antiviral responses similar to UL36 in HSV-1. Specifically, KSHV ORF64 and the murine gammaherpesvirus 68 (MHV68) DUB (also called ORF64) were able to deubiquitinate the RNA sensor, retinoic acid-inducible gene I (RIG-I), which prevents the induction of

type I IFN. Additionally, both KSHV and MHV68 replicated to higher levels in cells lacking RIG-I, indicating that RIG-I restricts their replication [83]. These studies, however, did not address whether the DUB of either KSHV or MHV68 had a direct effect on RIG-I during an infection.

In vivo analyses characterizing the role of gamma-herpesvirus DUBs conducted utilizing MHV68 have begun addressing the role of the gamma-herpesvirus DUB in small animals (*Mus musculus*). Like other gamma-herpesviruses, MHV68 enters latency in B-cells [84]. This small animal model system serves as a valuable system to determine the contribution of conserved gamma-herpesvirus genes to infection. Initial experiments revealed that MHV68 encodes a functional DUB [85]. Later studies examining the contributions of the MHV68 DUB to infection revealed that the DUB activity was not necessary for replication in cell culture, similar to other studies on herpesvirus DUB mutants. Interestingly, researchers discovered that a DUB mutant virus was rapidly cleared from the spleens of infected mice but was able to enter latency as well as the WT control [86]. This conclusion remains somewhat controversial, as a more recent study revealed that a mutant DUB MHV68 did not enter latency efficiently. This switch to latency was found to be dependent on the stimulator of interferon genes or STING protein [87].

Perhaps the most well characterized herpesvirus DUB is that of Epstein-Barr virus (EBV), BPLF1. EBV is a gamma-herpesvirus that infects over 95% of people worldwide. Normally asymptomatic, approximately 200,000 cases of cancer each year can be attributed to EBV infection [88]. Over the years BPLF1 has been attributed a number of

different functions. Initial studies revealed that in addition to possessing DUB activity [89], the DUB domain of BPLF1 (aa 1-246) interacts with the virally encoded ribonucleotide reductase large subunit (RR1). Deubiquitination of RR1 by BPLF1 reduces the ribonucleotide reductase activity in EBV, suggesting the DUB has a role in controlling replication [90].

BPLF1 is also unique from other herpesvirus DUBs in that it has the unique ability to deneddylate, proteins modified by NEDD8 [91]. NEDD8 is a ubiquitin-like protein responsible for post translational modification of the Cullin family of proteins, which serve as scaffolds for the assembly of multicomponent RING E3 ligases (CRLs) [92]. As Cullin proteins serve as major targets of neddylation and BPLF1 can act as a deneddylase, it was reasoned that BPLF1 might be targeting Cullins proteins. In fact, BPLF1 was shown to bind Cullins to regulate CRL activity, which led to the accumulation of CDT1, a critical protein that licenses DNA for replication [93], and subsequent deregulation of the cell cycle, and increased viral DNA synthesis [91]. In addition to promoting viral DNA synthesis, BPLF1 can promote the accumulation of host chromosomal lesions through the deubiquitination of PCNA and subsequent de-regulation of DNA lesion repair. This may be one mechanism by which EBV promotes the transformation of B-cells [94]. In addition to these functions in manipulating DNA replication and repair, BPLF1 has been shown to antagonize innate immune signaling. BPLF1 has been shown to deubiquitinate TRAF6, thereby inhibiting NFkB activation and subsequent antiviral responses [95, 96].

1.4.5 Beta-herpesvirus DUBs: roles During Infection

Systematic, functional analyses defining beta-herpesvirus DUB contributions to infection represent the minority of herpesvirus DUB studies. Although the only herpesvirus DUB structure currently known is that of the beta-herpesvirus MCMV DUB M48, targets of this DUB still elude researchers. However, studies of CMV DUBs have shown not only that the DUB is functional, but that it is active during infection. Early work from Schlieker and colleagues showed that the N-terminus of M48 possessed DUB activity and that this DUB activity is dependent on a catalytic triad of consisting of cysteine (C23), aspartic acid (D156), and histidine (H158) [89]. Additionally, this new class of DUB, termed the herpesvirus tegument ubiquitin specific proteases (htUSPs), contains a unique β-hairpin critical for ubiquitin and ubiquitin-like (Ubl) protein distinction [71].

More recent work by Kim and co-workers showed that the HCMV DUB, UL48, was expressed and active during infection. Like other herpesvirus DUBs, activity was not required for replication in cell culture. In fact, the contribution of UL48's DUB activity was only realized in multi-step growth analyses [97]. The UL48 DUB domain also contributes stability to viral particles, aiding in infectivity, and actively targets itself for deubiquitination leading to its stabilization [98]. Although these two studies from Jin-Hyun Ahn's laboratory identified several roles for CMV DUBs during infection, until recently, it was not known what contributions beta-herpesvirus DUBs made to infection in a natural host.

Uncovering the roles that herpesvirus DUBs assume during infection presents itself as an incredibly important set of tasks. As these DUBs are uniquely structured, they have the potential to serve as druggable targets. Continued research into the basic biology governing unique viral enzymatic contributions to infection is crucial to identify targets and develop pharmacological therapies. In Chapter 3, I will describe my work which identified a primary role for the M48 DUB during infection of mice. From our results and the significant structural similarity between the MCMV DUB and the HCMV DUB, we believe that the DUB of HCMV is a potential target for future pharmacological intervention.

Sub-Family	Species	DUB	Function
Alpha-herpesvirus	HSV-1	UL36	• Modest contribution to replication in cell culture (72) • Deubiquitination of TRAF3; decrease type I IFN response (72) • Deubiquitination of IκBa; decrease NFκB response (73)
	PRV	UL36	• Modest contribution to replication in cell culture (75) • Contributes to virulence; facilitates neuroinvasion (75) • Deubiquitinates itself to facilitate epithelial-to-neuron cell invasion; a "molecular switch" (77)
	MDV	UL36	• Modest contribution to replication in cell culture (80) • Contributes to lymphoma formation in chickens (79) • The DUB domain, not the catalytic residue, is essential for replication (80)
Beta-herpesvirus	HCMV	UL48	• Modest contribution to replication in cell culture (97) • DUB domain contributes to virion stability and infectivity (98)
	MCMV	M48	• Structural analyses suggest this DUB, as well as other DUBs, are unique in their structure (71)
Gamma-herpesvirus	KSHV	ORF64	• Deubiquitinates RIG-I; decrease in type I IFN response (82)
	MHV68	ORF64	• Encodes a functional DUB (85) • Modest contribution to replication in cell culture (86) • Contributes to lytic replication in spleens (86) • Deubiquitinates RIG-I; decrease in type I IFN response (82) • Conflicting data regarding role in latency (86, 87)
	EBV	BPLF1	• Deubiquitinates RR1, reducing ribonucleotide reductase activity, may have a role in EBV replication (90) • Dennedylates CRLs, leading to accumulation of CDT1, and increased viral DNA replication (91) • Deubiquitinates PCNA, de-regulating DNA lesion repair (94) • Deubiquitinates TRAF6, decreasing NFκB response (95, 96)

Table 1.1: Alpha-, beta-, and gamma-herpesvirus DUBs and their functions.

This table summarizes numerous functions that have been attributed to herpesvirus DUBs over the past 10-15 years. As evidenced by the amount of text, much of the work focusing on herpesvirus DUBs has been concentrated on alpha- and gamma-herpesvirues.

Chapter 2: Specific, sensitive detection of murine cytomegalovirus using electrochemical methods[1]

2.1 INTRODUCTION

Electrochemistry is a branch of chemistry that is concerned with the interrelation of electrical and chemical effects [26]. It is an exciting field of study that has proven incredibly useful for the development of a variety of valuable sensor technologies. These sensors can and have been developed to detect a number of different relevant biological markers as well as possible food contaminants [32]. In the case of biomarker detection, sensitive detection of a number of different biological markers can be useful as a point-of-care-diagnostic measure for a variety of different diseases such as cancer [99, 100] and various infectious diseases [101, 102].

[1] Large portions of this chapter have been previously published. Author contributions are described in the publications. Briefly, A.T.H. performed research, analyzed data, and helped to write the papers. J.E.D. and A.T.H. contributions were equal in publication 2 listed below.

1. **Dick JE, Hilterbrand AT, BoikaA, Upton JW, Bard AJ.** 2015. Electrochemical detection of a single cytomegalovirus at an ultramicroelectrode and its antibody anchoring. PNAS **112**(17): 5303-5308.
2. **Dick JE[*], Hilterbrand AT[*], Strawsine LM, Upton JW, Bard AJ**. 2016. Enzymatically enhanced collisions on ultramicroelectrodes for specific and rapid detection of individual viruses. PNAS **113**(23): 6403-6408.

[*]Co-first authors

One particular popular focus of electrochemistry is the study of distinct collisions at ultramicroelectrodes (UMEs). With diameters on the order of micrometers to nanometers, these tiny electrodes offer researchers the unique opportunity to observe small current events not detectable with larger electrodes. Collision electrochemistry has been applied to the study of a number of different hard nanoparticles, particularly particles made of various metals, metal oxides, and organic materials [36, 103-113]. While a number of techniques have been developed to observe and measure the results from collisions at an electrode, the most robust and reproducible method is one known as "blocking" [40] (Figure 1.3). In a blocking event, a particle in solution will encounter an electrode, irreversibly adhere to it, and subsequently block any flux of redox active species at the electrode [40]. The resulting blocking event can be observed as a current step using amperometry, or measurements of current flux. This blocking event results in a sharp decrease in current, which leads to a new current steady state until the next blocking even occurs.

Recent experiments utilizing collision electrochemistry methods have included the analysis of biologically relevant molecules of interest, like DNA and proteins [37, 114]. In fact, using collision electrochemistry, one can analyze singular collision events and learn about single molecule properties from these phenomena [37]. Due to the inherent sensitivity of this technique [38, 39], its application to pathogen detection is an intriguing possibility. However, no collision methodologies have been investigated for the detection of relevant pathogens, such as viruses. As described in Chapter 1, one of the

most prevalent viral pathogens worldwide is human cytomegalovirus (HCMV). As such, HCMV detection is a priority so that infected individuals might be treated.

Cytomegaloviruses (CMVs) are the prototypic members of the beta-herpesvirus family. These large (~200 nm diameter) dsDNA viruses establish lifelong latent infections after primary infection and do not cause significant disease in healthy individuals. However, immunocompromised individuals infected with human cytomegalovirus (HCMV) are at a significantly greater risk of morbidity and mortality [115], including patients receiving chemotherapeutics, AIDS patients, and organ transplant recipients. Moreover, HCMV congenital infection is a leading cause of birth defects and developmental disabilities including hearing and vision loss, microcephaly, and cognitive disabilities [116]. Thus, highly sensitive and rapid detection of CMV infection in patients is an important part of mitigating transmission and disease. Like most herpesviruses, HCMV is highly species specific. Therefore, valuable small animal model systems exist to study CMV / host relationships. Murine cytomegalovirus (MCMV) serves as an important model system for HCMV pathogenesis, sharing significant genetic and biological characteristics with HCMV. MCMV provides a powerful, genetically tractable infection system in a natural mouse host and has yielded significant insights into CMV biology [20].

One particularly saddening reality regarding HCMV infection is that diagnosis and confirmation is typically only done when patients present with possible HCMV-caused symptoms. As HCMV has a significant potential to cause terrible disease, it is rather interesting that it is only regularly screened for in expecting mothers in 9 countries

worldwide, not including the United States [24]. HCMV is also not regularly screened for in immunocompromised individuals. When detection of HCMV is required, relatively time consuming techniques, with varying degrees of sensitivity, exist for the detection of CMV, including ELISA methods, sensitive PCR techniques, culturing, and microscopy (Table 2.1). While fairly reliable, these methods require significant sample preparation and can take anywhere from hours to days to perform.

As such, rapid, sensitive tools are critically important for initial diagnoses and for the continued monitoring of individuals infected with HCMV. While the collision method of blocking allows for this sought after level of sensitivity (theoretical detection limit of 1 virus particle) and rapid detection, it is inherently non-specific [43]. In a sample containing a complex mixture of particles of different makeup, it would be impossible to discern between different particles simply based on the resulting current change upon collision and subsequent blocking of an electrode. For that reason, if collision electrochemistry is to be used for pathogen detection, one needs a way to specifically identify differences between the varieties of particles likely to be in solution.

Two methods developed for the specific detection of MCMV, in purified samples as well as from the urine of infected mice, are described in the following sections in Chapter 2. Both methodologies rely on the collision of particles with an electrode; however, they differ in the output read. In order to gain specificity in the detection schemes, both methods to be described rely on the use of a previously described neutralizing antibody against the MCMV glycoprotein, gB (Mab 97.3) [117]. In the first method, polystyrene beads, functionalized with an antibody that recognizes the F_C

portion of Mab 97.3, interact with MCMV and Mab 97.3, ultimately resulting in a decrease in the frequency of blocking collisions and an increase in the amount of current blocked when collisions do occur. The second method relies on that same neutralizing antibody, which is now functionalized with a glucose oxidase enzyme (GOx). Using electrochemistry very similar to that used in modern day glucometers [29], we show that MCMV collision events can be detected as discrete stepwise increases in current at an electrode, in contrast to the previous method. This proves powerful in that it is distinguishable from possible background collisions. These two methods, those opposite in the responses generated at the electrode, allow for the rapid, specific detection of MCMV.

Method	Advantages	Disadvantages
Presented Electrochemical Technique	• Rapid detection, comlete within one hour • Minimal sample preparation • Sub-picomolar detection • Dual measurments: ΔI and frequency	• False positive due to non-specific adsorption • Currently unquantifiable • Dependent on K_D of antibody
Real-Time Polymerase Chain Reaction (RTPCR)	• High sensitivity • Detection limit of 122-1953 genomes/ml depending on method	• Detection limit varies with sample • Limits of detection not readily reproducible
Enzyme-linked Immunosorbent Assay (ELISA)	• Tests IgM and IgG for exposure to HCMV (Abcam®, Calbiotech, Genway Biotech Inc.) • Specificity ~98%	• Does not detect virus directly (genome or infectious units) • Dependent on K_D of antibody
Culture Test	• "Gold standard" for HCMV detection • Infectious titer quantitation	• False negatives are possible • Not as sensitive as PCR based methods
Electron microscopy	• Direct, visual evidence of HCMV • Can use morphological details to classify pathogens	• Not suitable for highly dilute samples • Not high thoughput

Table 2.1: Comparison of several different HCMV detection techniques.

Several diagnostic measures exist for the detection of HCMV by indirect or direct methods. Each method has advantages and disadvantages over the others. These methods are presented in the table above.

2.2 RESULTS

2.2.1 Electrochemical detection of discrete MCMV collisions

Prior to the specific detection of MCMV, the electrochemical response upon blocking of an electrode needed to be determined for MCMV. Approximately 5.2 x 10^5 plaque forming units (PFUs) / ml (~0.86 pM) of virus were incubated with a 10 μm platinum UME in the presence of 500 mM potassium ferrocyanide (KFCN). This redox active species was chosen due to its incomplete dissolution [118-120]. If one were to use a redox active species which dissolves completely, agglomeration of colloidally suspended virions may occur, which would affect virion collision and detection. As seen in Figure 2.1b, discrete collision events caused by MCMV are observed at the electrode. As mentioned in Figure 1.3, when oxidation is blocked, by a virus for example, the observed blocking of anodic events is plotted as discrete current steps that are decreasing in value (going toward 0) (Figure 2.1b). By calculating the frequency of the collision events (# collisions / sec), one can obtain a diffusion coefficient (D) for a given particle, given by Eq. 1. From this diffusion coefficient, one can calculate the radius of a particle using the Stokes-Einstein relationship [41]:

$$r_{particle} = k_B T(6\pi\eta D)^{-1} \qquad \text{(Equation 2)}$$

where $r_{particle}$ is the radius of the particle, k_B is Boltzman's constant, T is temperature, and η is the viscosity of the continuous phase. Using these equations, the size of a particle can

be determined. These relationships were used in section 2.2.2 to discriminate between MCMV and MCMV bound to an antibody against the MCMV glycoprotein, gB.

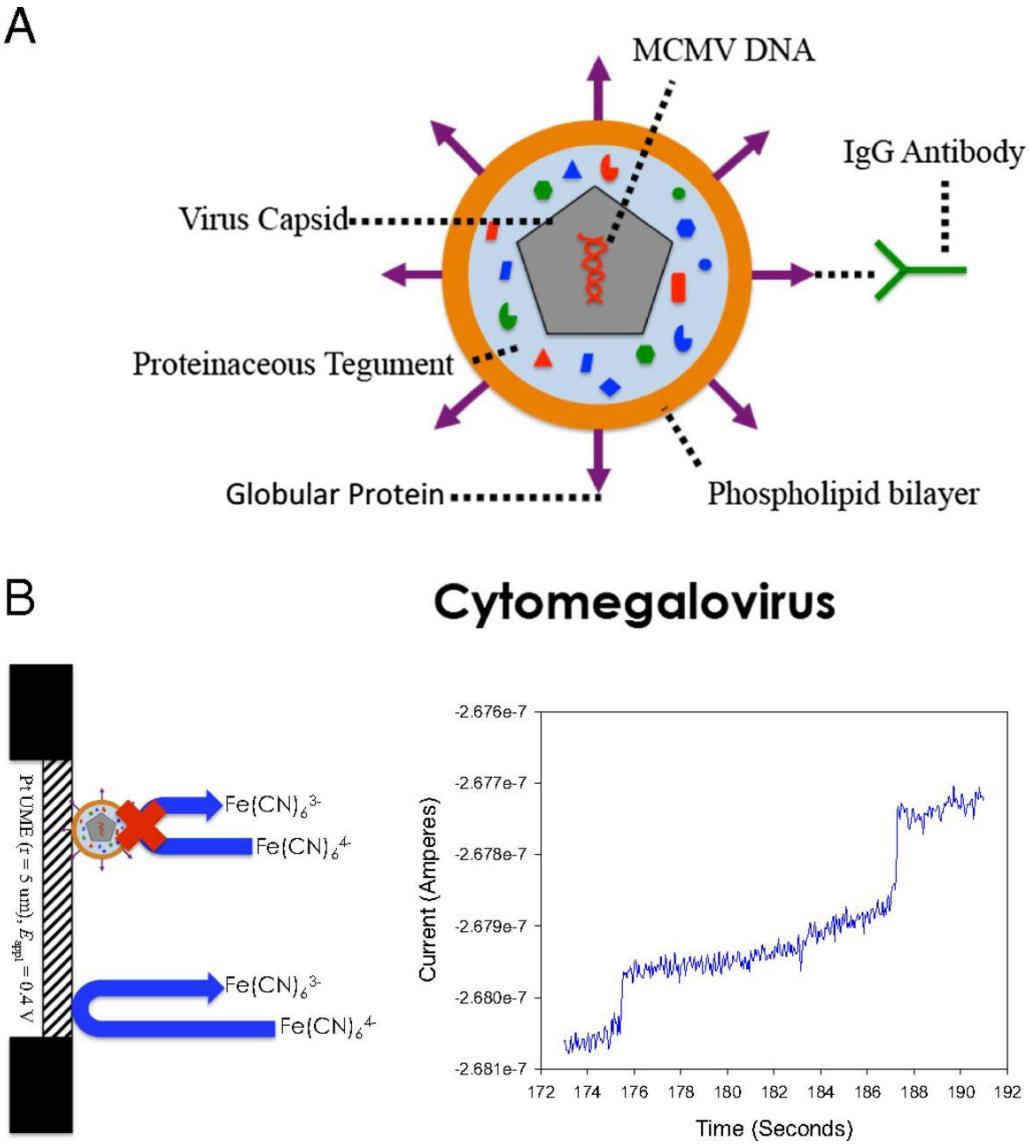

Figure 2.1: Electrochemical detection of MCMV by "blocking" in KFCN.

A) Cartoon diagram illustrating the general organization of an MCMV virion. B) MCMV adsorption event onto an electrode surface showing the blocking of the oxidation of KFCN at the electrode surface. The panel to the right shows a typical blocking response due to MCMV collisions. In this experiment, MCMV is blocking 500mM KFCN at a 10 µM Pt UME, where the applied voltage (E_{appl}) = +0.4 V vs. Ag/AgCl.

2.2.2 Electrochemical detection of discrete MCMV collisions with MCMV-specific antibody

Like other herpesviruses, the MCMV capsid is surrounded by a lipid bilayer known as the envelope. Throughout the envelope are a number of different MCMV glycoproteins important for various phenomena, such as viral entry, assembly, and egress [182]. One essential viral glycoprotein is glycoprotein B, or gB. This protein is necessary for the fusogenic steps resulting in MCMV lipid bilayer fusion with the plasma membrane of a susceptible cell [121]. Antibodies directed against gB can prevent infection, or neutralize the virus' ability to infect a cell [117]. As previously mentioned, blocking electrochemistry has the powerful capability to allow the researcher to discern particle size differences [37]. To showcase the ability of this electrochemical blocking technique to discern particle size differences, gB antibody (Mab 97.3), a kind gift from Dr. Michael Mach, was incubated with MCMV. The collision frequencies of MCMV-anti-gB were compared to MCMV alone. Utilizing Nanoparticle Tracking Analysis (NTA) via a Nanosight instrument, one can measure particle movements in solution by illuminating the particles with light from a laser. After recording these movements, software is able to trace the movement of the particles. From this, a diffusion coefficient can be calculated. By using the Stokes-Einstein relationship (Equation 2), one can back calculate the hydrodynamic radius of a particle. As illustrated in Table 2.2, the hydrodynamic radii of MCMV and MCMV-gB were readily determined. Of significant interest is the resulting difference seen in the radii. The difference of 17 nm ($MCMV\text{-}gB_{Radius} - MCMV_{Radius}$) agrees very well with the published length of IgG antibody,

which is approximately 14.5 nm [122]. Based on these measurements, it is very likely singular collision events are being recorded at the electrode. Additionally, it highlights the sensitivity of collision electrochemistry when using ultramicroelectrodes. While this blocking method has proved that MCMV and MCMV-Ab can be discriminated based on the calculated particle size, it still does not allow for specific detection of MCMV. If Mab 97.3 were to be incubated with a biological sample thought to contain MCMV, there would likely be a number of blocking events similar to MCMV-Ab. In that case, there would be no way to discern whether MCMV was present or not. Therefore, we set out to develop a more selective method for MCMV detection.

Sample	# of Events	ΔI (pA)	σ	f, Hz	σ	D, cm^2/s	D, cm^2/s^*	R, nm
MCMV	523	224	17	0.046	0.006	4.4×10^{-8}	6.4×10^{-8}	56
MCMV-Ab	506	293	21	0.034	0.008	3.3×10^{-8}	3.6×10^{-8}	73

*Values from nanoparticle tracking analysis.

Table 2.2: Statistics of MCMV and MCMV-gB antibody, values of current step sizes, frequencies of collision, diffusion coefficients, and radii.

2.2.3 Selectivity of MCMV detection by antibody anchoring of PSBs

As stated previously, the collision method is non-specific, meaning that any particle in solution could possibly collide with the measuring electrode and subsequently cause a current step. Because of this, it is necessary to include some means of specifically detecting MCMV by collision electrochemistry. In order to do this, 750 nm polystyrene beads (PSBs) functionalized with an antibody capable of recognizing the F_C portion of the gB antibody were mixed with MCMV and gB antibody. This experiment is illustrated in Figure 2.2a. In order to negate the potential background collisions that may occur as a result of unbound virus hitting the electrode, the redox active species (KFCN) was held at a concentration of 100 mM. By maintaining a dilute enough concentration of KFCN, unbound virus that blocks the electrode will not change current measurements at the electrode above that of the background. Therefore, holding KFCN at this concentration allows for the direct observation of PSBs and the effect the virus has on the beads without having to de-convolute the collisions of two different species. As shown in Figure 2.2b left panel, PSB collisions with the electrode cause observable current steps as measured by amperometry. However, when MCMV and gB antibody are added, the frequency of those collisions and height of the current steps changes dramatically. Due to the agglomeration of PSBs with MCMV and gB (Figure 2.5b-e), the frequency of collisions decreases dramatically as the larger aggregates do not diffuse as readily as before. Additionally, aggregates caused by the addition of virus and gB antibody block more of the UME, meaning individual current decreases are much greater than the average current changes measured with PSBs alone (Figure 2.2b, right graph).

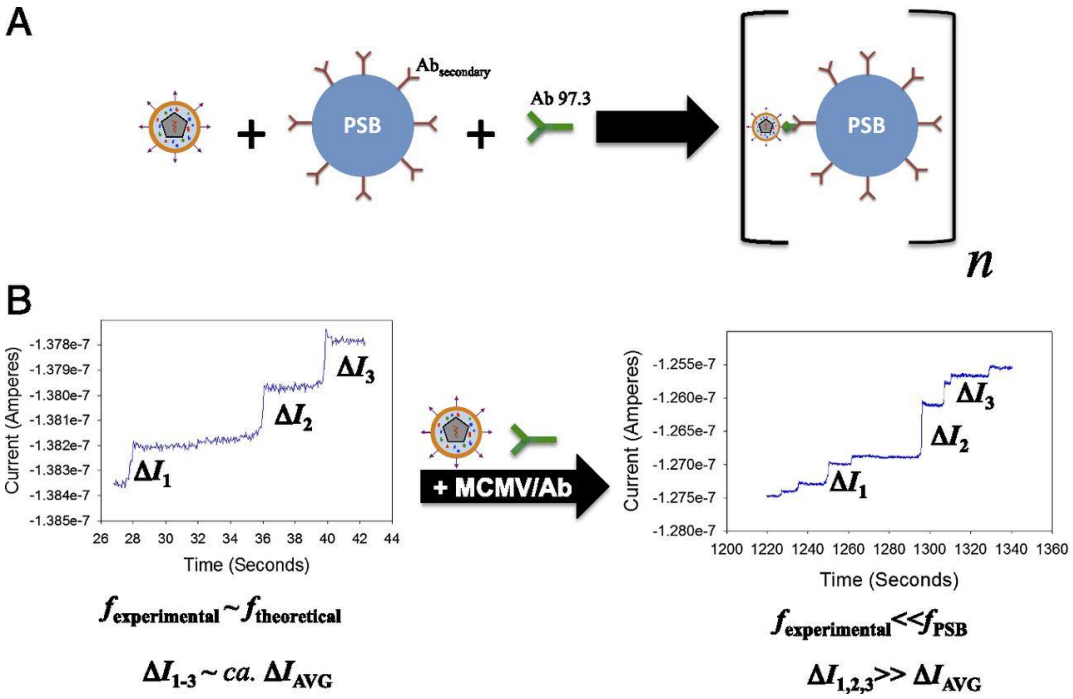

Figure 2.2: Selectivity of MCMV detection by antibody anchoring of PSBs.

A) Schematic representation of the collision experiments with PSBs radius, 750 nm, binding to the virus through the primary antibody (green Y). The secondary antibodies (maroon Ys) are specific to the Fc region of the primary antibody. B) Electrochemical current responses with and without virus. Without the virus, collisions of PSBs are observable with a characteristic frequency and current step height, ΔI. Upon addition of virus, the frequency drops, relative to the frequency of PSBs alone, and larger current steps can be observed.

To represent these observations in an averaged fashion over several blocking experiments, collision frequency percentages are plotted against binned current step ranges, measured in picoamperes (pA) (Figure 2.3a). When gB antibody and PSBs are mixed, observed current step ranges primarily fall between 101-150 pA. When PSBs and MCMV are mixed in a 1:1 ratio in the presence of gB antibody, a dramatic shift in the current step ranges is observed (201-250 pA). Additionally, an increase in the diversity of collision percentage frequencies is observed due to a greater distribution of current steps. It is hypothesized that this is due to higher order aggregates of MCMV, PSB, and antibody (Figure 2.5b-e). When murid gamma-herpesvirus 68 (MHV68) is mixed with the PSBs and gB antibody, a similar current step range as compared to PSBs and gB antibody was observed (101-150 pA), suggesting that the shift in current step ranges is dependent on MCMV.

To show that the gB antibody was specific to MCMV and not MHV68, we performed a neutralization assay and measured the resulting infectivity by plaque assay. Briefly, increasingly dilute concentrations of gB antibody were incubated with MCMV or MHV68. As expected, MCMV was sufficiently neutralized at high antibody concentrations and this effect decreased as the antibody concentration decreased. When the same neutralization assay was performed with MHV68, the infectivity of MHV68 was virtually unaffected (Figure 2.3b). These results tell us that the antibody is specific to MCMV, as it is incapable of neutralizing MHV68, likely because it is not able to efficiently bind to the MHV68 gB protein.

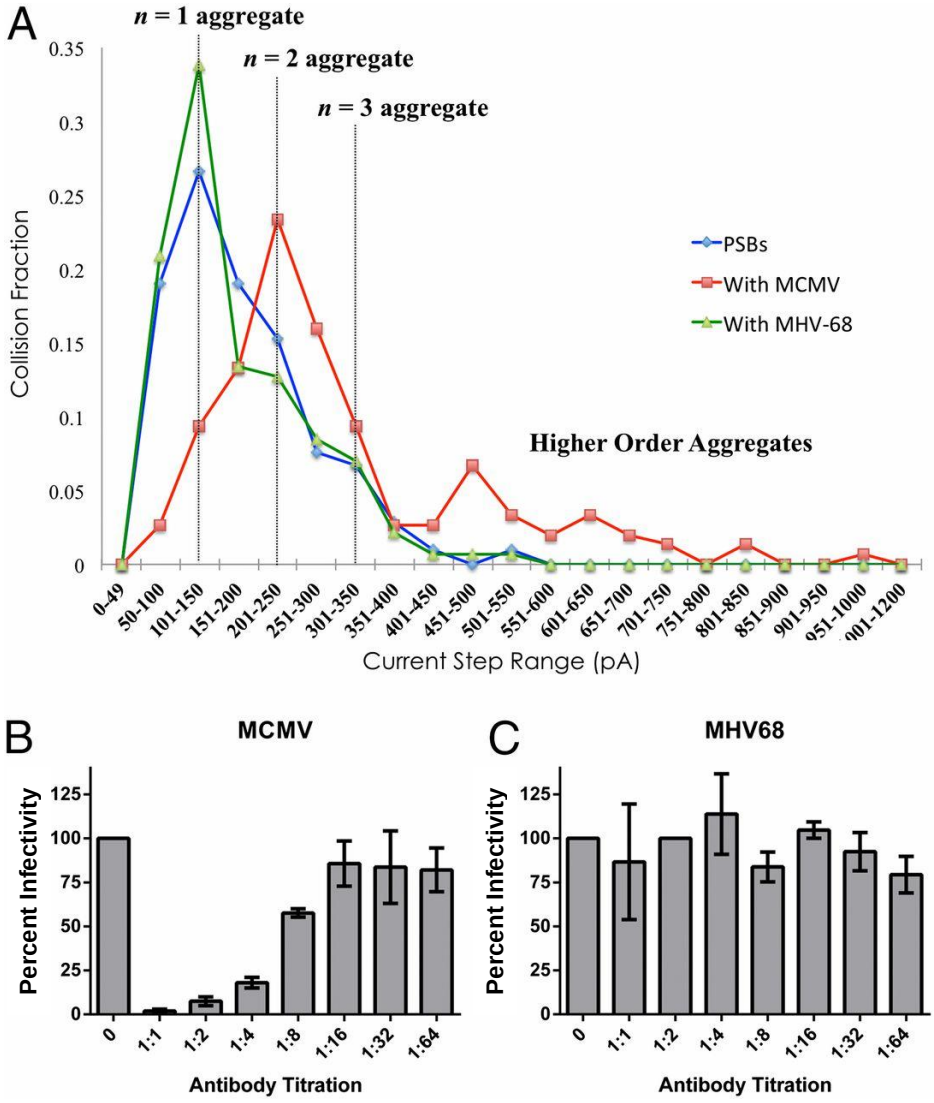

Figure 2.3: PSB aggregation is dependent on the MCMV-antibody interaction.

A) Current step distributions of the amount of collisions counted (collision fraction) as a function of current step binning. PSBs and virus are in a 1:1 mol ratio. Current step size distributions were determined for PSB and MAb 97.3 (blue trace), PSB and MAb 97.3 with MCMV (red trace), and PSB and MAb 97.3 with MHV68 (green trace). Aggregates of n = 1, 2, 3 and higher order were counted using amperometry of 100 mM KFCN dissolved in the aqueous continuous phase on a 10-µm Pt UME. The potential was held at +0.4 V vs. Ag/AgCl. (B and C) Plaque reduction neutralization tests for MCMV and MHV68 with MAb 97.3 (see text).

In addition to an increase in current step size upon the mixing of PSBs, gB antibody, and MCMV, a decrease in collision frequency at the electrode was also observed. These observations are plotted in Figure 2.4. When MCMV-gB antibody conjugate was mixed with PSBs at a 15:1 ratio (i.e. excess virus), collision frequencies decreased over 80% when compared to PSBs alone. This decrease in collision frequency is likely due to the larger aggregates formed when MCMV, antibody, and PSBs are combined (Figure 2.5b-e) as larger objects do not diffuse as readily as smaller objects. By tracking the changes in collision frequency and current step height, we demonstrated that a qualitative diagnosis for MCMV's presence can be made. While this method demonstrates that MCMV can be specifically detected using collision electrochemistry, in reality, we are actually measuring larger current decreases and a decrease in collision frequency. In other words, this iteration relies on a decrease in detection. So, in theory, any phenomenon that might cause PSB agglomeration would effectively result in the same output. As such, we continued our studies in a second publication in which MCMV particles were enzymatically labeled to generate positive current events (i.e. specific increases in current) that were readily differentiated from background non-specific blocking events.

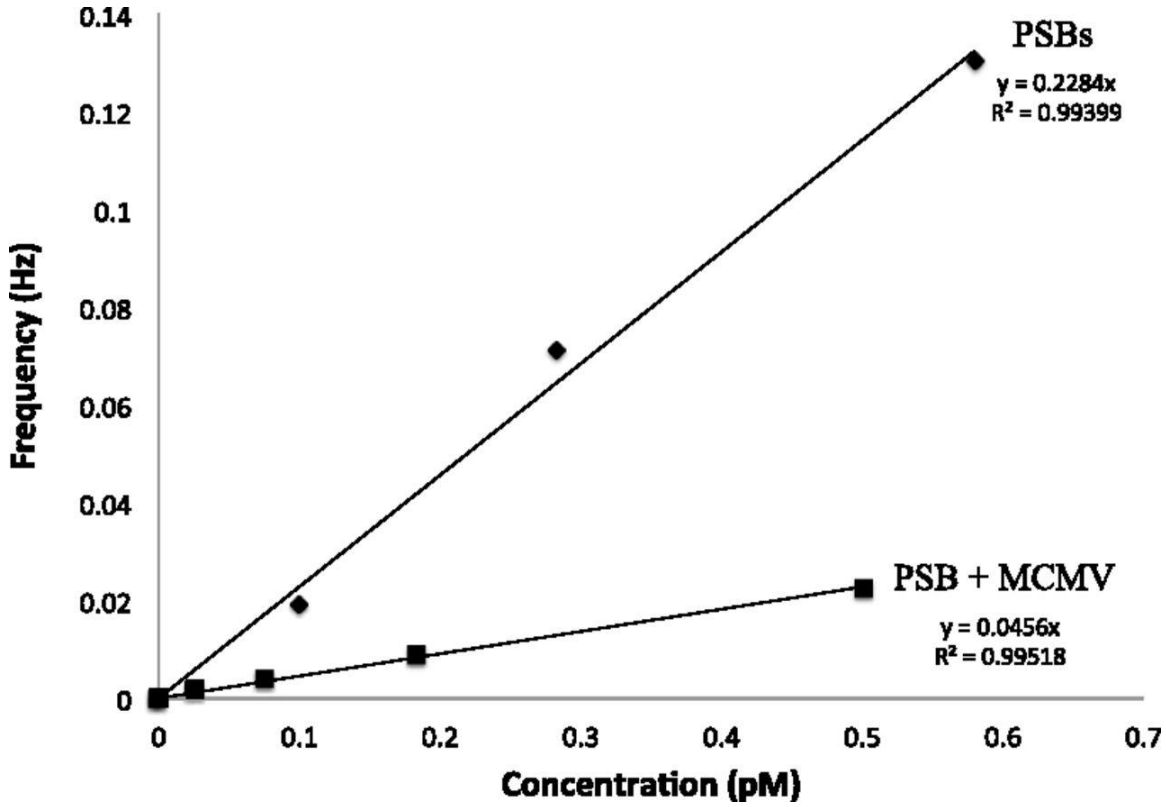

Figure 2.4: Frequency vs. concentration for PSBs and PSBs with excess MCMV-antibody.

Collisions were counted in amperometry of 100 mM KFCN dissolved in the aqueous continuous phase on a 10 um Pt UME. The potential was held at +0.5 V vs. Ag/AgCl.

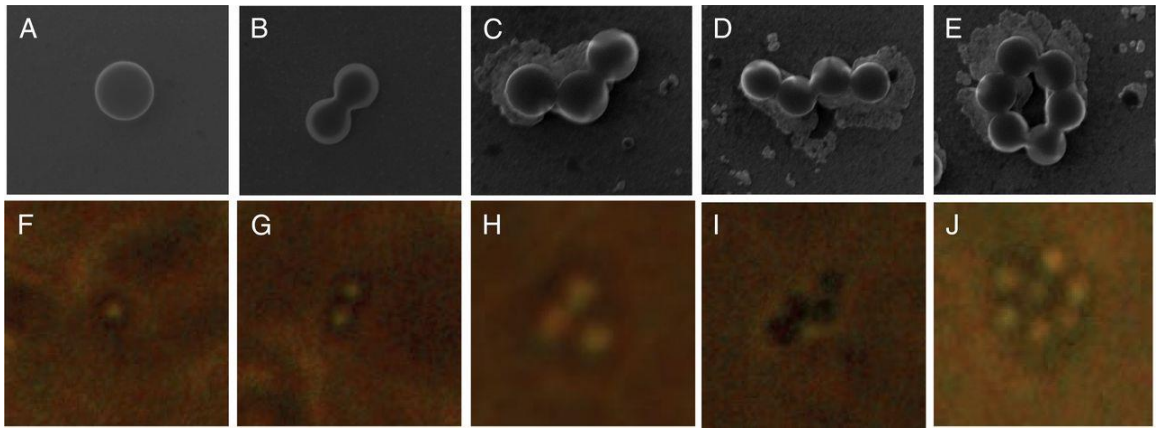

Figure 2.5: Scanning electron micrographs and optical microscope analogs of equimolar amounts of MCMV-antibody and PSBs.

A-E) Scanning electron micrographs of 0.283 pM PSBs and virus (1:1 stoichiometry), examples of n = 1, 2, 3, 4,… aggregates and their optical microscop analogs (F-J) taken with a 100X objective lens. In each case, the diameter of the bead was measured to be 750 nm.

2.2.4 Collisions of Antibody / GOx-coated MCMV

Previously, we reported the electrochemical detection of murine cytomegalovirus (MCMV) collisions on an UME [123]. In this paper, we have extended the collision of single viruses to a more specific analytical technique via enzymatic labeling. Glucose oxidase (GOx) catalyzes the oxidation of glucose to gluconolactone while reducing an oxidant molecule, such as ferrocenium methanol [29]. When oxygen is removed from solution, and the oxidation of ferrocene methanol to ferrocenium methanol is carried out at the electrode surface, the electrons from the glucose oxidation will reduce ferrocenium methanol back to ferrocene methanol, and feedback will be detected at the electrode surface, as shown in figure 2.6b [124]. This chemistry is similar to the chemistry used in usual glucometers [29]. This local feedback of ferrocene to the electrode surface causes an increase in the current response. Because the environmental noise of most potentiostats is on the order of 10–100 fA, and a single faradaic enzyme collision is capable of generating ca. 0.2 fA of current [125], single faradaic enzyme collisions cannot be discerned against the background. Hence, a single enzyme on an electrode surface cannot produce enough current to discern against the background. However, by covalently attaching GOx to a specific antibody, which in turn binds to the epitope on the virus for which the antibody is specific (Figure 2.6a), one can hypothesize that GOx will be specifically concentrated on the virus surface. Under these special circumstances, the GOx signal is significantly amplified so much so that the signals that are produced able to be detected on conventional potentiostats. In doing so, discrete current steps manifesting

as current increases can be interpreted as a GOx-coated virus colliding with an electrode (Figure 2.7d).

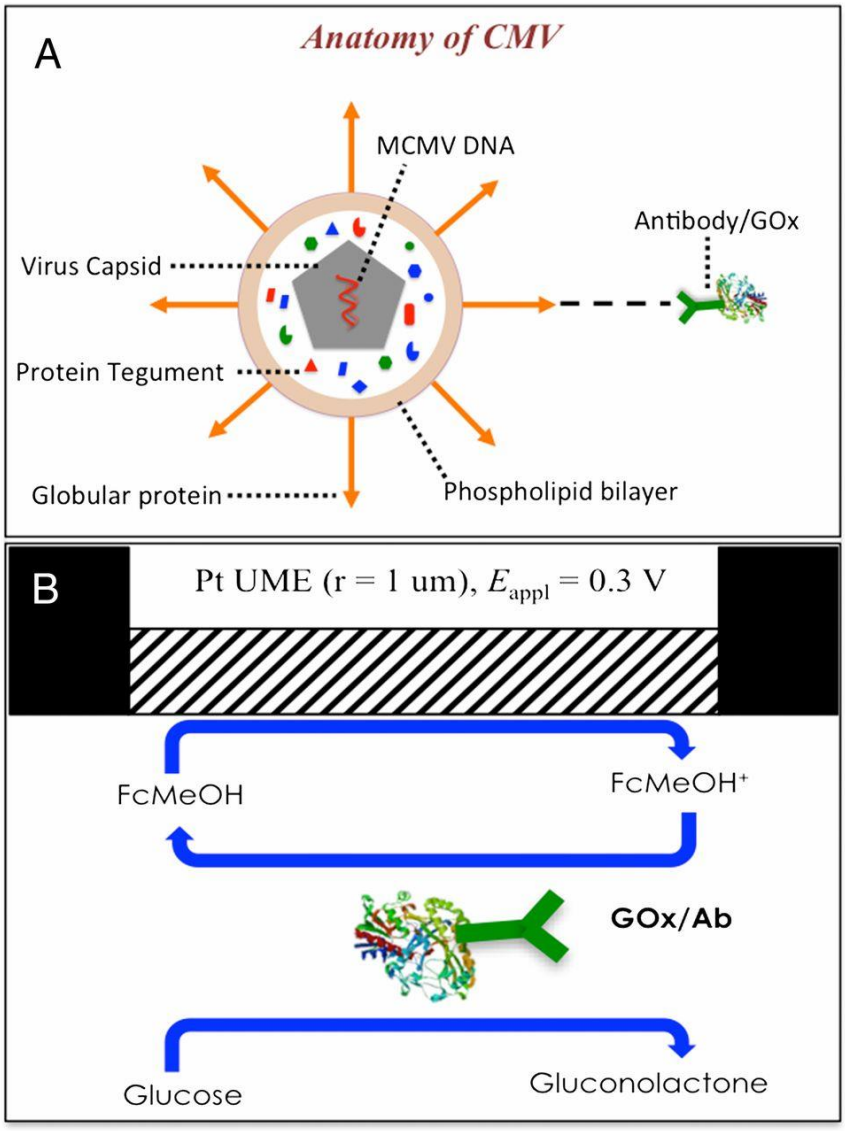

Figure 2.6: Schematic representation of the CMV virion and corresponding antibody/GOx interaction with a surface glycoprotein.

A) Schematic representation of the CMV virion and corresponding antibody/GOx interaction with a surface glycoprotein. B) Schematic representation of the antibody and GOx conjugate regenerating ferrocene methanol from ferrocenium methanol, the latter of which is continuously replenished via oxidation at an electrode surface, in the presence of glucose. The figure is not drawn to scale.

As shown in Figure. 2.7a, the virus itself will nonspecifically adsorb to the electrode surface, effectively blocking the redox reaction being carried out. We have previously demonstrated this phenomenon using MCMV [123]. Figure 2.7b gives the predicted amperometric response for this blocking experiment. In Figure 2.7c, GOx-labeled anti-gB antibody binds the surface of MCMV in solution, allowing the virus to pre-concentrate many enzymes for detection at the electrode surface, greatly amplifying the signal of just one GOx enzyme. The predicted amperometric response when the virus is surrounded by GOx is shown in Figure 2.7d. If the conjugation is incomplete or the antibody is not specific to the virus, no pre-concentration occurs, and blocking will be observed, consistent with numerous examples of blocking in the literature [36, 109, 126]. When the virus carries enough GOx enzymes to the electrode, feedback is generated, creating a discrete, positive current response.

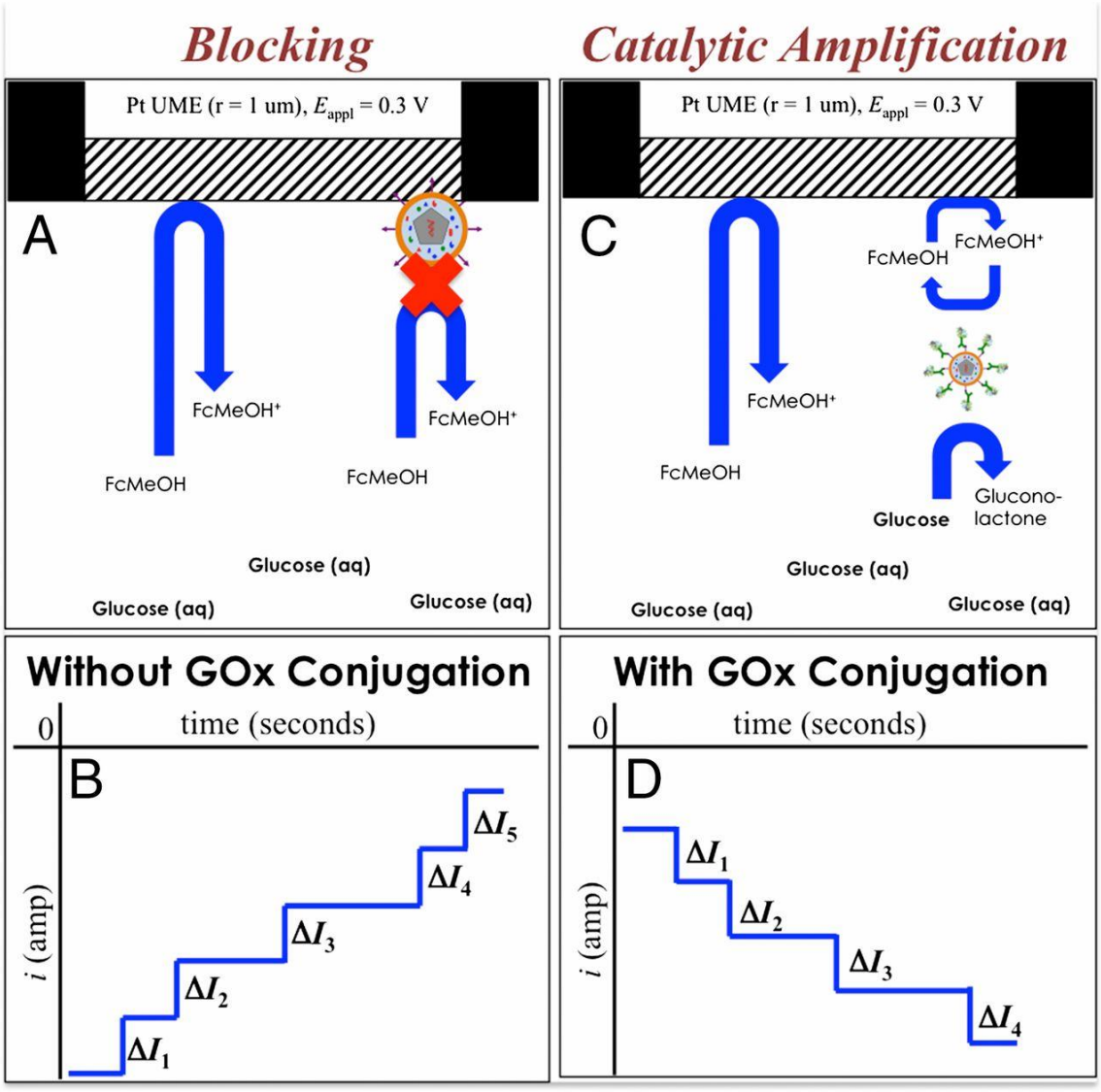

Figure 2.7: Schematic representing the predicted blocking and catalytic amplification responses.

A) Schematic representation of blocking caused by an MCMV virion. B) Schematic representation of the predicted amperometric response when MCMV alone is placed in a system containing the electrode, glucose, and ferrocene methanol. C) Schematic representing catalytic amplification upon GOx-antibody interaction with MCMV. D) Schematic representation of the predicted amperometric response when MCMV-GOx-antibody collide with an electrode and produce a catalytically amplified current response.

Figure 2.8 shows the amperometric i-t (current vs. time) response for the collisions of virus after incubation in the antibody/GOx solution in the presence of 1 mM ferrocene methanol and 50 mM glucose. As hypothesized (Figure 2.7d), step-wise current increases were observed in amperometry. The background current of about 348 pA is from the oxidation of ferrocene methanol to ferrocenium methanol. From the amperometric response, positive current steps with a slight deactivation are realized (anodic current is plotted negatively). The decay of the catalytic current is likely due to nonspecific adsorption of organic molecules, such as proteins and/or lipids, onto the electrode surface, blocking ferrocene oxidation sites. In the absence of virus, there is not enough buildup of GOx to cause a discrete event (Figure 2.9b). The current steadily increased over time due to nonspecific adsorption of the GOx/Ab conjugate on the electrode surface. No discrete steps were seen because one GOx enzyme is not able to generate enough current to manifest as a discrete event. Importantly, MCMV collisions with antibody-GOx conjugate without glucose resulted in blocking events only (Figure 2.9a) and MCMV with glucose and excess GOx resulted in blocking again as there was no antibody to facilitate the concentration of GOx around virions (Figure 2.9c). These results indicate that all components of the detection system need to be present to visualize discrete collision events.

From previous work by Savéant and coworkers, the current for a single GOx enzyme with ferrocenium methanol as the co-substrate to the enzyme is ~0.2 fA [36, 125]. The average current step height observed in the reported experiments was 0.8 ± 0.4 pA, implying that the amount of GOx enzyme on the virus surface is ~4,000, taking the

current produced by one enzyme as 0.2 fA. By estimating the size of the conjugate as a 5- to 10-nm^2, and taking the virus radius to be ~100 nm, the geometric capacity on the virus surface is between 1,300 and 5,000, which agrees with the electrochemical collision signal for a single virion. This estimate based on simple geometry does not consider the number of epitopes on the virus membrane or steric effects. We cannot completely rule out the possibility of the virus aggregating during incubation with the conjugate. From our previous study, virus aggregates were observed after adding PSBs functionalized with an antibody specific to the F_C of the gB antibody, and we demonstrated that aggregates diffuse more slowly compared with free virus, colliding with the electrode at a lower frequency [123]. In the studies presented here, current steps on the order of 4–6 pA, which could be interpreted as aggregates of virus, were infrequently observed in amperometry, occurring only three times in an analysis of over 80 anodic steps. It should be noted that these events were not counted during the statistical analysis of the anodic steps. Thus, although difficult to directly confirm, the results of our geometric analysis, coupled with the analysis of frequency of virus collisions, are consistent with detection of single MCMV virions in solution.

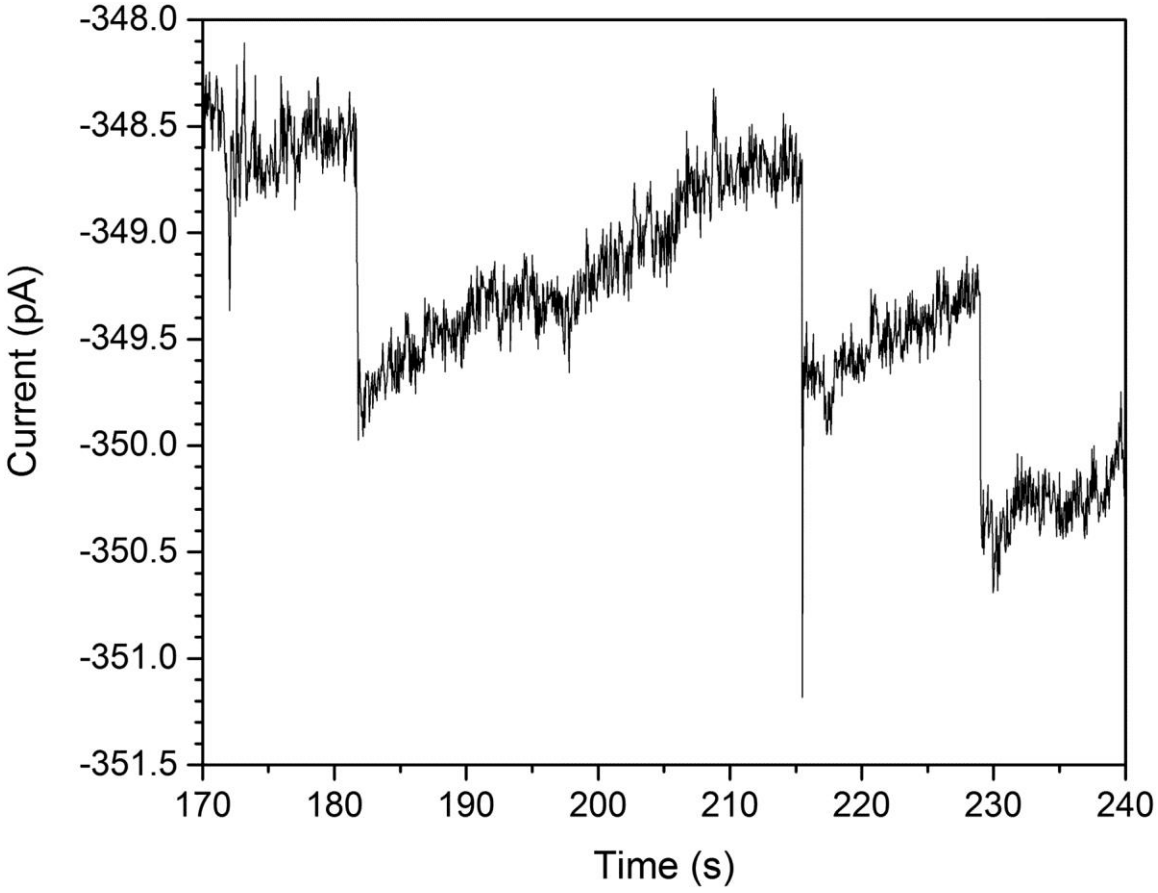

Figure 2.8: Amperometric i-t response of the virus in the presence of the antibody/GOx conjugate.

The purified virus (MCMV) was incubated with the GOx/antibody conjugate for 30 min before experimentation. Measurements were taken in 10 mM PBS, 1 mM ferrocene methanol, and 50 mM glucose on a 1-μm-radius Pt UME. The sampling rate for data acquisition was 50 ms.

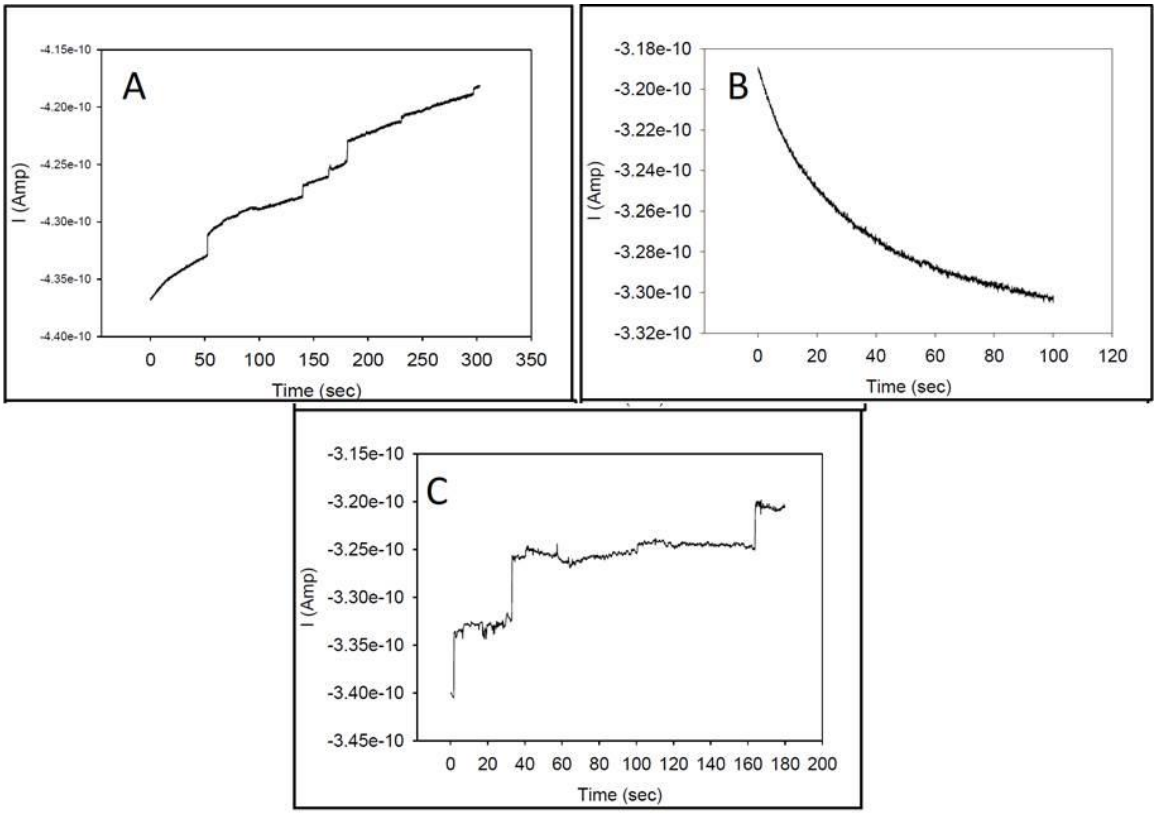

Figure 2.9: Amperometric response to control experiments demonstrating the specificity of the presented electrochemical technique.

A) Control amperometric i-t curve of MCMV collisions with the antibody/GOx conjugate in the absence of glucose demonstrating blocking. B) Control amperometric i-t curve of the antibody/GOx conjugate and glucose. C) Control amperometric i-t curve of MCMV in the presence of excess GOx with no antibody conjugation.

2.2.5 Discrimination of MCMV from Murid Gammaherpesvirus 68 (MHV68)

To demonstrate specific discrimination of MCMV from other particles of similar size or morphology, experiments were carried out in the presence of MHV68, a murine gamma-herpesvirus related to Epstein–Barr and Kaposi's sarcoma-associated herpesvirus. In the presence of anti-MCMV gB antibody/GOx conjugate, MHV68 shows only blocking at the electrode (Figure 2.10a). This indicates that MHV68 does not pre-concentrate GOx on its surface, because the epitope for Mab 97.3 is specific to MCMV gB and is in agreement with our previous work [123]. When MHV68 and MCMV are assessed in a mixture of viruses (2:1 MCMV:MHV68) in the presence of GOx–antibody conjugate, both blocking and positive current events are observed (Figure 2.10b). Because positive current events only occur when MCMV pre-concentrates enough GOx by its highly specific antibody interaction, the presence of additional blocking events, presumably by MHV68 virions, demonstrates that MCMV can be detected in the presence of other viruses or solution species that nonspecifically adsorb to the electrode surface. The specificity of the antibody allows for specific positive detection of MCMV by the electrochemical response.

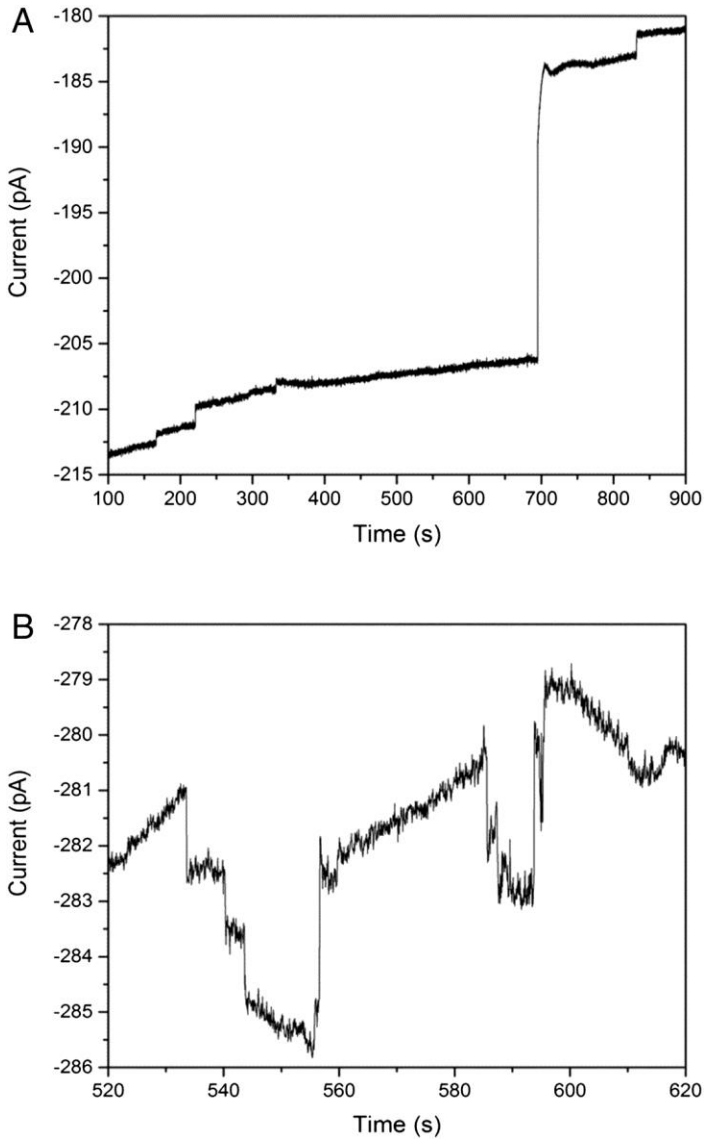

Figure 2.10: MHV68 can be differentiated amperometrically from MCMV.

A) Amperometric i-t curve of MHV68 in the presence of the antibody/GOx conjugate with glucose in solution and 50 mM PBS. MHV68 blocks the flux of ferrocene methanol to the surface of the electrode. (B) Amperometric i-t curve of a mixture of MHV68 and MCMV (2:1 MCMV to MHV68) with the antibody/GOx conjugate in a solution of 10 mM PBS, 50 mM glucose, and 1 mM ferrocene methanol showing positive and blocking current responses over the steady-state current level due to the collision of MCMV and MHV68, respectively. The steady-state current is the current due to the oxidation of ferrocene methanol on a 1-μm-radius Pt UME.

2.2.6 Detection of MCMV in the urine of infected mice

To demonstrate the feasibility of this digital electrochemical collision technique to detection of virus in a biological sample, we applied our technique of MCMV detection in urine from an infected mouse at various times post-infection. Like its HCMV counterpart, MCMV is readily secreted in the urine of infected mice [127]. Figure 2.11a gives a schematic representation of the electrochemical immunoassay, and figure 2.11b emphasizes the detection of virus in the urine sample. Mice were infected with 10^6 pfu MCMV by intraperitoneal (i.p.) injection, and urine was collected at the indicated times post infection. Urine samples were incubated with antibody/GOx and subjected to amperometry. Figure 2.11c shows representative results obtained 10 days after the initial infection, and discrete positive current steps can be seen with a deactivation. The enlarged response shows the step-like nature of the discrete events observed in electrochemistry. Experiments with urine from an uninfected mouse (0.5 ml PBS) showed no anodic step-like characteristics, indicating that a virus capable of concentrating GOx enzymes can only cause the positive anodic step (Figure 2.12a). During experiments in urine in the absence of virus, a slow decay in the steady-state current was observed. This decay is likely due to non-specific adsorption of proteins and other organic species in urine that are not electrochemically active, as evidence by the deactivation. Upon collision, a virus covered in GOx will begin reducing ferrocenium to ferrocene, providing the feedback loop that gives the positive step in current. Due to nonspecific adsorption that is evident in the urine background current decay, likely from urea and other organic molecules found in urine, the feedback loop becomes less

efficient, as emphasized in the enlarged portion of the amperometric i-t curve in Figure 2.11c. However, positive current events can be detected in infected mice (Figure 2.12b) which demonstrates that this technique can be used to detect viruses in biological samples.

Interestingly, the collision frequency in urine may yield insight into the shedding dynamics of the virus as a function of days post infection. In Figure 2.13, the frequency of collision is plotted as a function of days post infection. These frequency values are averaged from 5 infected mice tracked over the course of two weeks. Although MCMV is known to be shed in the urine of infected animals, the kinetics and amplitude of this passing during infection are not well characterized. The collision frequencies observed at 3, 5, 7, 10, and 14 days post infection mimic the viral load dynamics seen in other virally infected tissues, like the spleen and liver (see Chapter 3, Figures 3.3a and b). That is, there is a peak viral load reached and then subsequent clearance. As such, the electrochemical detection methodology proposed here may yield insight into the secretion of virus into the urinary system. Interestingly, the collision frequency observed on day 5 implies that the limit of detection is about 30 fM (femtomolar) of viral particles relying on diffusion alone.

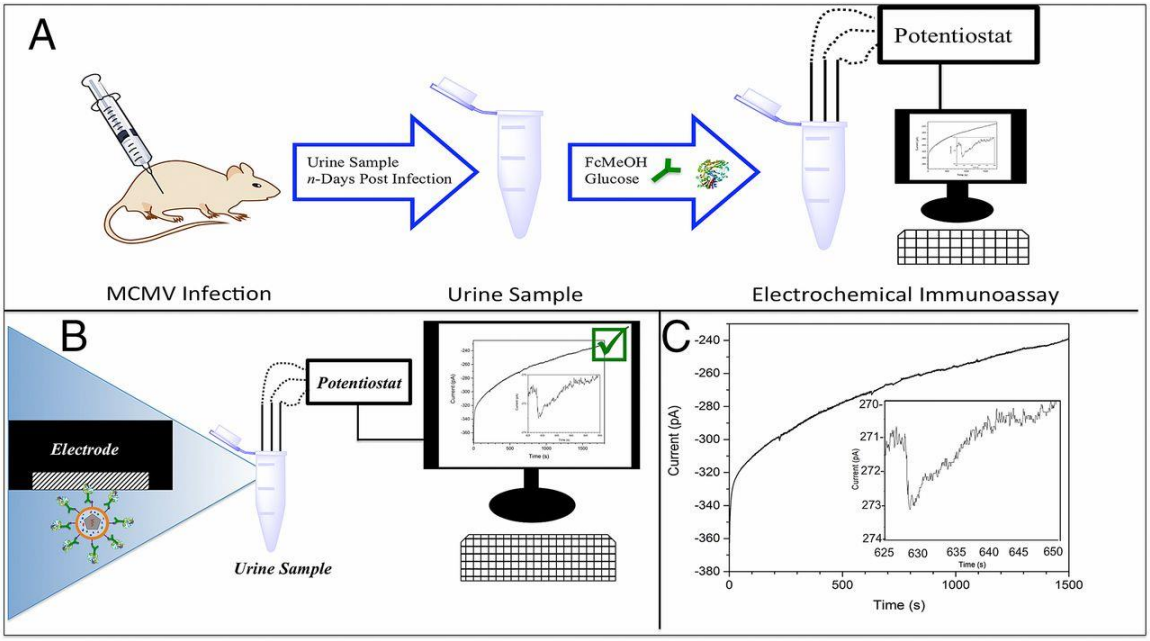

Figure 2.11: Workflow for MCMV detection in the urine of mice infected with MCMV.

A) Schematic representation of the electrochemical immunoassay. B) Enlargement of the assay emphasizing the detection of virus. C) Representative amperometry of 50 µL urine diluted with 400 µL of 1 mM ferrocene methanol and 100 mM glucose with a representative enlargement of a positive response for a sample collected 10 d after the initial infection.

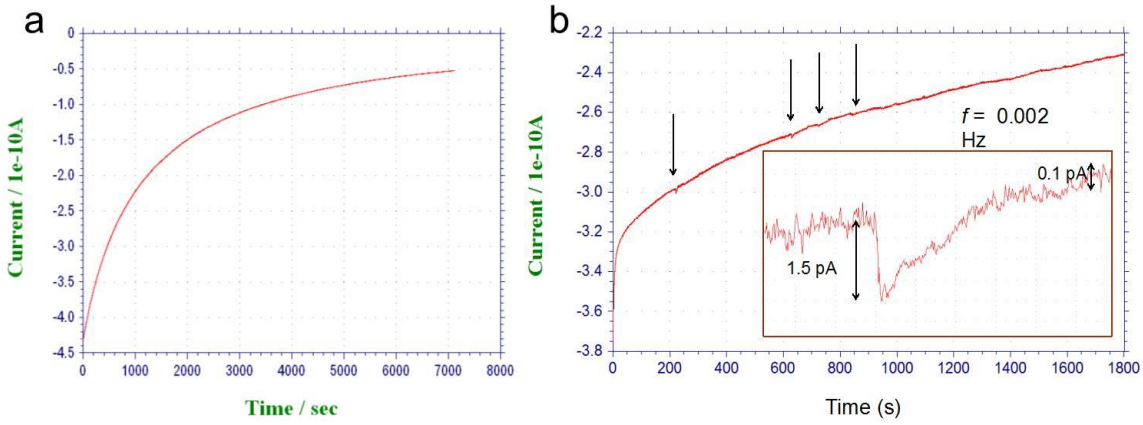

Figure 2.12: Representative amperometric i-t responses of mouse urine mixed with ferrocene methanol, glucose, and the GOx/antibody conjugate from uninfected on infected mice.

A) Amperometric i-t curve of representative uninfected mouse urine. The gradual decrease in the current response at the electrode is likely due to fouling of the electrode due to various organic molecules (e.g. urea, etc.) present in urine. B) Amperometric i-t curve of representative infected mouse urine. Discrete collision events are observed in the infected mouse urine that are not present in the uninfected mouse urine.

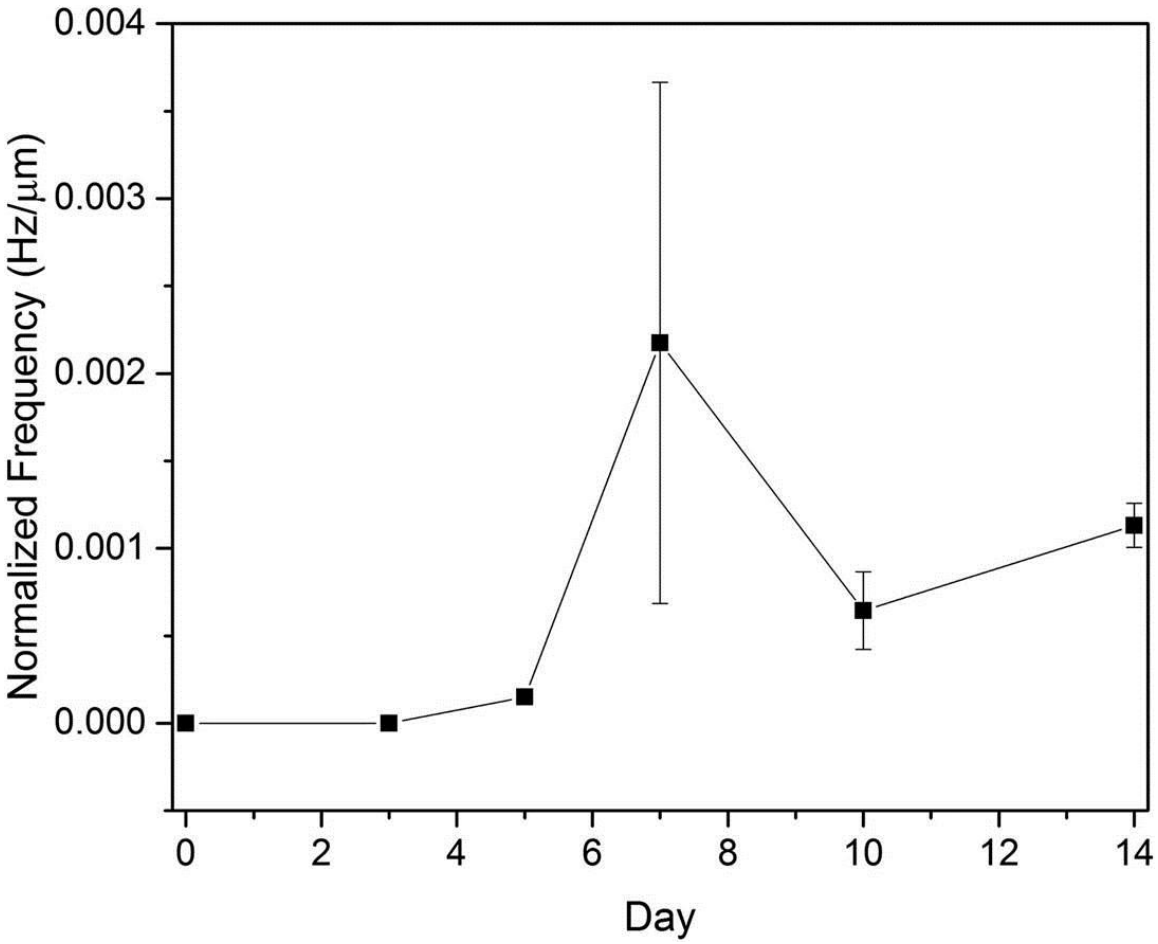

Figure 2.13: Frequency of collision versus day post infection of infected mouse urine.

Five C57Bl6/J mice were infected with 10^6 PFU of WT MCMV and urine was collected from individual mice over the course of 2 weeks. Collision frequencies from each of the urine samples from a given day post infection were averaged and plotted as a function of days post infection. Error bars represent standard deviation.

2.3 DISCUSSION

Facile, rapid diagnostic methods are essential for proper and expedient treatment for any number of infectious diseases. Electrochemical methods provide researchers with several avenues along which diagnostic instruments can and have been developed. For example, glucose meters, critical for diabetes patients to monitor blood glucose levels, utilize chemistry very similar to that described above [29]. Additionally, electrochemical methods have been developed and used for the monitoring of levels of various organic molecules, pesticides, antibiotics, and a number of bacterial pathogens in and on the food we eat [32]. While these methods are quite sensitive, we report the first instance of utilizing collision electrochemistry for the specific detection of a single viral particle from infected animals.

While collision electrochemistry has proven itself to be a powerful tool for the study of single molecules or particles [37], the method itself is not able to readily differentiate between the collisions of different species in a complex mixture. For this reason, specificity measures need to be taken in order to utilize this sensitive technology for the detection of particles of interest. In the case of pathogen detection by electrochemistry, biology offers a unique set of tools so that specificity may be reached.

Upon infection, pathogens, like cytomegalovirus, will ultimately elicit the adaptive immune response. One important arm of this response is the generation of high affinity antibodies that recognize the pathogen and increase the likelihood of clearance from the infected host by a variety of different mechanisms [128]. One such antibody usually generated recognizes an epitope in the viral glycoprotein known as gB. The same

is true for the mouse cytomegalovirus, MCMV. In addition to serving important roles in neutralizing infection, researchers can use these antibodies in the laboratory to learn more about the virus. In the stories described above, an MCMV gB antibody capable of neutralizing MCMV was utilized for the specific detection of MCMV in the presence of another virus as well as in the urine of infected mice. This detection was made possible by the covalent attachment of GOx to the antibody.

While the first method relies on a decrease in collision frequency and an increase in current step size, the second method provides an even more sensitive positive detection result by utilizing the chemistry of glucose oxidase. Generation of a constant flux of ferrocene methanol by glucose oxidase to be oxidized at the electrode causes discrete current steps where current momentarily increases before settling to a new steady state. While a signal to noise ratio of about 15:1 was generated using this methodology, greater current step sizes would be ideal in order to definitively conclude a collision event resulting in a current increase occurred. In other words, greater signal amplification is needed gain even more sensitivity and to reduce the possible rate of false positives. Additionally, sensitivity can be gained by optimizing the limit of quantitation. This can be done by introducing some sort of microfluidics, in which virus / antibody-GOx conjugates are reliably directed to an electrode or electrode array. This may increase detection and would potentially allow for the quantification of a given virus' concentration in solution (i.e. # collisions / unit volume passed / second). These possibilities are discussed in greater detail in Chapter 4.

While electrochemical analyses have been applied to the detection of a number of different pathogens (food pathogens, etc), we report the first specific digital pathogen detection scheme using collision electrochemistry. As detection methodologies improve and better point-of-care diagnostics are developed for pathogens, an equal effort needs to be taken for development of better treatment options. In the case of HCMV infection, current antiviral therapies can be very toxic. Additionally, clinical isolates of HCMV have demonstrated resistance to antiviral drugs. As such, novel, unique viral targets for drug treatment need to be identified and characterized to determine their promise as druggable targets. In the next chapter, we describe work that characterized a uniquely structure and highly conserved MCMV deubiquitinating enzyme and propose that it may be a viable target for future anti-CMV therapeutics.

Chapter 3: Murine cytomegalovirus deubiquitinase regulates viral chemokine levels to control inflammation and pathogenesis[2]

3.1 INTRODUCTION

The prototypic beta-herpesvirus, human cytomegalovirus (HCMV), remains a major causative agent of nongenetic birth defects, such as sensory loss, defects in neural development, and microcephaly [129]. Although immunocompetent patients typically present no obvious symptoms of infection, HCMV still represents a major cause of morbidity and mortality in immunocompromised or immunonaive individuals, including transplant recipients and infants infected prenatally [129]. In order to navigate the multitude of antiviral responses in an immunocompetent host, cytomegaloviruses devote a significant portion of their genome to counteracting or appropriating host responses to facilitate successful infection [130, 131]. HCMV encodes a number of proteins involved in various processes, such as type I interferon (IFN) [13, 132-134], cell death pathways [135], and major histocompatibility complex class I antigen presentation [136], that act to antagonize or appropriate antiviral responses. In addition to intracellular immune modulation, cytomegaloviruses encode cytokines and chemokines to modulate immune responses at a distance [137].

Due to the high degree of species specificity, tractable model systems are required for host/pathogen studies of the cytomegaloviruses. The use of the murine cytomegalovirus (MCMV) model system has provided significant insight into CMV

[2] Large portions of this chapter have been previously published.

1. **Hilterbrand AT, Boutz DR, Marcotte EM, Upton JW**. 2017. Murine Cytomegalovirus Deubiquitinase Regulates Viral Chemokine Levels to Control Inflammation and Pathogenesis. mBio **8**(1): e01864-16.

biology over the years [138]. HCMV and MCMV share significant genetic and biological characteristics; among them is the large tegument protein (LTP). This essential protein [70, 139, 140] encodes a structurally distinct deubiquitinase within its amino terminus [89]. Though not essential for replication [75, 85, 97, 141], the DUB activities possessed by LTPs in other herpesviruses have been ascribed a number of distinct functions.

Emerging evidence suggests that herpesvirus DUBs play roles in manipulating host antiviral responses to infection. Murine gammaherpesvirus 68 (MHV 68) and Kaposi's sarcoma-associated herpesvirus (KSHV) DUBs can deubiquitinate RIG-I, thus removing its ability to signal to downstream components and propagate type I IFN signaling [83]. The herpes simplex virus 1 (HSV-1) DUB, UL36, can target tumor necrosis factor (TNF) receptor-associated factor 3 (TRAF3), thereby blocking type I IFN production [72]. The Epstein-Barr virus (EBV) DUB, BPLF1, blocks NF-κB signaling via the deubiquitination of several proteins involved in Toll-like receptor (TLR) signaling, namely, TRAF6, NEMO, and IκBα [95]. Recent work also demonstrated a conserved function for herpesvirus DUBs in antagonizing stimulator of interferon gene (STING)-dependent interferon responses in bone marrow-derived dendritic cells (BMDCs) [87], further implicating herpesvirus DUBs in the modulation of antiviral signal transduction.

Additionally, several herpesvirus DUBs have been ascribed roles in pathogenesis. The DUB of pseudorabies virus (PRV) targets itself for deubiquitination, allowing transmission to nerve termini and subsequent axonal retrograde transport to facilitate neuroinvasion [77]. Inactivation of the Marek's disease virus (MDV) DUB led to a

decrease in lymphoma incidences in chickens [80]. Moreover, an MHV 68 DUB mutant showed rapid clearance from infected spleens [86] and a decrease in the establishment of STING-dependent latency [87]. Those studies indicated that herpesvirus DUBs contribute to replication and pathogenesis in their hosts. Recent work has also shown that the HCMV DUB is active during infection, contributes modestly to replication, and maintains virion stability and infectivity [97, 98]. However, *in vivo* analyses examining the contribution of CMV DUB activity to replication in a live host have not been conducted. In this report, we show that the MCMV DUB, M48, significantly contributes to the replication and dissemination of MCMV *in vivo* by regulating levels of MCK2, the virally encoded proinflammatory chemokine. In regulating MCK2 levels, aspects of MCK2 biology, namely, MCK2-dependent inflammatory responses and incorporation of MCK2 into virions, are also controlled. Interestingly, concomitant loss of MCK2 in the presence of a mutant DUB restored replication in most cell types in culture as well as in the spleen and liver of infected mice. These results highlight MCMV DUB contributions to acute infection *in vitro* and *in vivo* and provide important mechanistic insight into the role that it plays during infection in a natural host. It appears that MCK2-dependent responses are managed through DUB-dependent regulation of MCK2 levels.

3.2 RESULTS

3.2.1 MCMV DUB activity contributes modestly to replication in cell culture

In a previous study, we generated an MCMV DUB mutant (MCMV-M48^{C23S}) [87]. Briefly, MCMV-M48^{C23S} was generated by 2-step allelic exchange mutagenesis of

the pARK25 bacterial artificial chromosome (BAC) containing the K181 Perth strain of MCMV by first inserting a selection/counterselection cassette (SacB/Kan^{r}[kanamycin resistance]) into the open reading frame of M48. The catalytic cysteine of the M48 DUB was then replaced with a serine residue (Figures 3.1a and 3.2a). This mutation was repaired to restore the wild-type (WT) sequence by allelic exchange to control for spurious distal mutations, generating the MCMV-M48^{Rep} virus, which behaved similarly to WT virus *in vivo* (Figures 3.2e and f). Importantly, the C23S mutation was sufficient to inactivate M48 DUB activity (Figure 3.2d). To begin the characterization of MCMV-M48^{C23S}, we first sought to determine the contribution of MCMV M48 DUB activity to viral replication in culture. Single-step growth analyses of infected cells in culture revealed that MCMV-M48^{C23S} is modestly attenuated for growth in fibroblasts (Figure 3.1b) and endothelial cells (Figure 3.1c) compared to WT or the M48^{Rep} viruses. In contrast, mutant and control viruses replicated similarly in a macrophage cell line (Figure 3.1d), suggesting a potential cell type-specific role for DUB activity during lytic replication. Multistep growth of the mutant virus displayed similar levels of attenuation in all 3 cell types (Figure 3.1e-g). Together, these results reveal that M48 DUB activity plays a minor role in viral replication that is similar to the role ascribed to the DUB activity of the HCMV homologue, UL48 [97].

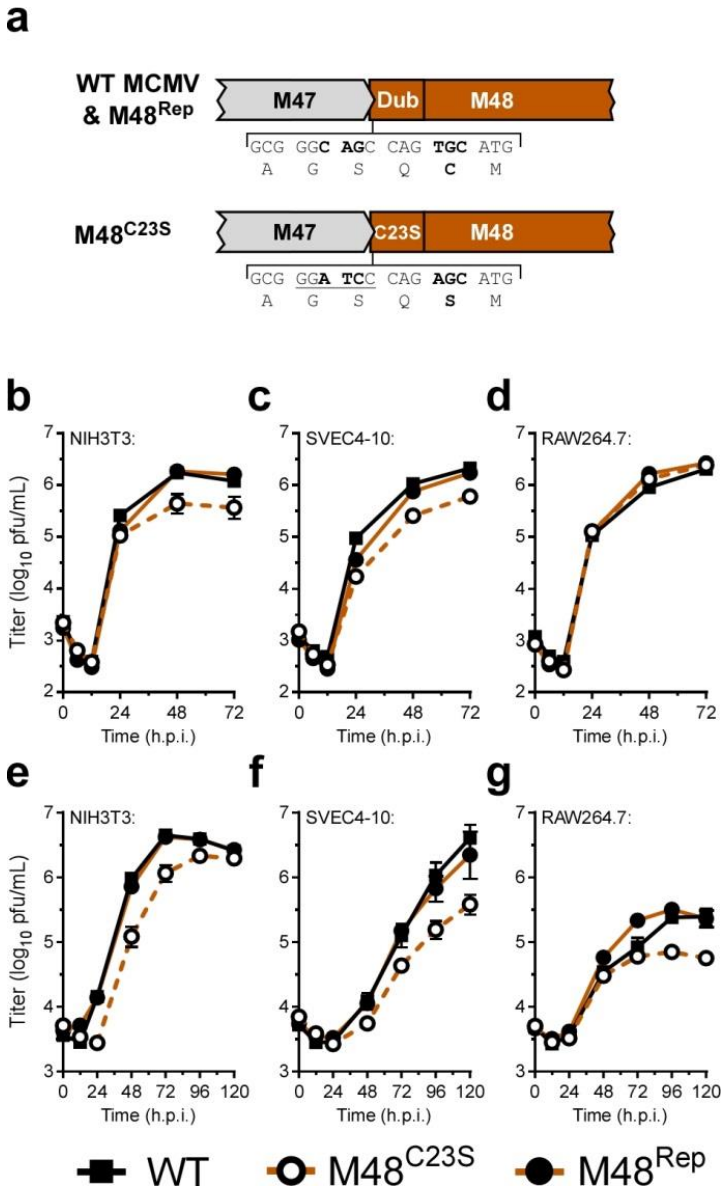

Figure 3.1: M48 DUB activity contributes modestly to replication in cell culture.

A) Schematic of the genomic location of and mutagenesis performed in the MCMV DUB, M48. B-G) Single-step (B to D) (MOI = 5.0) and multistep (E to G) (MOI = 0.05) growth curves in NIH3T3 fibroblasts (B and E), SVEC4-10 endothelial cells (C and F), or RAW264.7 macrophages (D and G). Each data point represents $n \geq 6$ replicates. The 0 h time point represents the time immediately post wash and addition of fresh complete media (h.p.i. = hours post infection).

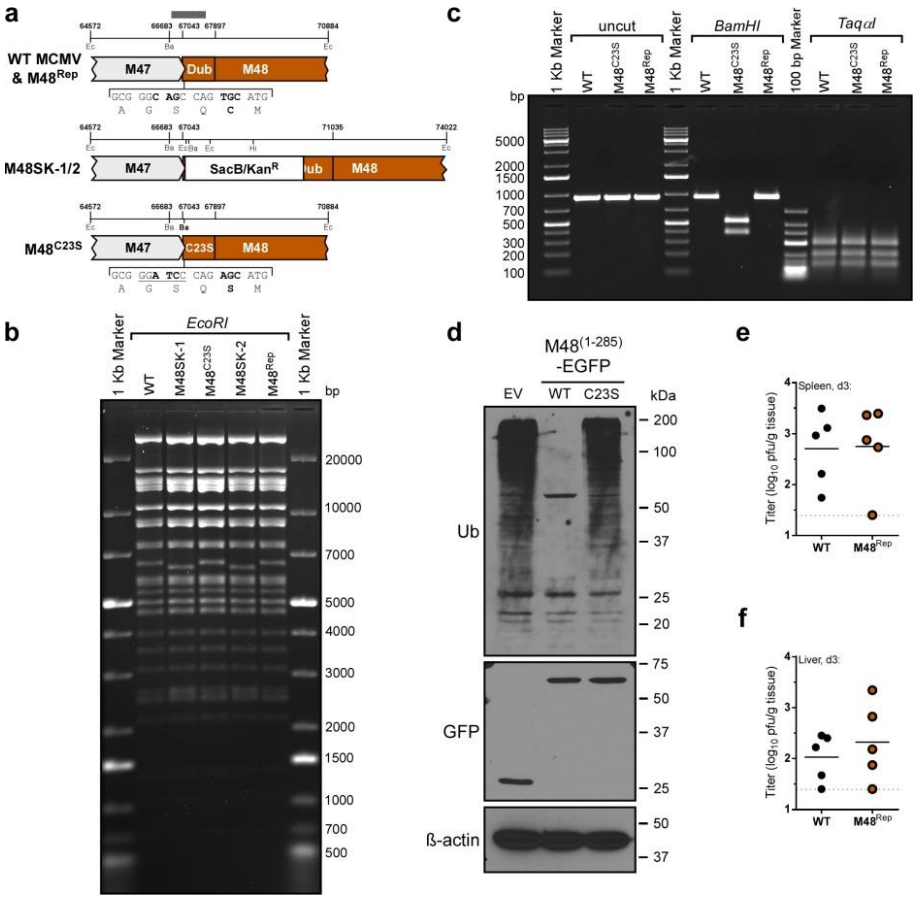

Figure 3.2: Generation of MCMV-M48^{C23S} and MCMV-M48^{Rep} recombinant viruses.

A) Schematic diagram depicting the genomic area around M48 as well as the mutagenesis strategy. Numbers represent MCMV genomic coordinates (GenBank accession number AM886412.1), and abbreviations indicate restriction enzymes sites (Hi, HindIII; Ec, EcoRI; Ba, BamHI). See materials and methods for a more detailed description of M48^{C23S} and M48^{Rep} generation. B) Restriction fragment length polymorphism analysis of WT, M48SK-1, M48^{C23S}, M48SK-2, and M48^{Rep} bacterial artificial chromosomes with EcoRI restriction enzyme. C) BamHI digest of PCR-amplified region surrounding the C23S mutation in which synonymous mutations were introduced generating a unique BamHI restriction site. Taqα1digestion was performed to show that surrounding sequence was not affected. Amplicons were also sequenced by Sanger sequencing. D) NIH3T3 cells were transfected with pEGFP-N1, pEGFP-N1-M48(1-285)^{WT} or pEGFP-N1-M48(1-285)^{C23S}. 24 hours post transfection, cell lysates were collected and immunoblot analysis was performed for the presence of ubiquitin conjugates. E and F) Splenic (E) and liver (F) titers for WT and M48^{Rep} virus were assessed to demonstrate that the repair virus replicated like its WT counterpart.

3.2.2 MCMV DUB activity is critical for replication in mice, and a mutant DUB virus elicits a greater inflammatory response

We next sought to determine the contributions of M48 DUB activity to replication in a natural host. C57BL/6J mice were inoculated with either MCMV-M48^{C23S} or MCMV-M48^{Rep} virus by intraperitoneal (i.p.) injection. Acute replication in spleen, liver, and salivary glands was assessed at the indicated times postinfection. Compared to the repaired virus, MCMV-M48^{C23S} was severely attenuated for acute replication in all organs assessed. Although replication of both mutant and repaired virus in the spleens of infected mice peaked at 5 days postinfection, MCMV-M48^{C23S} replication achieved peak levels 24-fold lower than those seen with MCMV-M48^{Rep} (Figure 3.3a). Viral titers in infected livers (Figure 3.3b) revealed that MCMV-M48^{C23S} replicated at or slightly above the limit of detection and displayed no obvious peak of replication, whereas MCMV-M48^{Rep} replicated to the expected levels in this organ [142]. MCMV-M48^{C23S} was detected in the salivary glands of animals by 14 days postinfection; however, the levels were approximately 240-fold lower than those seen with MCMV-M48^{Rep} (Figure 3.3c). Together, these results show that the DUB function of M48 is critical for MCMV replication in a natural host.

We continued our *in vivo* characterization of MCMV-M48^{C23S} by examining the resulting host response to the virus following footpad inoculation with MCMV-M48^{C23S} or MCMV-M48^{Rep}. Footpad inoculation allows the assessment of virus-induced inflammation at the site of inoculation, characterized by swelling of the infected footpad. Surprisingly, MCMV-M48^{C23S} caused a rapid onset of swelling by 3 days postinfection

not seen in the MCMV-M48^{Rep} virus-infected mice (Figure 3.3d). Thus, despite being attenuated for acute replication *in vivo*, the DUB-mutant virus elicited a more robust inflammatory response.

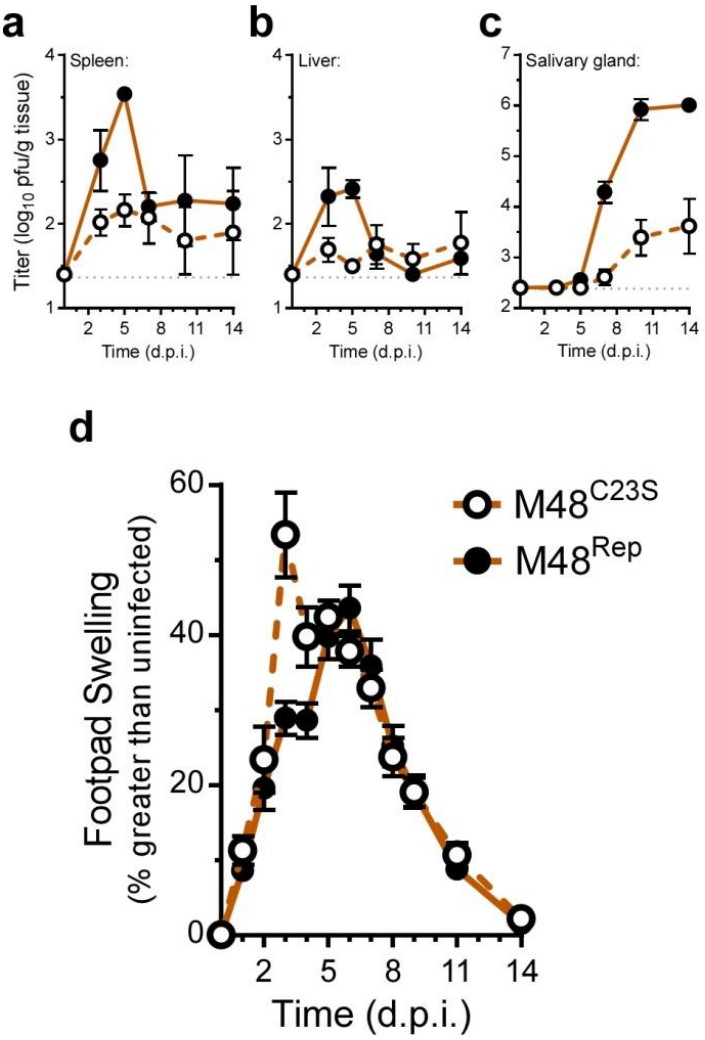

Figure 3.3: MCMV DUB activity is critical for replication in mice, and a mutant DUB virus elicits a greater inflammatory response.

A to C) Organ titers from C57BL6/J mice infected intraperitoneally (i.p.) with 10^6 PFU of either MCMV-M48^{C23S} or MCMV-M48^{Rep}. Spleen (A), liver (B), and salivary gland (C) were collected and assessed at the indicated days post infection (d.p.i.). Each data point represents an $n \geq 5$ mice. D) Footpad swelling of C57BL6/J mice infected with 10^6 PFU of either MCMV-M48^{C23S} or MCMV-M48^{Rep} via footpad injection. Swelling was measured by digital caliper over the course of 14 days, and data are plotted as percent increase over the measurements from uninfected mice. Each data point represents an $n \geq 5$ mice.

3.2.3 M48 DUB activity regulates MCK2 levels and can regulate secretion

As MCMV-induced swelling is influenced by the production of the MCMV-encoded C-C chemokine, MCK2 [143-145], we next investigated what role the DUB activity of M48 may play in regulating this chemokine. As swelling occurred rapidly in the footpads of MCMV-M48^{C23S}-infected mice, we hypothesized that MCK2 levels may be increased in MCMV-M48^{C23S}-infected cells. In order to test this, NIH3T3 fibroblasts were infected (multiplicity of infection [MOI] = 5.0) and lysates collected at 0, 12, 24, and 48 hours post infection (hpi). An immunoblot assessment of MCK2 protein levels in WT-, MCMV-M48^{C23S}-, or MCMV-M48^{Rep}-infected fibroblasts revealed elevated MCK2 levels in MCMV-M48^{C23S}-infected fibroblasts compared to the WT-infected or MCMV-M48^{Rep}-infected fibroblasts (Figure 3.4a). The levels of other representative immediate-early (IE1), early (E1), and late [M86/major capsid protein (MCP)] viral gene products were similar between the viruses during infection. These results suggest that M48 DUB activity negatively regulates MCK2 levels during infection.

To further test this hypothesis and assess the potential modulation of MCK2 by M48 DUB activity, M48 (WT or C23S) and MCK2 were cloned into the expression vectors pEGFP-N1 and p3XFLAG-CMV-14, respectively, and cotransfected into NIH3T3 murine fibroblasts. To directly address the effect of M48 DUB activity in regulating MCK2 secretion in the absence of infection, MCK2 was immunoprecipitated (IP) from the supernatants of cells cotransfected with epitope-tagged MCK2 and enhanced green fluorescent protein (EGFP)-tagged WT M48 or M48^{C23S} expression

constructs. While MCK2 exhibited low levels of secretion in samples transfected with MCK2 alone, cotransfection with either M48 or M48^{C23S}showed elevated levels of MCK2 in the supernatant (Figure 3.4b). Interestingly, MCK2 secretion was reproducibly higher in cells cotransfected with M48^{C23S}, consistent with a model in which the M48 gene product promotes secretion of MCK2, and the DUB activity of M48 negatively regulates this process. Immunoblot analysis of cell lysates coexpressing MCK2 and WT M48, but not M48^{C23S} or EGFP alone, showed marked accumulation of an ~30-kDa band corresponding to the unglycosylated form of MCK2 [146] (Figure 3.5a), suggesting that M48 DUB activity stabilizes or promotes accumulation of unglycosylated MCK2. This accumulation may result from a block of proteosomal degradation of MCK2, as evidenced by the accumulation of the unglycosylated 30-kDa band following a cycloheximide chase with MG132 pretreatment (Figure 3.5b). These results suggest that MCK2 expression may be controlled by endoplasmic reticulum-associated protein degradation (ERAD) and that M48 DUB activity prevents MCK2 proteasomal degradation after retrotranslocation from the ER. An important constituent of the ERAD process is the AAA ATPase, p97/VCP, which extracts proteins from the ER in an ATP-dependent fashion and facilitates their ultimate degradation by the proteasome [147]. Overexpression of a dominant-negative p97 (p97^{QQ}) blocks retrotranslocation of proteins, such as the Rem signal peptide of mouse mammary tumor virus (MMTV), from the ER [148]. Consistent with a role for ERAD in regulating MCK2 expression, cells cotransfected with p97^{QQ} showed a significant increase in MCK2 secretion (Figure 3.5c). This result is similar to the observed increase in MCK2 secretion in the presence of M48,

regardless of the presence or absence of DUB activity (Figure 3.4b). Together, these results (Figures 3.4 and 3.5) show that M48 plays DUB-dependent and -independent roles in the control of MCK2. Furthermore, they suggest that M48 may modulate ERAD or ERAD substrates like MCK2 to influence expression and secretion from infected cells and that this process is subject to fine control by M48 DUB activity.

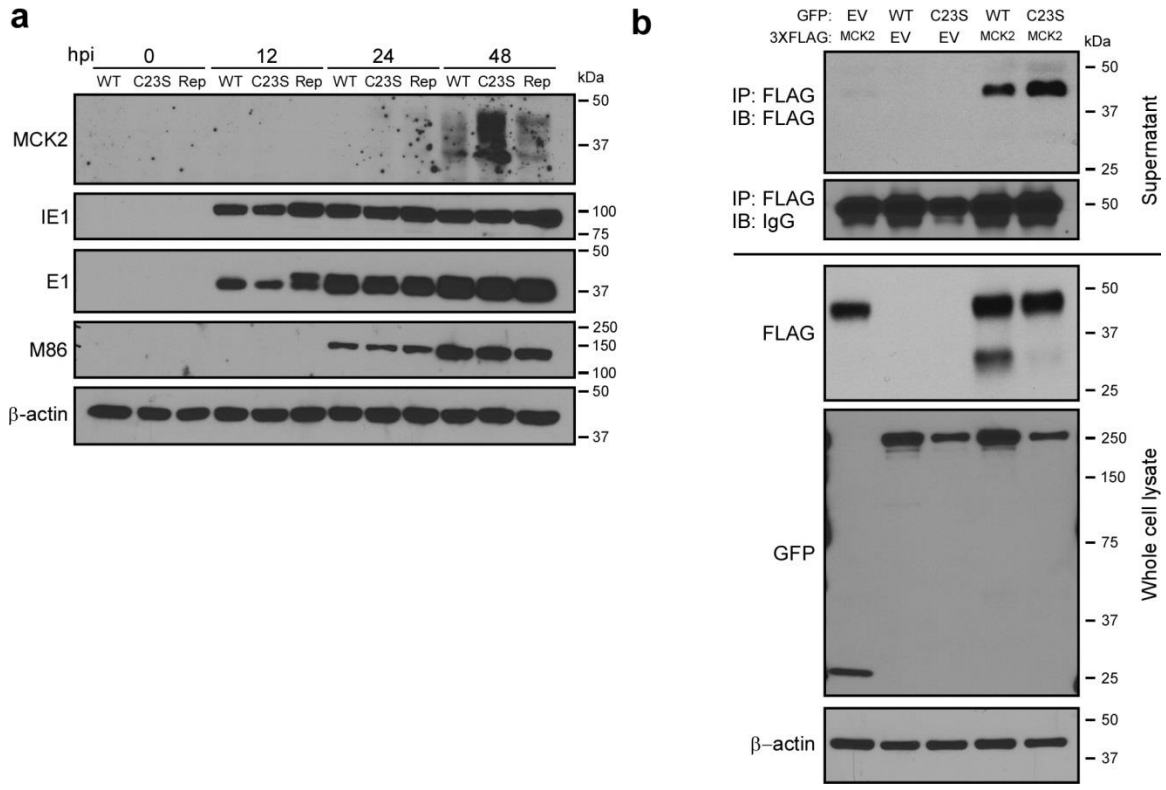

Figure 3.4: M48 DUB activity regulates MCK2 levels and can regulate secretion.

A) Immunoblot of whole-cell lysates from NIH3T3 fibroblasts infected with WT MCMV, MCMV-M48^{C23S}, or MCMV-M48^{Rep} (MOI = 5.0). Samples were collected at the indicated times post infection, and levels of MCK2, as well as those of representative immediate early (IE1), early (E1), and late [M86 (MCP)] viral antigens, were detected by immunoblotting. β-actin served as a loading control. B) Immunoblot (IB) analyses of supernatant immunoprecipitations (IP) (top panels) or whole-cell lysates (bottom panels) from NIH3T3 fibroblasts transfected with the indicated plasmids. At 24 hours post transfection, cell culture supernatants were collected and subjected to anti-FLAG immunoprecipitation as described in the Materials and Methods. Cells were collected at the same time, and lysates were generated and proteins separated by SDS-PAGE. Samples were immunoblotted with the indicated antibodies. Data are representative of results from 3 independent experiments.

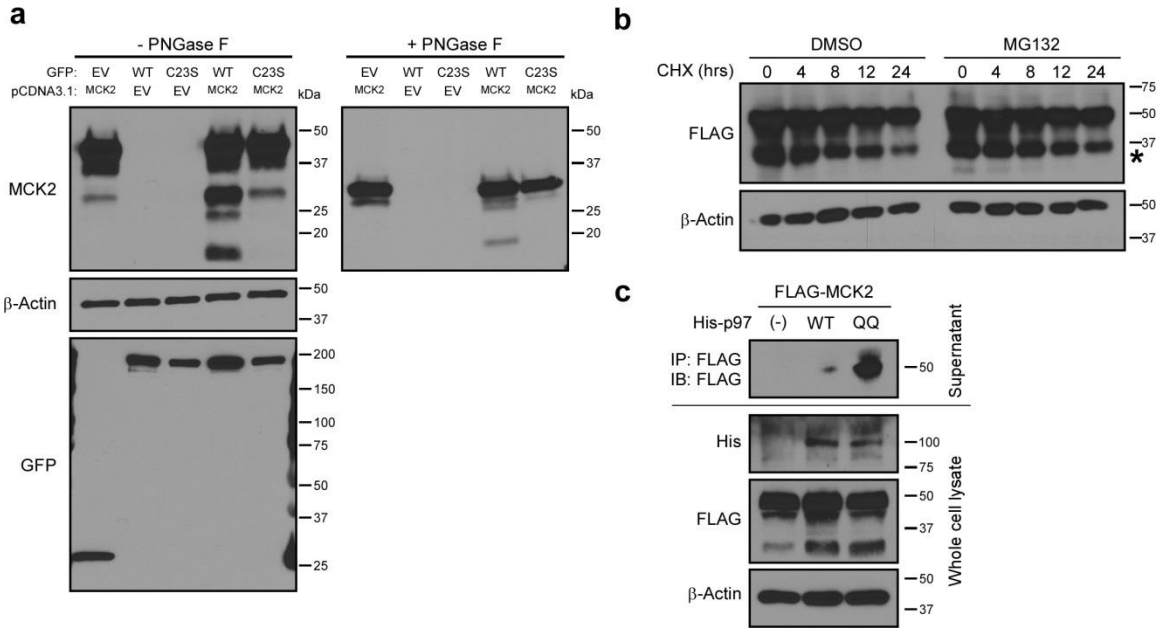

Figure 3.5: MCK2 levels and secretion are controlled by ERAD.

A) NIH3T3 cells were transfected with EGFP, M48, or M48^{C23S} and with pCDNA3.1 (EV) or MCK2. Immunoblot analysis was performed on whole-cell lysates (both untreated and treated with PNGase F). B) NIH3T3 cells were transfected with MCK2 and then subjected to pretreatment with either dimethyl sulfoxide (DMSO) or MG132 (20 μM) 24 hours post transfection for 1 hour prior to the addition of cycloheximide (CHX) (100 μg/ml). Whole-cell lysates were collected at 0, 4, 8, 12, and 24 hours post-CHX treatment, and MCK2 was subjected to immunoblot analysis. *, unglycosylated MCK2 product. C) NIH3T3 cells were transfected with MCK2 and pCDNA3.1 empty vector (EV), 6-His p97^{WT}, or 6-His p97^{QQ}. Secreted MCK2 was assessed as described for Figure 3.4B.

3.2.4 M48 DUB activity controls MCK2 incorporation into mature virions

In addition to serving as a chemokine during infection, MCK2 can also associate with the glycoprotein H/glycoprotein L (gH/gL) complex in mature virions. gH/gL/MCK2 glycoprotein complexes promote pH- and energy-dependent entry and facilitate entry into macrophages [149]. To determine if M48 DUB activity had an effect on virion-associated MCK2 levels, cell-free virions were purified by gradient centrifugation and subjected to immunoblot analysis. MCMV-M48^{C23S} virions contained higher MCK2 levels than MCMV-M48^{Rep} virions, while M86 (MCP) levels remained constant between samples (Figure 3.6a). Mass spectrometry (MS)-based proteomics analysis of purified virions confirmed these findings. Label-free relative quantitation consistently showed higher levels of MCK2 protein in MCMV-M48^{C23S} virions than in MCMV-M48^{Rep} virions (Figure 3.6b), indicating that, in addition to controlling MCK2 levels during infection, M48 DUB activity controls the amount of MCK2 incorporated into infectious virions. Interestingly, the MCK2 partner M115 (gL) also showed a modest and yet statistically significant increase in abundance, suggesting that MCK2 and gL may share a pathway for maturation and assembly regulated by the DUB. In contrast, no changes were observed in the relative levels of the major fusogenic glycoprotein M55 (gB) or of the components of the gM/gN glycoprotein complex, M100 (gM) and M73 (gN) [150] (Figure 3.6b).

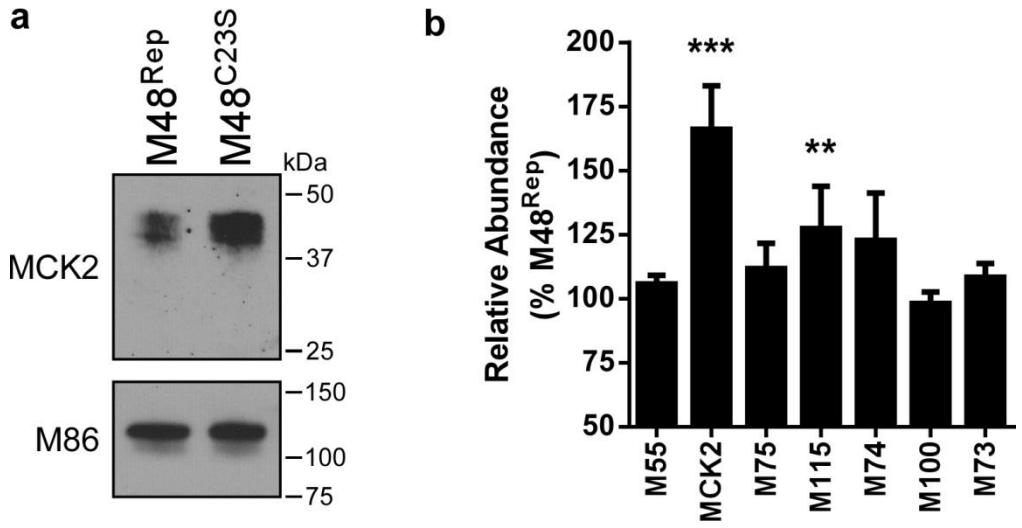

Figure 3.6: M48 DUB activity controls MCK2 incorporation into mature virions.

A) Immunoblot of lysates of MCMV-M48^{Rep} and MCMV-M48^{C23S} virions purified over a 20% to 70% linear sorbitol gradient. Equal amounts of virion lysate were loaded and MCK2 levels were assessed by immunoblotting. M86 (MCP) served as a loading control between samples. B) Relative peptide abundances of virion-associated glycoproteins M55 (gB), MCK2, M75 (gH), M115 (gL), M74 (gO), M100 (gM), and M73 (gN) in purified MCMV-M48^{C23S} virions compared to MCMV-M48^{Rep}. Ratios were calculated as averages of target ion peak areas normalized to M86 (MCP) for three independent experiments. Error bars represent standard errors of the means. **, $P < 0.01$; ***, $P < 0.001$ (by Wilcoxon signed-rank test).

3.2.5 Deletion of MCK2 rescues MCMV-M48^{C23S} replication *in vitro* and *in vivo*

Given our results suggesting that M48 DUB activity controls MCK2 protein levels, we hypothesized that the MCMV-M48^{C23S} attenuation was at least partly due to the greater amounts of MCK2 being produced. If so, genetic ablation of MCK2 would restore replication of the DUB mutant virus. To directly test this hypothesis, two additional recombinant viral mutants were constructed. Both the WT and M48^{C23S} viruses were modified by introducing a translational stop and a single-nucleotide frameshift within the first exon (*m131*) of *Mck2*, generating MCMV-m131^{stop} and MCMV-m131^{stop}M48^{C23S} (Figures 3.7a, 3.8a-c). In order to confirm a loss of MCK2 expression, gradient-purified virions were subjected to immunoblot analyses, with the results clearly demonstrating loss of MCK2 expression (Figure 3.7b).

Characterization of MCMV-m131^{stop} and MCMV-m131^{stop}M48^{C23S} was initiated with single-step and multistep growth analyses in cell culture for NIH3T3 fibroblasts, SVEC4-10 endothelial cells, and RAW264.7 macrophages. Surprisingly, the single-step and multistep growth curves of MCMV-m131^{stop} and MCMV-m131^{stop}M48^{C23S} showed no difference in replication kinetics in fibroblast and endothelial cell lines (Figure 3.7c, d, f, and g), suggesting that the modest replication defect for MCMV-M48^{C23S} (Figure 3.1b, c, e, and f) can be attributed to MCK2. Although MCMV-m131^{stop} and MCMV-m131^{stop}M48^{C23S} replicated similarly in single-step replication analysis on RAW264.7 macrophages (Figure 3.7e), MCMV-m131^{stop}M48^{C23S} levels remained modestly attenuated during multistep replication (Figure 3.7h). This result is

similar to that shown in Figure 3.1g, where MCMV-M48^{C23S} replicated at titers 4-fold to 5-fold lower than MCMV-M48^{Rep} or WT MCMV, suggesting that DUB-dependent functions may govern replication in macrophages independently of MCK2.

To further investigate the role of MCK2 dysregulation in MCMV-M48^{C23S}replication in a natural host, animals were infected with *Mck2*-deficient viruses by i.p. injection. Concomitant loss of MCK2 reversed the acute replication defect of MCMV-M48^{C23S} to WT levels in spleen and livers of infected mice over a time course of 14 days postinfection (Figure 3.9a and b). *Mck2*-deficient viruses were not detected in salivary glands of infected mice (Figure 3.9c), consistent with a role for MCK2 in virus dissemination. To determine if the rapid onset of footpad swelling was dependent on MCK2 expression, animals were infected via footpad injection with either MCMV-m131^{stop} or MCMV-m131^{stop}M48^{C23S}. Mice infected with either MCMV-m131^{stop} or MCMV-m131^{stop}M48^{C23S} showed identical levels of swelling and recovery over the 14-day time course with no rapid onset of swelling (Figure 3.9d) as seen in the MCMV-M48^{C23S}-infected mice (Figure 3.3d). This suggests that the DUB-dependent swelling phenotype observed in MCMV-M48^{C23S}-infected mice (Figure 3.3d) was mediated by MCK2. Taken together, these results indicate that M48 DUB activity regulates MCK2 biology by controlling its expression, maturation, or secretion during infection.

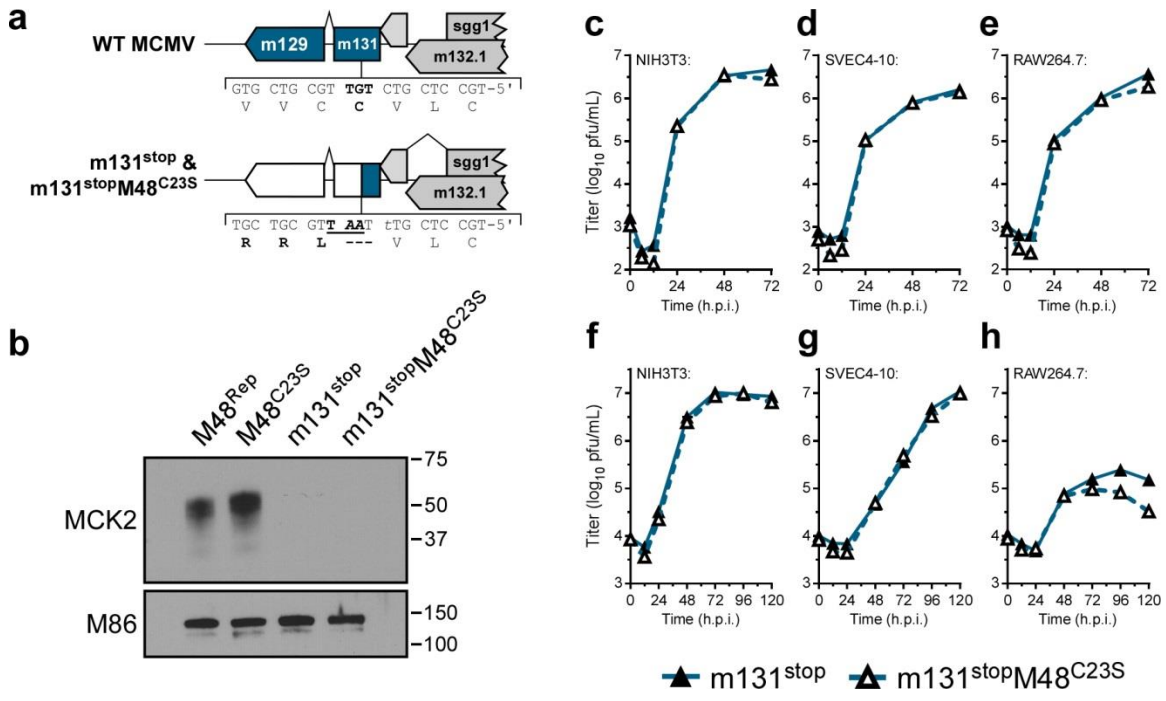

Figure 3.7: Concomitant loss of MCK2 rescues MCMV-M48^{C23S} replication in culture.

A) A schematic representing the genomic location and generation of mutant viruses lacking MCK2 expression (m131^{stop} or m131^{stop}M48^{C23S}). B) Immunoblot of gradient-purified virions of the indicated genotype to confirm loss of MCK2 expression. C to H) Single-step (C-E) (MOI = 5.0) and multistep (F-H) (MOI = 0.05) growth curves in NIH3T3 fibroblasts (C and F), SVEC4-10 endothelial cells (D and G), or RAW264.7 macrophages (E and H). Each data point represents *n* = 3 biological replicates.

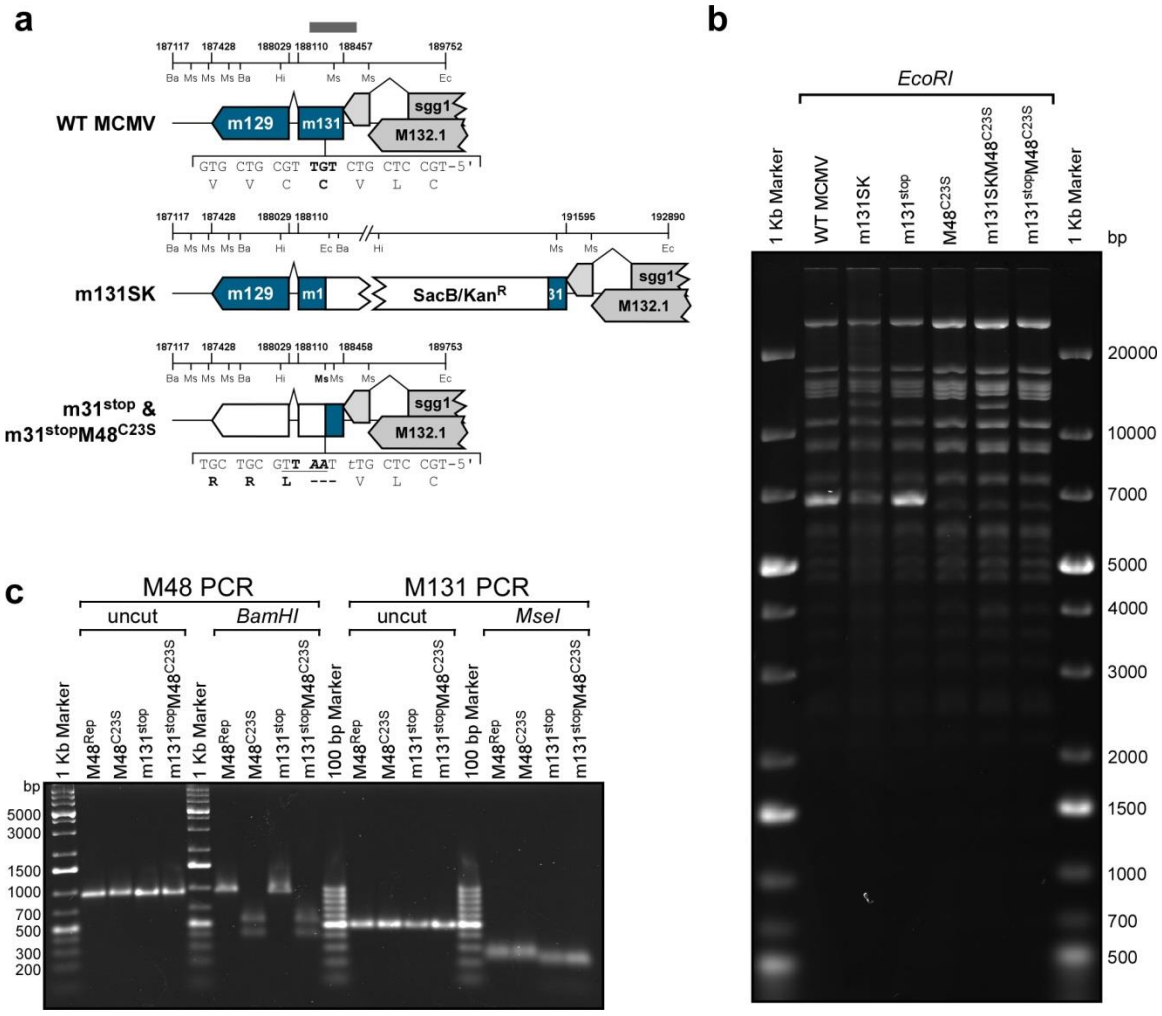

Figure 3.8: Generation of viruses lacking MCK2 expression.

A) Schematic diagram depicting the genomic area around MCK2 (m129-m131) as well as the mutagenesis strategy to generate MCK2-deficient viruses. Numbers represent MCMV genomic coordinates (GenBank accession number AM886412.1) and abbreviations indicate restriction enzyme sites (Hi, HindIII; Ec, EcoRI; Ba, BamHI). See materials and methods for a more detailed description of $m131^{stop}$ and $m131^{stop}M48^{Rep}$ generation. B) RFLP analysis of WT, m131SK, $m131^{stop}$, $M48^{C23S}$, $m131SKM48^{C23S}$, and $m131^{stop}M48^{C23S}$ BACs digested with EcoRI. C) Amplicons from M48 and m131 surround the respective mutation sites. $M48^{C23S}$ mutants ($M48^{C23S}$ and $m131^{stop}M48^{C23S}$) showed digestion by BamHI. An MseI restriction site introduced into m131 in the form of a stop codon is shown by MseI digest of amplicons surrounding the mutagenized m131 region.

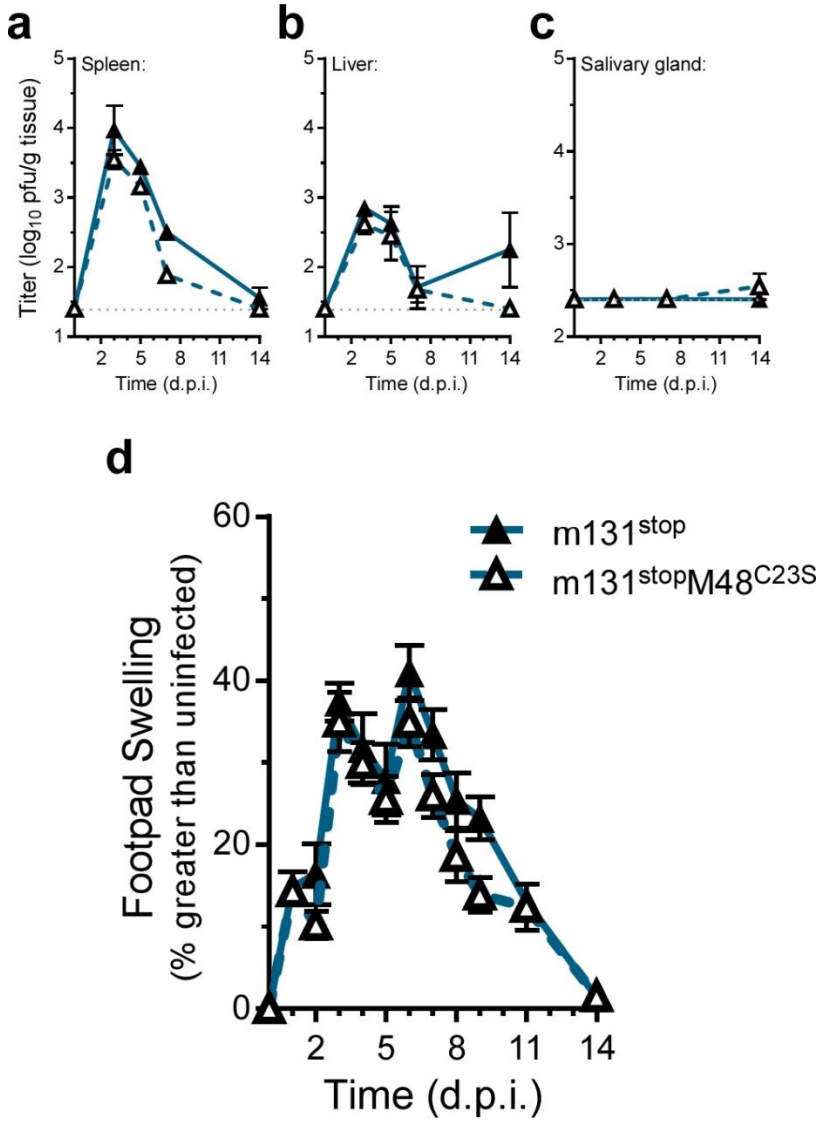

Figure 3.9: Concomitant loss of MCK2 in the presence of the DUB mutation rescues MCMV-M48^{C23S} replication in the spleens and livers and ameliorates footpad swelling.

A-C) C57BL6/J mice were infected with 10^6 PFU of MCMV-m131^{stop} or MCMV-m131^{stop}M48^{C23S} via i.p. injection. Viral load in the spleens (A), livers (B), and salivary glands (C) was assessed at the indicated times post infection. Each data point represents $n \geq 5$ mice. D) Footpad swelling of C57BL6/J mice infected with 10^6 PFU of either MCMV-m131^{stop} or MCMV-m131^{stop}M48^{C23S} via footpad injection. Swelling was measured by digital caliper over the course of 14 days, and data are plotted as percent increase over the measurements from uninfected mice. Each data point represents $n \geq 5$ mice.

3.3 DISCUSSION

In this report, we describe a systematic investigation into the role of the MCMV DUB *in vitro* and *in vivo*. Specific mutation of a catalytic cysteine within the DUB domain of M48 (C23S) revealed a minor role for M48 DUB activity in MCMV replication in cultured cells (see Figure 3.1b-g) but substantial attenuation in a natural host (Figure 3.3a-c). Importantly, these results are consistent with previous reports demonstrating that the DUB activity of the HCMV orthologue of M48, UL48, is present during infection and modestly contributes to replication in cell culture [97]. Interestingly, our work revealed that a major role for M48 DUB activity is control of MCK2, the viral chemokine, both *in vitro* and *in vivo*. Loss of M48 DUB function results in increased MCK2 levels (Figure 3.4a), manifesting as enhanced inflammation at localized sites of infection in mice (Figure 3.3d) and resulting in attenuation of MCMV replication (Figures 3.3a-c and 3.9a and b). Concomitant loss of MCK2 restored most observed DUB-dependent phenotypes *in vitro* and *in vivo* (Figures 3.7 and 3.9), providing compelling genetic evidence for a mechanism of intrinsic control over the virus-encoded chemokine.

Accumulating evidence implicates cellular DUBs in the control of a number of host proinflammatory pathways. The host deubiquitinase, A20, is critical for regulating NF-κB activation and subsequent activation of proinflammatory cytokines [151, 152]. Additionally, recent work has shown that the cellular DUB, Trabid, negatively regulates expression of interleukin-12 (IL-12) and IL-23 via the modification of ubiquitinated

histones [153]. OTULIN, the Met1-linked deubiquitinase, controls levels of Met1-linked ubiquitin chains, modulating activation of NF-κB responses and TNF-α levels [154]. While herpesvirus DUBs have been implicated in the control of host inflammatory signal transduction [72, 83, 95], M48 appears unique in that it manages levels of MCK2, a virally encoded chemokine. While our results do not exclude the possibility that M48 DUB activity may regulate other pathways, they provide the first example of a herpesvirus DUB controlling levels of a viral chemokine.

In order to determine whether MCK2 production contributed to the observed phenotypes of the MCMV-M48^{C23S} virus, we took a genetic approach and ablated MCK2 expression. Surprisingly, concomitant loss of MCK2 in the presence of the mutant DUB restored replication in most cell types in culture (Figure 3.7c-h). Fibroblasts and endothelial cells infected with MCMV-m131^{stop} or MCMV-m131^{stop}M48^{C23S} displayed similar replication kinetics in single-step and multistep replication analyses. Although the mechanism of attenuation of MCMV-M48^{C23S} in fibroblast and endothelial cells is likely complex, recent findings suggest that increased levels of virion-associated MCK2 (Figure 3.6a and b) promote an endocytic mode of entry over fusion at the plasma membrane [149]. Endocytic entry of herpesviruses results in delayed gene expression and increased antiviral gene transcription [155], both of which could contribute to attenuation of virus replication. Increased levels of these antiviral proteins may occur in MCMV-M48^{C23S}-infected cells, resulting in modest attenuation. We have recently shown that MCMV-M48^{C23S} elicited a greater stimulator of interferon gene (STING)-dependent type

I IFN response in cultured dendritic cells [87]. However, whether virion-associated MCK2 levels and STING-dependent responses during infection are connected remains to be determined.

Interestingly, while no difference in replication was observed in single-step growth kinetics on macrophages (Figure 3.7e), loss of MCK2 in the presence of the mutant DUB failed to alleviate the modest growth defect in multistep growth (Figure 3.7h), similarly to that seen in Figure 3.1g. These results imply that DUB-dependent, MCK2-independent mechanisms may be necessary for efficient replication in macrophages. Since macrophages and monocytes are important CMV target cells *in vivo*, a potential role for DUB-dependent functions in cell tropism warrants further investigation.

Surprisingly, replication of MCMV-M48^{C23S} in the spleens and livers of infected mice was restored with targeted deletion of MCK2. Previous work examining the contributions of MCK2 to pathogenesis has shown that, while MCK2 is necessary for dissemination to the salivary glands, it is dispensable for replication and spread in the spleen and liver [144, 145, 156]. Our results are consistent with these findings showing that MCK2 is not a major contributor to the early stages of infection in target organs. We extend these observations to show that overproduction and/or dysregulation of MCK2, as seen in MCMV-M48^{C23S}-infected cells, attenuates acute replication *in vivo*.

MCK2 is necessary for effective dissemination of MCMV to the salivary glands of infected mice [144, 145, 157, 158]. However, MCMV-M48^{C23S}, which fails to appropriately control MCK2 production or secretion, remained impaired for dissemination to the salivary glands regardless of the route of inoculation (Figures 3.9c and 3.10). Thus, it is tempting to speculate that careful calibration of MCK2 levels facilitates a successful infection. Recent work utilizing recombinant MCMVs expressing viral or mammalian neutrophil-attracting chemokines (mouse CXCL1 or HCMV CXCL1) showed that overexpression of pro-inflammatory chemokines is detrimental to MCMV dissemination to the salivary gland [159]. Our work is consistent with those findings in that uncontrolled MCK2 levels impair dissemination of MCMV. However, as expected, neither the MCMV-m131^{stop} nor the -m131^{stop}M48^{C23S} viruses were reliably detected in the salivary glands of infected mice (Figure 3.9c), indicating that MCK2 is required for dissemination. Thus, it is difficult to conclude that MCK2 overproduction is the only contributor to a decrease in mutant DUB virus dissemination. DUB-dependent, MCK2-independent contributions to MCMV dissemination and/or salivary gland replication may exist. The modest replication defect seen in multistep replication kinetics in macrophages (Figures 3.1g and 3.7h) could indicate the existence of DUB-dependent contributions to monocyte infection and dissemination independent of MCK2.

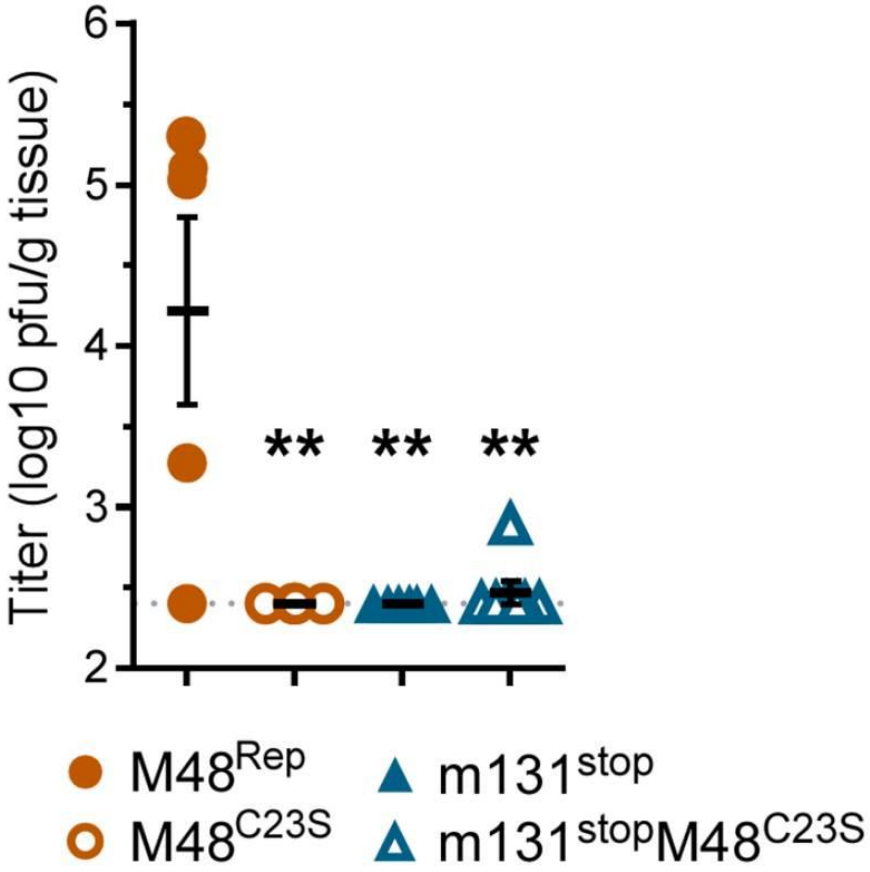

Figure 3.10: Salivary gland titers from mice infected via a footpad (f.p.) route of inoculation.

The salivary glands from the f.p.-infected mice in Figures 3.3a-c and 3.9a-c were collected at 14 d.p.i., homogenized, and infectious viral loads were determined by plaque assay.

In fact, when bottom-up proteomics analyses are applied to cells infected with either MCMV-M48^{C23S} or MCMV-M48^{Rep} virus, distinct differences manifest in two viral proteins (Table 3.1). Specifically, viral proteins sgg1 and m137 are elevated in MCMV-M48^{Rep} infected cells compared to MCMV-M48^{C23S} infected cells. While the specific functions of m137 are unknown, aside from the fact that it appears to contribute to virulence [160], sgg1, or salivary gland growth gene 1, has been shown to be critical for replication in the salivary glands of infected mice [161]. Sgg1 is a virally encoded type 1 transmembrane protein encoded by the m133 open reading frame of MCMV [162]. Sgg1 is not essential for replication in cell culture or in many organ types in mice. However, sgg1 is critical for replication in the salivary gland. It is important to note that sgg1 does not contributing to the dissemination of MCMV to the salivary glands, but is responsible for MCMV replication in the acinar cells of infected salivary glands [163], though the exact mechanism by which it mediates this is currently unknown. While we originally hypothesized that MCMV-M48^{C23S} attenuation may be due to increased levels of MCK2, these results suggest another DUB-dependent mechanism in governing the levels of sgg1. Interestingly, these data are opposite to what is observed regarding MCK2 levels in MCMV-M48^{C23S} versus MCMV-M48^{Rep} infected cells (Figure 3.4a). These data suggest that M48 DUB activity utilizes different mechanisms to control the levels of specific viral proteins during infection.

Protein	Origin	Function	$M48^{C23S}$ (PSMs)		$M48^{Rep}$ (PSMs)	
			#1	#2	#1	#2
sgg1	MCMV	• Salivary gland replication (161, 163)	8	ND	63	53
m137	MCMV	• Virulence factor (160)	4	ND	52	62

Table 3.1: Peptide spectrum matches (PSMs) of sgg1 and m137 from infected fibroblasts.

NIH3T3 cells were infected at an MOI = 5.0 and lysates were collected 48 hours post infection. Peptides were prepared (see materials and methods) and subjected to LC-MS/MS analysis. PSMs of sgg1 and m137 are presented here. Two biological replicates for MCMV-$M48^{C23S}$ and MCMV-$M48^{Rep}$ are shown here.

In addition to attenuation of acute replication, MCMV-M48^{C23S} induced a robust inflammatory response following footpad inoculation. We showed that this phenotype is restored to WT levels by concomitant loss of MCK2 (Figure 3.9d). This result clearly indicates that the rapid swelling observed in MCMV-M48^{C23S}-infected mice was due to MCK2 overproduction. Unlike previous footpad studies performed with MCK2-null viruses [144, 145, 157, 158], we observed considerable swelling in the footpads of mice infected with MCMV-m131^{stop} or MCMV-m131^{stop}M48^{C23S}. This inconsistency may be due to several factors. In previous works, the K181+ strain and its MCK2 mutant derivatives were used, while our studies utilized the BAC-derived K181 Perth strain (pARK25) of MCMV. Additionally, most studies of MCK2-dependent inflammation have employed BALB/c mice, whereas we report results from C57BL/6 mice. While the source of these differences in the results of control experiments warrants further investigation, we clearly demonstrated that the rapid swelling seen in MCMV-M48^{C23S}-infected mice is ameliorated by ablating MCK2 expression. This is compelling evidence that loss of DUB control over MCK2 expression, maturation, or secretion mediates the inflammatory phenotype of MCMV-M48^{C23S} *in vivo*.

Although the specific substrate(s) of M48 DUB activity during infection remains unknown, we anticipate that significant targets include endoplasmic reticulum- and/or Golgi-associated components. Interestingly, the M48 homologue encoded by HCMV, UL48, has been shown to interact with the endoplasmic reticulum protein RRBP1/ES130 [164], a ribosome binding protein critically implicated in the function of the secretory pathway [165, 166]. Although the functional relevance was not addressed, considered together with the data reported here, a possible model emerges wherein beta-herpesvirus DUBs may be localized to the ER, allowing control over secreted or transmembrane protein maturation, whether host or virus in nature. This association at the ER might allow M48 to affect secretory events via RRBP1 by modulating ERAD, or through another currently unknown mechanism (Figure 3.13). While it is unknown whether M48 itself interacts with any ER-resident proteins, fluorescence microscopy shows that WT M48 localizes in a very perinuclear fashion. Interestingly, mutant DUB M48 seems to localize in a more diffuse pattern when compared to WT M48 (Figure 3.11). This difference in localization may lead to a difference in interacting partners, and subsequently, a different target repertoire.

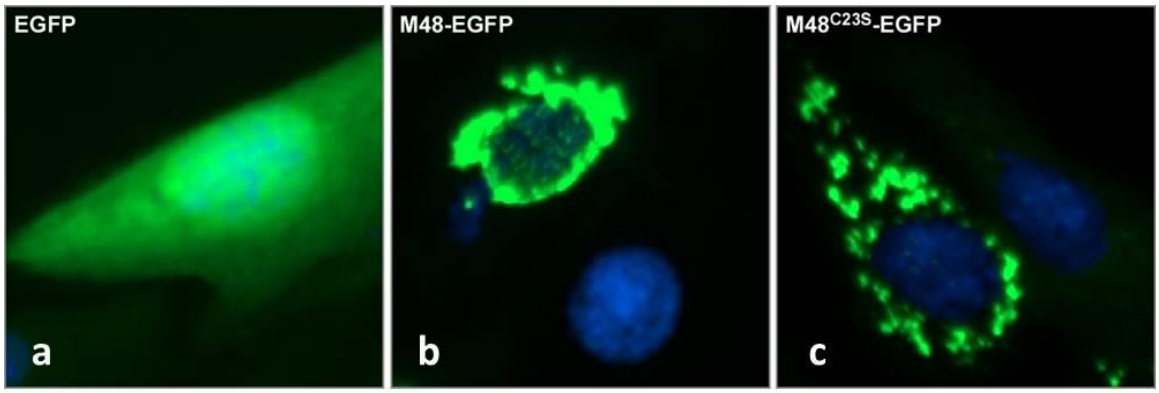

Figure 3.11: Fluorescence imaging of M48 and M48^{C23S} localization in uninfected cells.

A-C) NIH3T3 cells were transfected with either and eGFP expression vector (A), M48-eGPF (B), or M48^{C23S}-eGFP (C). 24 hours post transfection, cells were fixed, permeabilized, and counterstained with Hoechst stain. Cells were imaged on an EVOS FL inverted fluorescence microscope.

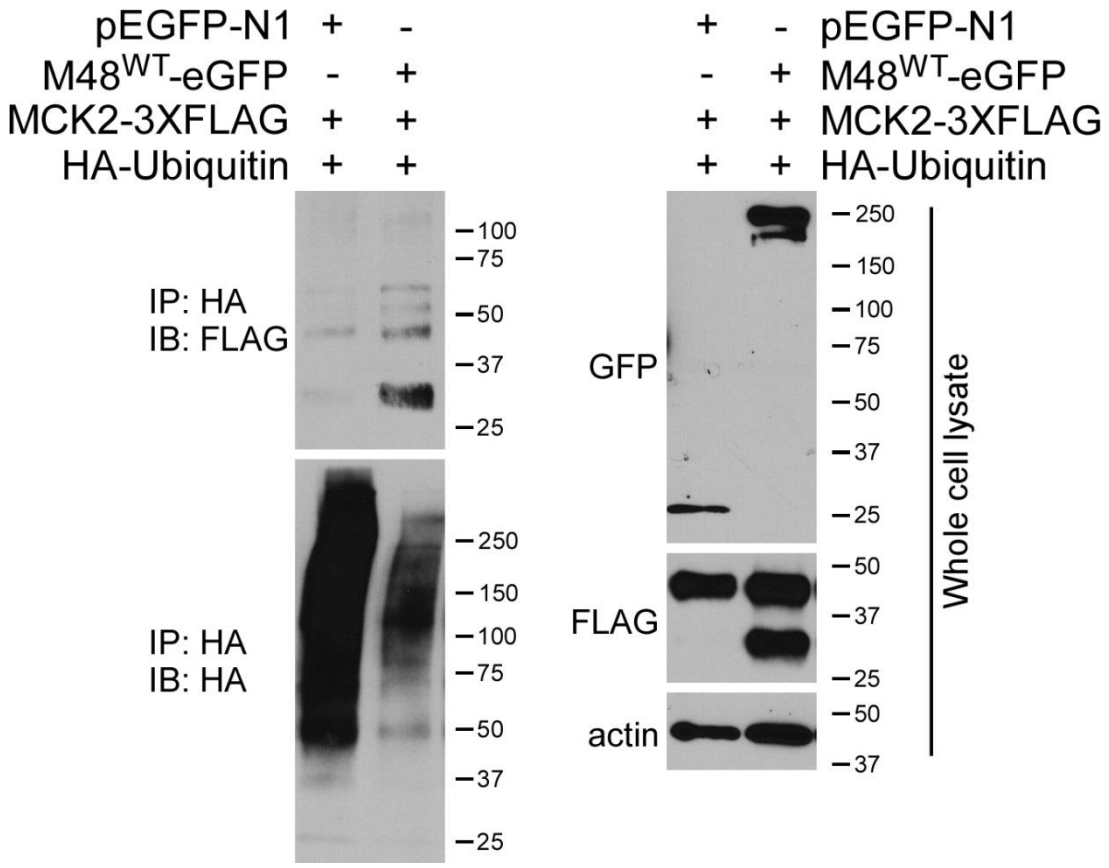

Figure 3.12: MCK2 ubiquitination in the presence of M48.

NIH3T3 cells were co-transfected with M48-eGFP, MCK2-3XFLAG, and HA-Ub. 24 hours post transfection, lysates were collected and subjected to anti-HA immunoprecipitation. The immunoblots performed are indicated next to their respective panels.

While we do not know what the direct targets of M48 DUB activity are at this time, we have begun to rule out some possible candidates. One obvious candidate is MCK2 itself; i.e. is MCK2 a direct target of M48 DUB activity. Interestingly, MCK2 does not appear to be a primary target of M48 deubiquitination. In cells co-transfected with M48-eGFP, MCK2-3XFLAG, and HA-Ubiquitin, MCK2 is more heavily ubiquitinated than cells co-transfected with eGFP, MCK2 and HA-Ubiquitin (Figure 3.12). While not indicative of any cellular targets of M48 DUB activity, these results do suggest that the DUB is not directly modulating the ubiquitinated status of MCK2.

In conclusion, we have revealed a novel mechanism by which a herpesvirus DUB controls the host response to infection and appropriates that response for successful infection. While the function of the viral chemokine MCK2 in eliciting and coopting host inflammatory responses has been previously described [143-145, 157, 158], we show that there is DUB-dependent control of MCK2 expression during infection. Thus, a unique interplay between M48 DUB activity and MCK2 function orchestrates a critical step in CMV pathogenesis, representing a potential target for therapeutic intervention.

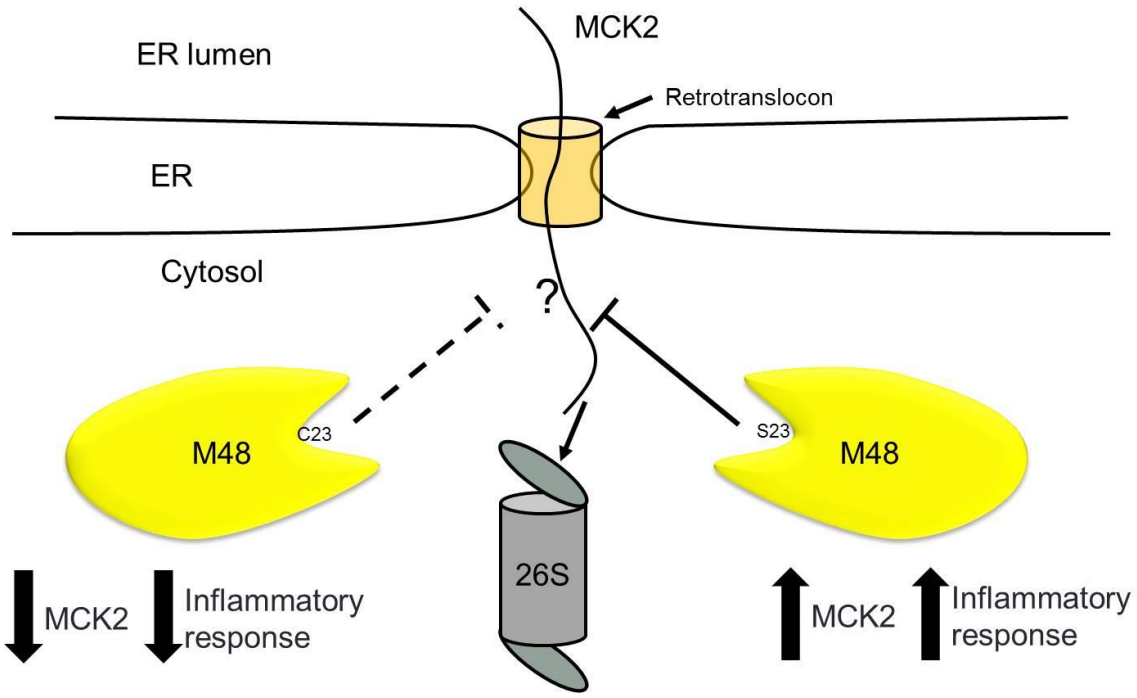

Figure 3.13: Proposed model for M48-dependent regulation of MCK2.

If M48 is expressed in the presence of MCK2, its degradation is blocked. Interestingly, a WT M48 DUB selectively promotes the degradation of MCK2, leading to its tamed expression and a decrease in inflammation. In the presence of the mutant DUB, MCK2 degradation is still blocked, but there is no selectivity in the amount allowed to be degraded, leading to an increase in MCK2 levels, ultimately resulting in increased inflammation. In the case of the WT DUB, these targets of DUB activity are under active investigation.

Chapter 4: Conclusions and Future Directions

4.1 Continued Research and Development on Pathogen Electrochemical Biosensors

4.1.1 Summary of dissertation research

We recently reported two significant advancements in the field of collision electrochemistry. We demonstrated that MCMV could be specifically detected in solution by tagging the virus with antibody and binding to polystyrene beads (PSBs), and then observing the formation of aggregates [123]. Building off this work, we then focused on the development of a positive detection method for MCMV utilizing an enzymatically enhanced collision technique to detect virus in the urine of infected mice [43]. Overall, these studies have demonstrated the potential use of collision electrochemistry to detect pathogens in complex solutions, and offer an easy-to-use and rapid diagnostic technique for CMV infection.

4.1.2 Future of pathogen electrochemical sensors utilizing collision electrochemistry

While the enzymatic detection of MCMV represents an impressive step forward, the technique does suffer from several foreseeable problems. First, we rely on an antibody for viral detection. It is not unreasonable that antibody epitopes may vary, which decreases the efficacy of this method. One way in which this problem could be solved is by using multiple antibodies, which effectively would increase the possibility of positive detection. Assuming detection using antibodies causes few problems, there is still an issue regarding the small signal to noise ratio currently inherent to our system.

Although our present signal to noise ratio of approximately 15:1 allows the detection of distinct events by amperometry, a greater signal to noise ratio would be ideal. To achieve this, one could take advantage of the electrochemical amplification properties of nanoparticles, such as platinum. These nanoparticles could be labeled with an MCMV- or HCMV-specific antibody, similar to the manner in which Spain and colleagues electrochemically detected prostate specific antigen [167]. Subsequent collisions with an electrode would then produce a robust current response greater (S:N on the order of 100:1) than that of the background.

Additional method optimization also includes the mode of mass transfer of particles to the electrode. Currently, our method relies on the diffusion of particles to the electrode. Because detection dependent on diffusion is directly related to the concentration of the particle, samples that are relatively dilute will be difficult to reliably detect the presence of viral particles. In this case, it would be necessary to implement some sort of ultramicroelectrode (UME) array, thus increasing the chances of a collision [168]. Directing the mass transfer of particles by utilizing fluidics device over an electrode array would significantly increase the chances of a positive detection event [169]. Lastly, while our method could be used for point-of-care diagnostics and continued monitoring, if a new patient tests positive for HCMV using this technique, additional confirmation in the way of cell culture or PCR-based assays would still be necessary in order to confirm the diagnosis before moving forward with treatment.

Overcoming these hurdles will allow for the rapid development of similar detection schemes for any number of different pathogens, including viral, bacterial,

fungal and parasitic infections. Recent work from Sepunaru and co-workers showed that electrochemically amplified detection of influenza could be achieved by incubating the virus with silver nanoparticles and observing the collisions of influenza / Ag-nanoparticles with an electrode [101]. While significant signal was observed upon influenza particle collision at an electrode, this method would not work on a more complex sample not entirely comprised of influenza virus as the silver nanoparticles would likely non-specifically stick to any particle in solution. Therefore, while significant strides have been made in using electrochemistry to detect pathogens, continued research and development is necessary for implementation of these collision methods in the clinic.

4.2 IDENTIFYING AND VERIFYING NOVEL TARGETS FOR ANTI-VIRAL CYTOMEGALOVIRUS TREATMENT

4.2.1 The cytomegalovirus deubiquitinating enzyme as a viable therapeutic target

Unique enzymatic contributions to HCMV infection are likely to be important to viral replication. As such, a major area of research has been to target these enzymes through the use of small molecule inhibitors. In chapter 3, I described our recent work characterizing the important role of the uniquely structured and conserved MCMV DUB in mediating infection dynamics *in vivo*. Because this DUB is structurally distinct from its cellular counterparts, it is possible that with additional research, this DUB could serve as another potential target for pharmacological intervention. Interestingly, this idea is not new as small molecule inhibitors of cellular DUBs are of significant interest due to the tumorigenic potential of some cellular DUBs [170]. As such, currently developed inhibitors may serve as solid platforms for anti-CMV DUB drug discovery.

Though herpesvirus DUBs share some structural similarities to the papain superfamily of proteases, their interactions with ubiquitin are unique [71]. The M48 DUB is structurally distinct and seems to derive its specificity for ubiquitin in a beta-hairpin region that is critical for its interaction with the ubiquitin hydrophobic patch (M48 a.a. 108-115). Though the catalytic triad (C23, H158, and D156) responsible for the cleavage of ubiquitin is not unique to the herpesvirus DUBs, targeted inhibition of the DUB's ability to act on ubiquitin may be possible by targeting the beta-hairpin. Excitingly, predicted structural analyses using the Phyre2 modeling software [171] suggest significant structural conservation between M48 and the HCMV DUB, UL48. They even seem to share homology in the beta-hairpin. Several of the same residues mediating the interaction with the hydrophobic ubiquitin patch appear to be conserved (M48 → L110, Y113, and C115; UL48 → L114, Y117, and C119) (Figure 4.1). To determine the contributions of the hairpin to MCMV infection, genetic studies mutagenizing these key residues should be conducted. Assuming they contribute to pathogenesis in some capacity, the conserved beta-hairpin, along with other distinct structural components [71] may be amenable to targeted anti-viral therapies.

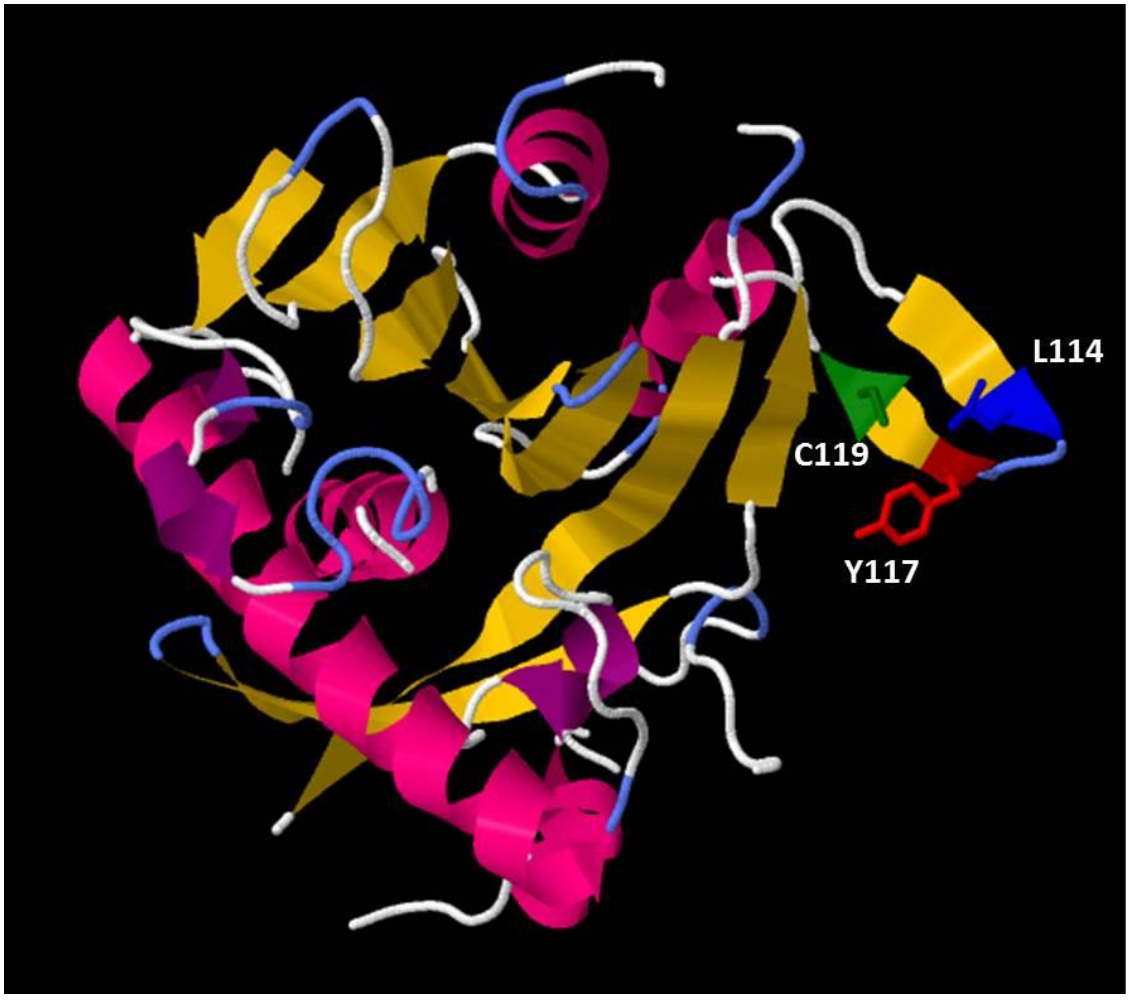

Figure 4.1: UL48 (amino acids 1-300) modeled and mapped to M48.

Amino acids 1-300 of UL48 (Towne strain) were submitted on the protein fold recognition engine, Phyre2. The resulting .pdb file was opened in Jmol and the conserved residues located in the beta-hairpin were mapped (L114→ blue, Y117→red, C119→green).

4.2.2 Cytomegalovirus deubiquitinating enzyme mutants as vaccine vectors

In addition to the development of anti-HCMV therapeutics, the use of HCMV as a vaccine vector has been heavily researched due to its ability to successfully activate both the innate and adaptive arms of the immune response [128]. In fact, recent work has utilized rhesus CMV (RCMV) as a vaccine vector in which simian immunodeficiency virus (SIV) antigens have been genetically inserted and subsequently expressed. The substantial immune response elicited by RCMV also causes an immune response against the SIV antigens. Subsequent challenges with SIV were unproductive in 50% of the monkeys as a result of the immunization provided [172 , 173]. Due to the increased inflammatory response and type I interferon response elicited by a mutant DUB MCMV [87, 174], it may be that a mutant DUB HCMV elicits both a more robust and potent immune response. While it remains to be determined if the HCMV DUB functions in the same manner as the MCMV DUB, co-transfection of the HCMV DUB UL48 (WT or mutant) with MCK2 resulted in increased MCK2 secretion in the presence of the mutant DUB similar to the result seen in Figure 3.4b (Figure 4.2). These results suggest at least some conserved functionality between the two proteins. Future efforts will seek to determine host immune responses to mutant DUB MCMV and other non-human primate CMVs to determine what these precise immunological changes are. Results from these studies will not only yield important insight into CMV-mediated immune responses, but may serve to aid in the development of future CMV vector vaccines.

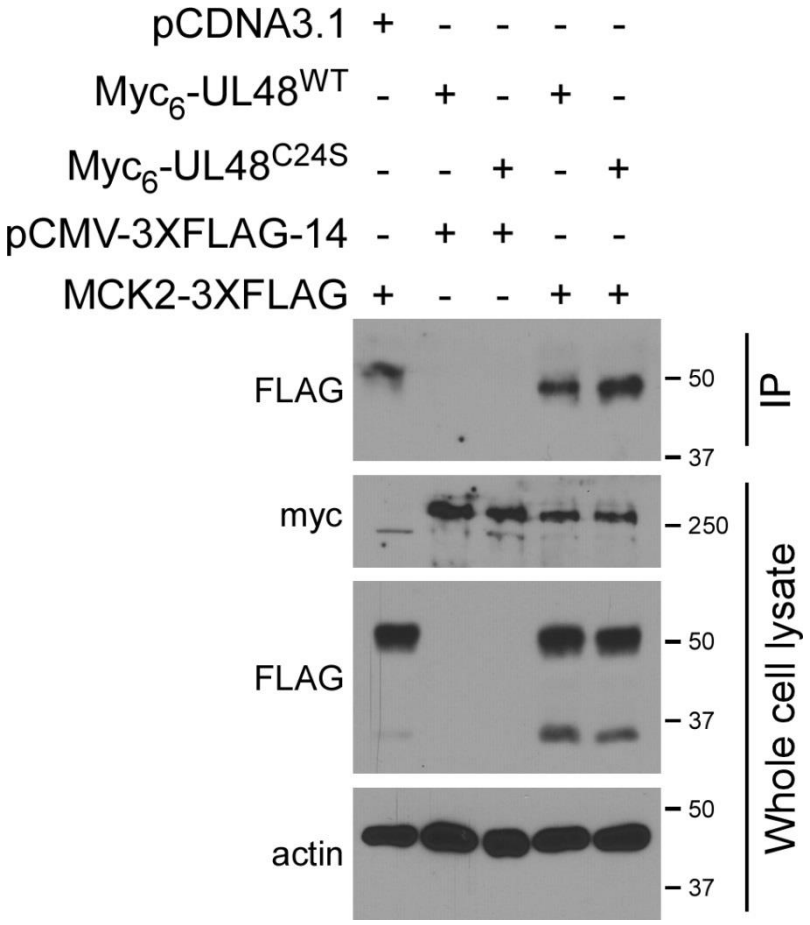

Figure 4.2: Mutant DUB UL48 facilitates an increased MCK2 secretion.

NIH3T3 cells were co-transfected with UL48 (WT or mutant DUB) and MCK2. MCK2 secretion was assessed as previously described (Figure 3.4b). Expression of the indicated proteins was done by immunoblot of the whole cell lysate.

4.3 Overall Conclusions

In conclusion, we have demonstrated the feasibility of a rapid, facile point of care diagnostic technique that, if implemented in the clinic in the future, would allow for early detection and treatment against HCMV infection. Additionally, we have characterized and identified a major role for a highly conserved MCMV deubiquitinating enzyme. As this enzyme represents a uniquely structured viral protein, it may serve as an additional target against which anti-CMV drugs can and will be developed. These two studies fundamentally represent substantial steps forward in CMV diagnosis and identification of possible targets for CMV treatment. Though significant knowledge has been gained as a result of these studies, continued improvements to CMV diagnosis and identification of unique viral contributions to infection must be made in order that CMV-caused diseases may one day be a thing of the past.

Chapter 5: Materials and Methods

5.1 CHAPTER 2 MATERIALS AND METHODS [123]

5.1.1 Chemicals

Water used in each experiment was Milli-Q water. Ferrocyanide was purchased from Fisher Scientific and used without further purification. Ferrocenedimethanol was purchased and used without further purification. Goat anti-mouse IgG (Fc) coated polystyrene particles (0.7–0.9 μm) were purchased from Spherotech and stored at 4 degrees centigrade. Before using the solution, the bottle was vortexed for 1 min and sonicated using a Q500 ultrasonic processor (Qsonica). Potassium nitrate (KNO_3, 99.8%) was purchased from Fisher Scientific. All chemicals were used as received.

5.1.2 Electrochemistry

Electrochemical experiments were performed using a CHI model 900B potentiostat (CH Instruments). The Pt UME was prepared following the general procedure developed in our laboratory [175].The three-electrode cell was placed in a faraday cage and grounded to a pipe. An Ag/AgCl (1 M KCl) wire was used (BASi) as the reference electrode, and a Pt wire was used as the auxiliary electrode. Generally, experiments were performed in a 20-mL glass vial with a homemade vial cap to position the electrodes in the solution.

5.1.3 Optical analysis

DLS was obtained using a Zetasizer Nano ZS (Malvern). NTA was also used to analyze the virus particles by Nanosight. Here, scattering light from a laser illuminates particles. A movie of these particles is taken, and the software traces the movement of the nanoparticle. This movement allows the software to calculate a diffusion coefficient and use the Stokes–Einstein relation to back-calculate the hydrodynamic radius. SEM images were obtained using an FEI Quanta 650 ESEM. The optical images were taken using a Nikon Eclipse TE300 inverted microscope with a 100× objective lens and a camera attachment to the eyepiece.

5.1.4 Virus propagation and purification

Bacterial artificial chromosome derived wild-type MCMV (strain K181-Perth) and MHV68 WUMS [obtained from American Type Culture Collection (ATCC) #VR1465] were generated on NIH 3T3 fibroblasts (ATCC, #CRL-1658) as previously described [176, 177]. Viral stocks were propagated, clarified, and concentrated as previously described [145]. Sorbitol density gradient purification was performed as previously described to purify the virus [178]. Briefly, concentrated virus was resuspended in complete DMEM supplemented with 10% bovine calf serum, layered over 20% sucrose cushion, and centrifuged 60 min at 32,800 × *g*. Pelleted virus was resuspended in Tris-buffered saline (0.05 M Tris, 0.10 M NaCl, pH 7.4), placed onto a 20–70% continuous linear sorbitol gradient, and subjected to ultracentrifugation at 70,000 × *g* for 60 min at 16 °C. Virion band was visualized using light scatter from an overhead

light source, and collected by needle aspiration. Samples were subjected to a second round of ultracentrifugation to remove additional contaminants.

5.1.5 Antibody and bead adsorption

Mouse monoclonal anti-gB neutralizing antibody (Clone MAb97.3) was provided by Michael Mach, University of Erlangen, Germany. Preparation of the MCMV-A samples was as follows: Infectivity experiments were completed to gauge how much antibody would render the virus noninfectious under the assumption that a noninfectious virus is saturated with antibody. A 1:1 (vol/vol) virus to antibody solution was mixed together and allowed to incubate at 37 degrees centigrade for 1 hour. A new sample was made for each experiment, and experiments were performed in triplicate. For the MHV68, a similar method of preparation was performed as for MCMV. For the PSB measurements, a similar procedure was followed. Here, the PSBs were added to the virus and antibody mixture. The PSB, MCMV, MAb 97.3 mixture was incubated at room temperature for another hour.

5.2 CHAPTER 2 MATERIALS AND METHODS [43]

5.2.1 Chemicals

Ferrocene methanol (98%) was purchased from Sigma-Aldrich. Solutions of ferrocene methanol were prepared by sonicating the solution for at least 20 min to dissolve ferrocene. This solution as then passed through a 100-nm pore filter. Glucose

was purchased from Fisher Scientific and used without further purification. In each case, nanopure water was used for the experiments.

5.2.2 Electrochemistry

Electrochemical experiments were performed using a CHI model 900B potentiostat (CH Instruments). The three-electrode cell was placed in a faraday cage and grounded to a pipe. An Ag/AgCl (1 M KCl) wire was used (BASi) as the reference electrode, and a Pt wire was used as the auxiliary electrode.

5.2.3 Electrode fabrication

The Pt UME was prepared following the general procedure developed in our laboratory [175]. Electrodes were fabricated using a laser puller (Sutter Instruments) followed by a soft mechanical polishing until the electrode was 0.5–3 μm in radius. Briefly, a 25-μm-diameter Pt wire was placed in a glass capillary pulled to nanometer dimensions after a laser pulse locally heated and melted the glass and Pt. This electrode was then mechanically polished to the necessary size.

5.2.4 Glucose oxidase conjugation

GOx was covalently attached to purified anti-gB neutralizing antibody. Briefly, MCMV gB antibody, Mab97.3 kindly provided by Michael Mach, University of Erlangen, Erlangen, Germany, was purified from supernatant by way of affinity purification using agarose beads conjugated to protein A/G (Santa Cruz). Purified

antibody was eluted from the protein A/G beads with 0.15% TFA. The elution solvent was removed via vacuum concentration (Speed Vac; Thermo Fisher) and resuspended in 1× PBS (137 mM NaCl, 2.7 mM KCl, 10 mM Na_2HPO_4, and 1.8 mM KH_2PO_4). Antibody concentration was determined via Bradford assay. The conjugation reaction was performed using a Glucose Oxidase Conjugation Kit (ab102887; Abcam) as per the manufacturer's instructions. The conjugate was incubated in the electrochemical samples for 30 min at 4 °C.

5.2.5 Virus purification

Both MCMV and MHV68 virions were prepared as previously described [123]. Briefly, concentrated virus was resuspended in complete DMEM supplemented with 10% (vol/vol) bovine calf serum, layered over 20% (wt/vol) sucrose cushion, and centrifuged 60 min at 32,800 × *g*. Pelleted virus was resuspended in Tris-buffered saline (0.05 M Tris and 0.10 M NaCl, pH 7.4), placed onto a 20–70% (wt/vol) continuous linear sorbitol gradient, and subjected to ultracentrifugation at 70,000 × *g* for 60 min at 16 °C. The virion band was visualized using light scatter from an overhead light source and collected by needle aspiration. Samples were subjected to a second round of ultracentrifugation to remove additional contaminants.

5.2.6 Animal infections

C57BL/6J mice were infected with 10^6 pfu of WT MCMV via i.p. route of infection. Urine collection was performed at 3, 5, 7, 10, and 14 d post-infection. Control mice were infected with media only. Animals were maintained by the Animal Resources

Center (ARC) at the University of Texas at Austin in accordance with Institutional guidelines, and all procedures were approved by the University of Texas at Austin Institutional Animal Care and Use Committee.

5.3 CHAPTER 3 MATERIALS AND METHODS

5.3.1 Plasmids and transfections

Transfections were performed with GenJet *in vitro*transfection reagent (Ver. II; SignaGen Laboratories) per the manufacturer's instructions. Carboxy-terminal 3XFLAG epitope-tagged MCK2 was generated by PCR amplification of nucleotides 188352 to 187431 from pARK25 (Redwood et al, 2005), a bacterial artificial chromosome (BAC) containing the K181 (Perth) strain MCMV (GenBank accession number AM886412.1). Amplicons were cloned into the *EcoRI* and *XbaI*sites of p3XFLAG–CMV-14 (Sigma-Aldrich). An untagged MCK2 expression construct was similarly generated by PCR and the resulting amplicon cloned into the *KpnI* and *BamHI* sites of pcDNA3.1(+). Carboxy-terminal EGFP-tagged M48 and $M48^{C23S}$ were generated by PCR amplification of nucleotides 67043 to 67897 (amino acids [a.a.] 1 to 285) or 67043 to 73483 (full length) of either WT BAC or $M48^{C23S}$ BAC, respectively. Both the full-length and $M48^{(1–285)}$ constructs were cloned into the *HindIII* and *KpnI* sites of pEGFP-N1 (Clontech). Plasmids pQE9-His-p97(wt) and pQE9-p97(QQ) (Addgene plasmids 14666 and 14667, respectively) were a gift from Graham Warren (Meyer et al, 2000; Ye et al, 2001). Insertions were amplified by PCR with an N-terminal 6-His tag and cloned into the *KpnI* and *BamHI* sites of pcDNA3.1(+).

5.3.2 Cells

NIH3T3 murine fibroblasts (ATCC CRL-1658) were propagated in Dulbecco's modified Eagle's medium (DMEM; Sigma-Aldrich) containing 10% heat-inactivated bovine calf serum (BCS; Life Technologies, Inc.) and 1% penicillin-streptomycin-glutamine (Life Technologies, Inc.). RAW264.7 murine macrophages (ATCC TIB-71) and SVEC4-10 endothelial cells (ATCC CRL-2181) were propagated in DMEM (Sigma) containing 10% heat-inactivated fetal calf serum (Life Technologies, Inc.) and 1% penicillin-streptomycin-glutamine (Life Technologies, Inc.).

5.3.3 BAC mutagenesis and recombinant viruses

pSIM6 plasmid, containing genes necessary for λ-red recombination, was introduced into bacteria containing pARK25 (Redwood et al, 2005). Recombineering for K181-BAC mutagenesis was performed as previously described (Upton et al, 2010). Genome integrity was confirmed by restriction fragment length polymorphism analysis, and mutagenesis was verified by PCR, restriction digest, and sequencing of the targeted region of *M48* and *m131*. BAC-derived parental and recombinant viruses were generated and purified as previously described (Redwood et al, 2005). Viruses were propagated, clarified, and concentrated, and the titers were determined by plaque assay on NIH3T3 cells as previously described (Saederup et al, 1999). Growth curve experiments were performed in 12-well plates at the indicated multiplicity of infection (MOI) in 0.4 ml for 2 h at 37°C. After adsorption, cells infected at an MOI of 5.0 were washed twice with

phosphate-buffered saline (PBS) and refed. Cells infected at an MOI of 0.05 in a volume of 0.4 ml were given additional complete DMEM to reach a volume of 1 ml. Cells and supernatants were harvested at the indicated times, and titers were determined via plaque assay on NIH3T3 fibroblasts.

5.3.4 Immunoprecipitation and immunoblotting

Culture supernatants collected from MCK2/M48-cotransfected cells were cleared of cell debris by spinning at 5,000 × *g* for 15 min. IPs were performed by adding anti-FLAG M2-agarose slurry (Sigma-Aldrich) followed by incubation on an orbital rotator overnight at 4°C. Cell lysates and IP samples were separated by SDS-PAGE on 10% acrylamide gels or Mini-Protean TGX precase 4% to 20% gradient gels (Bio-Rad). Proteins were transferred to nitrocellulose membranes (GE Healthcare Life Sciences) and subjected to immunoblot analysis with indicated antibodies. The following antibodies were used in immunoblot analyses: mouse anti-MCK2 (clone 11D7; gift from Peggy MacDonald, the Rockefeller University), mouse anti-m123/IE1 (Chroma101; Center for proteomics, University of Rijeka), mouse anti-m112-113/E1 (Chroma103; Center for proteomics, University of Rijeka), rabbit anti-M86 (MCP) (gift from Laura Hanson, Texas Woman's University), mouse anti-β-actin (clone AC-74; Sigma-Aldrich), mouse anti-GFP (clone 4B10; Cell Signaling Technology, Inc.), mouse anti-FLAG M2-peroxidase (clone M2; Sigma-Aldrich), mouse anti-ubiquitin (clone P4D1; Santa Cruz), mouse anti-6-His (THE His Tag antibody; GenScript), anti-mouse IgG-horseradish

peroxidase (IgG-HRP) (Vector Laboratories), and anti-rabbit IgG-HRP (Vector Laboratories).

5.3.5 PNGase F treatment

PNGase F treatments were performed according to the protocol of the manufacturer (NEB) for denaturing conditions. Briefly, whole-cell lysate in NP-40 lysis buffer (1% NP-40, 150 mM NaCl, 50 mM Tris-HCl—pH 8.0) was diluted with denaturing buffer and boiled for 10 min. Reaction buffer (10×; diluted to 1×), NP-40 (1%), and PNGase F were added, and the reaction mixture was incubated at 37°C for 1 h. Samples were then analyzed by immunoblotting.

5.3.6 Virus purification

Virions were purified over a 20% to 70% linear sorbitol gradient as described previously [123]. Briefly, extracellular virions were collected from infected cell supernatants via centrifugation at 20,000 × *g* for 1.5 h at 4°C. Virion pellets were collected and then passed over a 20% sucrose cushion for 1 h at 16°C and 32,800 × *g*. The cushion-purified virus was resuspended in 1 ml of TN buffer (50 mM Tris-HCl and 100 mM NaCl, pH 7.4), briefly sonicated, and placed on the top of the linear gradient. Gradients were centrifuged at 76,000 × *g* in an SW41 swinging-bucket rotor for 1 h at 16°C. Virion-containing bands were collected by aspiration, diluted in buffer, and pelleted by centrifugation at 100,000 × *g* for 3 h at 16°C.

5.3.7 Sample preparation for LC-MS/MS analysis

Pelleted virions were resuspended in TN buffer, and 2,2,2-trifluoroethanol (TFE) (Sigma-Aldrich) was added to reach a final concentration of 50% TFE. Proteins were reduced with 5 mM tris(2-carboxyethyl)phosphine (TCEP) for 45 min at 55°C followed by alkylation with 15 mM chloroacetamide at room temperature, in the dark, for 30 min. Excess chloroacetamide was quenched with 20 mM dithiothreitol (DTT), and samples were diluted 10-fold to reach a final concentration of 5% TFE–digestion buffer (50 mM Tris [pH 8.0], 2 mM $CaCl_2$). Trypsin was added to reach a final concentration of 1:50 (enzyme/protein), and the digests were incubated at 37°C for 5 h. The digests were quenched by addition of formic acid to reach a final concentration of 1%. Tryptic digests were vacuum centrifuged to reduce the volume to approximately 100 to 150 μl. Buffer exchange was performed with Hypersep SpinTip C18 SPE tips (Thermo Scientific) according to the manufacturer instructions. Briefly, resin was washed 3 times with a 60% acetonitrile–0.1% formic acid solution and then equilibrated with buffer A (0.1% formic acid–water). Peptides were passed over the resin, after which bound peptides were washed 3 times with buffer A and eluted with the 60% acetonitrile–0.1% formic acid solution. Eluted peptides were briefly dried via vacuum centrifugation and resuspended in 5% acetonitrile–0.1% formic acid. Peptides were stored at −80°C until liquid chromatography-tandem mass spectrometry (LC-MS/MS) analysis.

5.3.8 LC-MS/MS analysis

Samples were analyzed by liquid chromatography-tandem mass spectrometry (LC-MS/MS), with a minimum of three replicate injections analyzed per sample. Peptides were separated by reverse-phase chromatography on a Dionex Ultimate 3000 nanoRSLC system (Thermo Scientific) with an Acclaim PepMap 100 RSLC C_{18} column (Thermo Scientific) (15 cm), using an acetonitrile gradient (3% to 38% over 215 min). Eluting peptides were directly analyzed by nano-electrospray ionization-tandem mass spectrometry on an Orbitrap Velos Pro mass spectrometer (Thermo Scientific). Full spectra (MS1) were collected at a resolution of 100,000. Fragmentation spectra (MS2) were collected in a data-dependent manner, with ions required to carry a charge of +2 or greater for MS2 selection, and up to 20 MS2 scans were collected per round. Dynamic exclusion was employed, whereby ions selected twice within 30 s were excluded from selection for 45 s.

5.3.9 MS data analysis and protein quantitation

A searchable protein sequence database was constructed from MCMV (strain K181) and mouse reference proteomes (UniProt) and common contaminants (from the MaxQuant website; **http://maxquant.org/downloads.htm**). MS spectra were searched against this database using SEQUEST (Proteome Discoverer 1.4; Thermo Scientific). The database was curated to include the m129/m131 spliced product. Fully tryptic peptides with up to 2 missed cleavages were considered. Mass tolerance filters of 10 ppm (MS1) and 0.5 Da (MS2) were applied. Modifications of cysteine carbamidomethylation (static;

+57.0215 Da) and methionine oxidation (dynamic; +15.9949 Da) were allowed, with no more than three modifications allowed per peptide-spectrum match (PSM). False-discovery rates (FDR) for PSMs were determined by decoy database error modeling using Percolator (Proteome Discoverer 1.4; Thermo Scientific), and a set of high-confidence PSMs were selected for further analysis at an FDR of <1%. Extracted-ion chromatograms (XICs) of MCMV-derived peptides were manually inspected using the Skyline software package [179] to identify target ions exhibiting minimal interference and limited variability across replicate injections. The top three highest-quality target ions were selected for each protein of interest and XIC peak areas exported for calculation of relative abundances. XIC peak areas were first normalized to the major capsid protein M86 (MCP) by dividing XIC peak areas by the mean of the values determined for the three M86 (MCP) target ions. Normalized values were averaged across replicate injections and used to calculate the target ion ratios between $M48^{C23S}$ and $M48^{Rep}$ samples. Finally, mean averages and standard deviations of target ion ratios were calculated for each protein.

5.3.10 Animal experiments

C57BL/6J mice were obtained from the Jackson Laboratory. Animals were bred and maintained at the Animal Resources Center (ARC) at the University of Texas at Austin in accordance with Institutional guidelines, and all procedures were approved by the University of Texas at Austin Institutional Animal Care and Use Committee. Six- to 10-week-old male and female animals were infected with 10^6 PFU by inoculation into a

rear footpad or by intraperitoneal (i.p.) injection, as previously described [180]. Upon sacrifice, organs were placed into 1 ml of complete DMEM, subjected to a single freeze/thaw cycle (−80°C), and disrupted by sonication. Organ homogenates were serially diluted, and the titers were determined by plaque assay on NIH3T3 fibroblasts. Footpad measurements were taken at the indicated time points with a digital caliper, as previously described [144]. Unless otherwise indicated, each time point represents *n* of ≥5.

5.3.11 Fluorescence microscopy

NIH3T3 cells were grown to the desired confluency in a 6-well plate before being transfected with 1 μg of either pEGFP-N1 empty vector (EV), pEGFPN-1-M48, or pEGFPN-1-M48^{C23S}. 24 hours post transfections, cells were washed twice with 1X phosphate buffered saline (PBS) before being fixed in 4% paraformaldehyde for 20 minutes at room temperature. After 3 washes in 1X PBS, cells were permeabilized with 0.5% Triton X-100 (in 1X PBS) on ice for 10 minutes. After 3 more washes with 1X PBS, cells were incubated at room temperature with Hoechst stain for 10 minutes. After 1 more wash with 1X PBS, cells were visualized under an EVOS FL inverted fluorescence microscope.

5.4 CHAPTER 4 MATERIALS AND METHODS

5.3.1 Plasmids and transfections

Transfections were performed with GenJet *in vitro*transfection reagent (Ver. II; SignaGen Laboratories) per the manufacturer's instructions. Carboxy-terminal 3XFLAG epitope-tagged MCK2 was generated by PCR amplification of nucleotides 188352 to 187431 from pARK25 [176], a bacterial artificial chromosome (BAC) containing the K181 (Perth) strain MCMV (GenBank accession number AM886412.1). Amplicons were cloned into the *EcoRI* and *XbaI*sites of p3XFLAG–CMV-14 (Sigma-Aldrich). Wildtype UL48 (myc_6-UL48) as well as mutant DUB UL48 (myc_6-UL48^{C24S}) were kindly provided by Jin-Hyun Ahn (Department of Molecular Cell Biology, Samsung Biomedical Research Institute, Sungkyunkwan University School of Medicine, Suwon, Republic of Korea) [97].

5.3.4 Phyre2 analysis

Amino acids 1-300 of HCMV UL48 (Towne strain; GenBank FJ616285.1) were analyzed using the online protein fold recognition server, Phyre2 [171]. The obtained results indicated that 80% of the UL48 sequence (1-300) matched with 100% confidence to the previously crystalized M48 DUB [71]. Conserved residues in the beta-hairpin of UL48 were mapped using Jmol [181].

5.3.5 Immunoprecipitation and immunoblotting

Culture supernatants collected from MCK2/M48-cotransfected cells were cleared of cell debris by spinning at 5,000 × *g* for 15 min. IPs were performed by adding anti-FLAG M2-agarose slurry (Sigma-Aldrich) followed by incubation on an orbital rotator

overnight at 4°C. Cell lysates and IP samples were separated by SDS-PAGE on 10% acrylamide gels or Mini-Protean TGX precast 4% to 20% gradient gels (Bio-Rad). Proteins were transferred to nitrocellulose membranes (GE Healthcare Life Sciences) and subjected to immunoblot analysis with indicated antibodies. The following antibodies were used in immunoblot analyses: mouse anti-FLAG M2-peroxidase (clone M2; Sigma-Aldrich), rabbit anti-myc-peroxidase (Sigma-Aldrich), and mouse anti-β-actin (clone AC-74; Sigma-Aldrich).

References

1. Gupta, R.K., et al., Evolving uses of oral reverse transcriptase inhibitors in the HIV-1 epidemic: from treatment to prevention. Retrovirology, 2013. 10: p. 82.

2. Cytomegalovirus (CMV) and Congenital CMV Infection. 2016; Available from: https://www.cdc.gov/cmv/overview.html.

3. Sun, X., et al., Sero-epidemiological survey of human cytomegalovirus-infected children in Weifang (Eastern China) between 2009 and 2012. Virol J, 2013. 10: p. 42.

4. Davison, A.J., Comparative analysis of the genomes, in Human Herpesviruses: Biology, Therapy, and Immunoprophylaxis, A. Arvin, et al., Editors. 2007: Cambridge.

5. Kling, C. and D. Kabelitz, Congenital HCMV and assisted reproduction: Why not use the chance for primary screening? Arch Gynecol Obstet, 2015. 291(6): p. 1205-11.

6. Bhat, V., et al., Cytomegalovirus infection in the bone marrow transplant patient. World J Transplant, 2015. 5(4): p. 287-91.

7. Kepler, G.M., et al., A Model for HCMV Infection in Immunosuppressed Patients. Math Comput Model, 2009. 49(7-8): p. 1653-1663.

8. Peggs, K.S. and S. Mackinnon, Cytomegalovirus: the role of CMV post-haematopoietic stem cell transplantation. Int J Biochem Cell Biol, 2004. 36(4): p. 695-701.

9. Santos, C.A., Cytomegalovirus and Other beta-Herpesviruses. Semin Nephrol, 2016. 36(5): p. 351-361.

10. Anderholm, K.M., C.J. Bierle, and M.R. Schleiss, Cytomegalovirus Vaccines: Current Status and Future Prospects. Drugs, 2016. 76(17): p. 1625-1645.

11. El Chaer, F., D.P. Shah, and R.F. Chemaly, How I treat resistant cytomegalovirus infection in hematopoietic cell transplantation recipients. Blood, 2016. 128(23): p. 2624-2636.

12. Lurain, N.S. and S. Chou, Antiviral drug resistance of human cytomegalovirus. Clin Microbiol Rev, 2010. 23(4): p. 689-712.

13. Bowman, L.J., J.I. Melaragno, and D.C. Brennan, Letermovir for the management of cytomegalovirus infection. Expert Opin Investig Drugs, 2017. 26(2): p. 235-241.

14. Verghese, P.S. and M.R. Schleiss, Letermovir Treatment of Human Cytomegalovirus Infection Antiinfective Agent. Drugs Future, 2013. 38(5): p. 291-298.

15. Kollias, C.M., et al., Animal models of herpes simplex virus immunity and pathogenesis. J Neurovirol, 2015. 21(1): p. 8-23.

16. Jurak, I. and W. Brune, Induction of apoptosis limits cytomegalovirus cross-species infection. EMBO J, 2006. 25(11): p. 2634-42.

17. Qin, W., et al., Generating Mouse Models Using CRISPR-Cas9-Mediated Genome Editing. Curr Protoc Mouse Biol, 2016. 6(1): p. 39-66.

18. Rawlinson, W.D., H.E. Farrell, and B.G. Barrell, Analysis of the complete DNA sequence of murine cytomegalovirus. J Virol, 1996. 70(12): p. 8833-49.

19. Schleiss, M.R., Nonprimate models of congenital cytomegalovirus (CMV) infection: gaining insight into pathogenesis and prevention of disease in newborns. ILAR J, 2006. 47(1): p. 65-72.

20. Krmpotic, A., et al., Pathogenesis of murine cytomegalovirus infection. Microbes Infect, 2003. 5(13): p. 1263-77.

21. Cytomegalovirus (CMV) and Congenital Infection: Diagnosing CMV. 2016; Available from: https://www.cdc.gov/cmv/clinical/features.html.

22. Prince, H.E. and M. Lape-Nixon, Role of cytomegalovirus (CMV) IgG avidity testing in diagnosing primary CMV infection during pregnancy. Clin Vaccine Immunol, 2014. 21(10): p. 1377-84.

23. Ross, S.A., et al., Diagnosis of Cytomegalovirus Infections. Infectious disorders drug targets, 2011. 11(5): p. 466-474.

24. Adler, S.P., Screening for cytomegalovirus during pregnancy. Infect Dis Obstet Gynecol, 2011. 2011: p. 1-9.

25. Cahill, A.G., et al., Screening and treating for primary cytomegalovirus infection in pregnancy: where do we stand? A decision-analytic and economic analysis. Am J Obstet Gynecol, 2009. 201(5): p. 466 e1-7.

26. Bard, A.J. and L.R. Faulkner, Electrochemical Methods: Fundamentals and Applications. 2001.

27. Adams, K.L., M. Puchades, and A.G. Ewing, In Vitro Electrochemistry of Biological Systems. Annu Rev Anal Chem (Palo Alto Calif), 2008. 1: p. 329.

28. Zhu, C., et al., Electrochemical sensors and biosensors based on nanomaterials and nanostructures. Anal Chem, 2015. 87(1): p. 230-49.

29. Heller, A. and B. Feldman, Electrochemical glucose sensors and their applications in diabetes management. Chem Rev, 2008. 108(7): p. 2482-505.

30. Jayanthi, V.S., A.B. Das, and U. Saxena, Recent advances in biosensor development for the detection of cancer biomarkers. Biosens Bioelectron, 2016. 91: p. 15-23.

31. Zhan, W. and A.J. Bard, Electrogenerated chemiluminescence. 83. Immunoassay of human C-reactive protein by using Ru(bpy)3(2+)-encapsulated liposomes as labels. Anal Chem, 2007. 79(2): p. 459-63.

32. Wang, Y. and T.V. Duncan, Nanoscale sensors for assuring the safety of food products. Curr Opin Biotechnol, 2016. 44: p. 74-86.

33. Walter, N.G., et al., Do-it-yourself guide: how to use the modern single-molecule toolkit. Nat Methods, 2008. 5(6): p. 475-89.

34. Ha, T., Single-molecule methods leap ahead. Nat Methods, 2014. 11(10): p. 1015-8.

35. Fan, F.R. and A.J. Bard, Electrochemical detection of single molecules. Science, 1995. 267(5199): p. 871-4.

36. Quinn, B.M., P. van 't Hof, and S.G. Lemay, Time-resolved electrochemical detection of discrete adsorption events. Journal of the American Chemical Society, 2004. 126(27): p. 8360-8361.

37. Dick, J.E., C. Renault, and A.J. Bard, Observation of Single-Protein and DNA Macromolecule Collisions on Ultramicroelectrodes. Journal of the American Chemical Society, 2015. 137(26): p. 8376-8379.

38. Dick, J.E. and A.J. Bard, Recognizing Single Collisions of PtCl6(2-) at Femtomolar Concentrations on Ultramicroelectrodes by Nucleating Electrocatalytic Clusters. J Am Chem Soc, 2015. 137(43): p. 13752-5.

39. Dick, J.E. and A.J. Bard, Toward the Digital Electrochemical Recognition of Cobalt, Iridium, Nickel, and Iron Ion Collisions by Catalytic Amplification. J Am Chem Soc, 2016. 138(27): p. 8446-52.

40. Park, J.H., et al., Single Collision Events of Conductive Nanoparticles Driven by Migration. Journal of Physical Chemistry C, 2013. 117(13): p. 6651-6657.

41. Einstein, A., Über die von der molekularkinetischen Theorie der Wärme geforderte Bewegung von in ruhenden Flüssigkeiten suspendierten Teilchen. Annalen der Physik, 1905. 322(8): p. 549-560.

42. Dick, J.E., Electrochemical detection of single cancer and healthy cell collisions on a microelectrode. Chem Commun (Camb), 2016. 52(72): p. 10906-9.

43. Dick, J.E., et al., Enzymatically enhanced collisions on ultramicroelectrodes for specific and rapid detection of individual viruses. Proc Natl Acad Sci U S A, 2016. 113(23): p. 6403-8.

44. Li, J., Q.Y. Chai, and C.H. Liu, The ubiquitin system: a critical regulator of innate immunity and pathogen-host interactions. Cell Mol Immunol, 2016. 13(5): p. 560-76.

45. Pertea, M. and S.L. Salzberg, Between a chicken and a grape: estimating the number of human genes. Genome Biol, 2010. 11(5): p. 206.

46. Yau, R. and M. Rape, The increasing complexity of the ubiquitin code. Nat Cell Biol, 2016. 18(6): p. 579-86.

47. Ordureau, A., et al., Defining roles of PARKIN and ubiquitin phosphorylation by PINK1 in mitochondrial quality control using a ubiquitin replacement strategy. Proc Natl Acad Sci U S A, 2015. 112(21): p. 6637-42.

48. Cunningham, C.N., et al., USP30 and parkin homeostatically regulate atypical ubiquitin chains on mitochondria. Nat Cell Biol, 2015. 17(2): p. 160-9.

49. Ordureau, A., et al., Quantitative proteomics reveal a feedforward mechanism for mitochondrial PARKIN translocation and ubiquitin chain synthesis. Mol Cell, 2014. 56(3): p. 360-75.

50. Sarraf, S.A., et al., Landscape of the PARKIN-dependent ubiquitylome in response to mitochondrial depolarization. Nature, 2013. 496(7445): p. 372-6.

51. Wickliffe, K.E., et al., K11-linked ubiquitin chains as novel regulators of cell division. Trends Cell Biol, 2011. 21(11): p. 656-63.

52. Matsumoto, M.L., et al., K11-linked polyubiquitination in cell cycle control revealed by a K11 linkage-specific antibody. Mol Cell, 2010. 39(3): p. 477-84.

53. Qin, Y., et al., RNF26 temporally regulates virus-triggered type I interferon induction by two distinct mechanisms. PLoS Pathog, 2014. 10(9): p. e1004358.

54. Birsa, N., et al., Lysine 27 ubiquitination of the mitochondrial transport protein Miro is dependent on serine 65 of the Parkin ubiquitin ligase. J Biol Chem, 2014. 289(21): p. 14569-82.

55. Wang, Q., et al., The E3 ubiquitin ligase AMFR and INSIG1 bridge the activation of TBK1 kinase by modifying the adaptor STING. Immunity, 2014. 41(6): p. 919-33.

56. Zhou, H.L., et al., The p97-UBXD8 complex destabilizes mRNA by promoting release of ubiquitinated HuR from mRNP. Genes Dev, 2013. 27(9): p. 1046-58.

57. Yuan, W.C., et al., K33-Linked Polyubiquitination of Coronin 7 by Cul3-KLHL20 Ubiquitin E3 Ligase Regulates Protein Trafficking. Mol Cell, 2014. 54(4): p. 586-600.

58. Reyes-Turcu, F.E., K.H. Ventii, and K.D. Wilkinson, Regulation and cellular roles of ubiquitin-specific deubiquitinating enzymes. Annu Rev Biochem, 2009. 78: p. 363-97.

59. Clague, M.J., J.M. Coulson, and S. Urbe, Cellular functions of the DUBs. J Cell Sci, 2012. 125(Pt 2): p. 277-86.

60. Randow, F.L., P.J., Viral avoidance and exploitation of the ubiquitin system. Nat Cell Biol, 2009. 11(5).

61. Gan, J., et al., Manipulation of ubiquitin/SUMO pathways in human herpesviruses infection. Rev Med Virol, 2016. 26(6): p. 435-445.

62. Lanfranca, M.P., H.H. Mostafa, and D.J. Davido, HSV-1 ICP0: An E3 Ubiquitin Ligase That Counteracts Host Intrinsic and Innate Immunity. Cells, 2014. 3(2): p. 438-54.

63. Brulois, K., et al., Kaposi's sarcoma-associated herpesvirus K3 and K5 ubiquitin E3 ligases have stage-specific immune evasion roles during lytic replication. J Virol, 2014. 88(16): p. 9335-49.

64. Smith, C.M., et al., Murine gammaherpesvirus-68 inhibits antigen presentation by dendritic cells. PLoS One, 2007. 2(10): p. e1048.

65. van den Boomen, D.J. and P.J. Lehner, Identifying the ERAD ubiquitin E3 ligases for viral and cellular targeting of MHC class I. Mol Immunol, 2015. 68(2 Pt A): p. 106-11.

66. Kattenhorn, L.M., et al., A deubiquitinating enzyme encoded by HSV-1 belongs to a family of cysteine proteases that is conserved across the family Herpesviridae. Mol Cell, 2005. 19(4): p. 547-57.

67. Guo, H., et al., Role of tegument proteins in herpesvirus assembly and egress. Protein Cell, 2010. 1(11): p. 987-98.

68. Bechtel, J.T. and T. Shenk, Human cytomegalovirus UL47 tegument protein functions after entry and before immediate-early gene expression. J Virol, 2002. 76(3): p. 1043-50.

69. Cardone, G., et al., The UL36 tegument protein of herpes simplex virus 1 has a composite binding site at the capsid vertices. J Virol, 2012. 86(8): p. 4058-64.

70. Das, S., et al., Identification of human cytomegalovirus genes important for biogenesis of the cytoplasmic virion assembly complex. J Virol, 2014. 88(16): p. 9086-99.

71. Schlieker, C., et al., Structure of a Herpesvirus-Encoded Cysteine Protease Reveals a Unique Class of Deubiquitinating Enzymes. Molecular cell, 2007. 25(5): p. 677-687.

72. Wang, S., et al., Herpes simplex virus 1 ubiquitin-specific protease UL36 inhibits beta interferon production by deubiquitinating TRAF3. J Virol, 2013. 87(21): p. 11851-60.

73. Ye, R., et al., Herpes Simplex Virus Type 1 Ubiquitin-specific Protease UL36 abrogates NF-kappaB Activation in DNA Sensing Signal Pathway. J Virol, 2016.

74. Liang, C., et al., A high-temperature passaging attenuated Pseudorabies vaccine protects piglets completely against emerging PRV variant. Res Vet Sci, 2017. 112: p. 109-115.

75. Bottcher, S., et al., Mutagenesis of the active-site cysteine in the ubiquitin-specific protease contained in large tegument protein pUL36 of pseudorabies virus impairs viral replication in vitro and neuroinvasion in vivo. J Virol, 2008. 82(12): p. 6009-16.

76. Lee, J.I., et al., A herpesvirus encoded deubiquitinase is a novel neuroinvasive determinant. PLoS Pathog, 2009. 5(4): p. e1000387.

77. Huffmaster, N.J., et al., Dynamic ubiquitination drives herpesvirus neuroinvasion. Proc Natl Acad Sci U S A, 2015. 112(41): p. 12818-23.

78. McPherson, M.C. and M.E. Delany, Virus and host genomic, molecular, and cellular interactions during Marek's disease pathogenesis and oncogenesis. Poult Sci, 2016. 95(2): p. 412-29.

79. Jarosinski, K., et al., A herpesvirus ubiquitin-specific protease is critical for efficient T cell lymphoma formation. Proc Natl Acad Sci U S A, 2007. 104(50): p. 20025-30.

80. Veiga, I.B., et al., Marek's disease virus (MDV) ubiquitin-specific protease (USP) performs critical functions beyond its enzymatic activity during virus replication. Virology, 2013. 437(2): p. 110-7.

81. Dittmer, D.P. and B. Damania, Kaposi sarcoma-associated herpesvirus: immunobiology, oncogenesis, and therapy. J Clin Invest, 2016. 126(9): p. 3165-75.

82. Gonzalez, C.M., L. Wang, and B. Damania, Kaposi's sarcoma-associated herpesvirus encodes a viral deubiquitinase. J Virol, 2009. 83(19): p. 10224-33.

83. Inn, K.S., et al., Inhibition of RIG-I-mediated signaling by Kaposi's sarcoma-associated herpesvirus-encoded deubiquitinase ORF64. J Virol, 2011. 85(20): p. 10899-904.

84. Rajcani, J. and M. Kudelova, Murine herpesvirus pathogenesis: a model for the analysis of molecular mechanisms of human gamma herpesvirus infections. Acta Microbiol Immunol Hung, 2005. 52(1): p. 41-71.

85. Gredmark, S., et al., A functional ubiquitin-specific protease embedded in the large tegument protein (ORF64) of murine gammaherpesvirus 68 is active during the course of infection. J Virol, 2007. 81(19): p. 10300-9.

86. Gredmark-Russ, S., et al., A gammaherpesvirus ubiquitin-specific protease is involved in the establishment of murine gammaherpesvirus 68 infection. J Virol, 2009. 83(20): p. 10644-52.

87. Sun, C., et al., Evasion of innate cytosolic DNA sensing by a gammaherpesvirus facilitates establishment of latent infection. J Immunol, 2015. 194(4): p. 1819-31.

88. Young, L.S., L.F. Yap, and P.G. Murray, Epstein-Barr virus: more than 50 years old and still providing surprises. Nat Rev Cancer, 2016. 16(12): p. 789-802.

89. Schlieker, C., et al., A deubiquitinating activity is conserved in the large tegument protein of the herpesviridae. J Virol, 2005. 79(24): p. 15582-5.

90. Whitehurst, C.B., et al., The Epstein-Barr virus (EBV) deubiquitinating enzyme BPLF1 reduces EBV ribonucleotide reductase activity. J Virol, 2009. 83(9): p. 4345-53.

91. Gastaldello, S., et al., A deneddylase encoded by Epstein-Barr virus promotes viral DNA replication by regulating the activity of cullin-RING ligases. Nat Cell Biol, 2010. 12(4): p. 351-61.

92. van der Veen, A.G. and H.L. Ploegh, Ubiquitin-like proteins. Annu Rev Biochem, 2012. 81: p. 323-57.

93. Rialland, M., F. Sola, and C. Santocanale, Essential role of human CDT1 in DNA replication and chromatin licensing. J Cell Sci, 2002. 115(Pt 7): p. 1435-40.

94. Whitehurst, C.B., et al., Epstein-Barr virus BPLF1 deubiquitinates PCNA and attenuates polymerase eta recruitment to DNA damage sites. J Virol, 2012. 86(15): p. 8097-106.

95. van Gent, M., et al., Epstein-Barr virus large tegument protein BPLF1 contributes to innate immune evasion through interference with toll-like receptor signaling. PLoS Pathog, 2014. 10(2): p. e1003960.

96. Saito, S., et al., Epstein-Barr virus deubiquitinase downregulates TRAF6-mediated NF-kappaB signaling during productive replication. J Virol, 2013. 87(7): p. 4060-70.

97. Kim, E.T., et al., Cleavage specificity of the UL48 deubiquitinating protease activity of human cytomegalovirus and the growth of an active-site mutant virus in cultured cells. J Virol, 2009. 83(23): p. 12046-56.

98. Kim, Y.E., et al., Involvement of the N-Terminal Deubiquitinating Protease Domain of Human Cytomegalovirus UL48 Tegument Protein in Autoubiquitination, Virion Stability, and Virus Entry. J Virol, 2016. 90(6): p. 3229-42.

99. Zhang, L., Z. Xu, and S. Dong, Electrogenerated chemiluminescence biosensor based on Ru(bpy)3(2+) and dehydrogenase immobilized in sol-gel/chitosan/poly(sodium 4-styrene sulfonate) composite material. Anal Chim Acta, 2006. 575(1): p. 52-6.

100. Uludag, Y., et al., An integrated lab-on-a-chip-based electrochemical biosensor for rapid and sensitive detection of cancer biomarkers. Anal Bioanal Chem, 2016. 408(27): p. 7775-7783.

101. Sepunaru, L., et al., Rapid electrochemical detection of single influenza viruses tagged with silver nanoparticles. Chemical Science, 2016. 7(6): p. 3892-3899.

102. Monzo, J., et al., Fundamentals, achievements and challenges in the electrochemical sensing of pathogens. Analyst, 2015. 140(21): p. 7116-7128.

103. Xiao, X. and A.J. Bard, Observing single nanoparticle collisions at an ultramicroelectrode by electrocatalytic amplification. J Am Chem Soc, 2007. 129(31): p. 9610-2.

104. Zhou, Y.G., N.V. Rees, and R.G. Compton, The electrochemical detection and characterization of silver nanoparticles in aqueous solution. Angew Chem Int Ed Engl, 2011. 50(18): p. 4219-21.

105. Zhou, H.J., F.R.F. Fan, and A.J. Bard, Observation of Discrete Au Nanoparticle Collisions by Electrocatalytic Amplification Using Pt Ultramicroelectrode Surface Modification. Journal of Physical Chemistry Letters, 2010. 1(18): p. 2671-2674.

106. Zhou, Y.G., et al., The charge transfer kinetics of the oxidation of silver and nickel nanoparticles via particle-electrode impact electrochemistry. Phys Chem Chem Phys, 2012. 14(41): p. 14354-7.

107. Haddou, B., N.V. Rees, and R.G. Compton, Nanoparticle-electrode impacts: the oxidation of copper nanoparticles has slow kinetics. Physical Chemistry Chemical Physics, 2012. 14(39): p. 13612-13617.

108. Kwon, S.J., F.R.F. Fan, and A.J. Bard, Observing Iridium Oxide (IrOx) Single Nanoparticle Collisions at Ultramicroelectrodes. Journal of the American Chemical Society, 2010. 132(38): p. 13165-13167.

109. Boika, A., S.N. Thorgaard, and A.J. Bard, Monitoring the Electrophoretic Migration and Adsorption of Single Insulating Nanoparticles at Ultramicroelectrodes. Journal of Physical Chemistry B, 2013. 117(16): p. 4371-4380.

110. Cheng, W., X.F. Zhou, and R.G. Compton, Electrochemical Sizing of Organic Nanoparticles. Angewandte Chemie-International Edition, 2013. 52(49): p. 12980-12982.

111. Fernando, A., S. Parajuli, and M.A. Alpuche-Aviles, Observation of Individual Semiconducting Nanoparticle Collisions by Stochastic Photoelectrochemical Currents. Journal of the American Chemical Society, 2013. 135(30): p. 10894-10897.

112. Sardesai, N.P., D. Andreescu, and S. Andreescu, Electroanalytical Evaluation of Antioxidant Activity of Cerium Oxide Nanoparticles by Nanoparticle Collisions at Microelectrodes. Journal of the American Chemical Society, 2013. 135(45): p. 16770-16773.

113. Stuart, E.J.E., et al., Electrochemical Observation of Single Collision Events: Fullerene Nanoparticles. Acs Nano, 2014. 8(8): p. 7648-7654.

114. Kwon, S.J. and A.J. Bard, DNA analysis by application of Pt nanoparticle electrochemical amplification with single label response. J Am Chem Soc, 2012. 134(26): p. 10777-9.

115. Griffiths, P., I. Baraniak, and M. Reeves, The pathogenesis of human cytomegalovirus. J Pathol, 2015. 235(2): p. 288-97.

116. Dollard, S.C., S.D. Grosse, and D.S. Ross, New estimates of the prevalence of neurological and sensory sequelae and mortality associated with congenital cytomegalovirus infection. Rev Med Virol, 2007. 17(5): p. 355-63.

117. Cekinovic, D., et al., Passive immunization reduces murine cytomegalovirus-induced brain pathology in newborn mice. J Virol, 2008. 82(24): p. 12172-80.

118. Davies, C.W., The conductance of potassium ferrocyanide solutions. Journal of the American Chemical Society, 1937. 59: p. 1760-1761.

119. Kolthoff, I.M. and W.J. Tomsicek, The oxidation potential of the system potassium ferrocyanide-potassium ferricyanide at various ionic strengths. Journal of Physical Chemistry, 1935. 39(7): p. 945-954.

120. Panckhurst, M.H. and K.G. Woolmington, A Spectrophotometric Study of Ionic Association in Aqueous Solutions. Proceedings of the Royal Society of London Series a-Mathematical and Physical Sciences, 1958. 244(1236): p. 124-139.

121. Rapp, M., et al., Identification of the murine cytomegalovirus glycoprotein B gene and its expression by recombinant vaccinia virus. J Virol, 1992. 66(7): p. 4399-406.

122. Tan, Y.H., et al., A nanoengineering approach for investigation and regulation of protein immobilization. ACS Nano, 2008. 2(11): p. 2374-84.

123. Dick, J.E., et al., Electrochemical detection of a single cytomegalovirus at an ultramicroelectrode and its antibody anchoring. Proc Natl Acad Sci U S A, 2015. 112(17): p. 5303-8.

124. Bourdillon, C.D., C.; Gueris, J.; Moiroux, J.; Saveant, J.M., A fully active monolayer enzyme electrode derivatized by antigen-antibody attachment. J Am Chem Soc, 1993. 115(26): p. 12264-12269.

125. Bourdillon, C.D., C.; Moiroux, J.; Saveant, J.M., New insights into the enzymatic catalysis of the oxidation of glucose by native and recombinant glucose oxidase mediated by electrochemically generated one-electron redox cosubstrates. J Am Chem Soc, 1993. 115(2-10).

126. Fosdick, S.E., et al., Correlated electrochemical and optical tracking of discrete collision events. J Am Chem Soc, 2013. 135(16): p. 5994-7.

127. Li, Z., et al., A mouse model of CMV transmission following kidney transplantation. Am J Transplant, 2012. 12(4): p. 1024-8.

128. La Rosa, C. and D.J. Diamond, The immune response to human CMV. Future Virol, 2012. 7(3): p. 279-293.

129. Boppana, S.B. and K.B. Fowler, Persistence in the population: epidemiology and transmisson, in Human Herpesviruses: Biology, Therapy, and Immunoprophylaxis, A. Arvin, et al., Editors. 2007: Cambridge.

130. Cicin-Sain, L., et al., Targeted deletion of regions rich in immune-evasive genes from the cytomegalovirus genome as a novel vaccine strategy. J Virol, 2007. 81(24): p. 13825-34.

131. Mocarski, E.S., Jr., Immunomodulation by cytomegaloviruses: manipulative strategies beyond evasion. Trends Microbiol, 2002. 10(7): p. 332-9.

132. Kim, Y.E. and J.H. Ahn, Positive role of promyelocytic leukemia protein in type I interferon response and its regulation by human cytomegalovirus. PLoS Pathog, 2015. 11(3): p. e1004785.

133. Li, T., J. Chen, and I.M. Cristea, Human cytomegalovirus tegument protein pUL83 inhibits IFI16-mediated DNA sensing for immune evasion. Cell Host Microbe, 2013. 14(5): p. 591-9.

134. Xie, M., et al., Human cytomegalovirus exploits interferon-induced transmembrane proteins to facilitate morphogenesis of the virion assembly compartment. J Virol, 2015. 89(6): p. 3049-61.

135. Fliss, P.M. and W. Brune, Prevention of cellular suicide by cytomegaloviruses. Viruses, 2012. 4(10): p. 1928-49.

136. Halenius, A., C. Gerke, and H. Hengel, Classical and non-classical MHC I molecule manipulation by human cytomegalovirus: so many targets-but how many arrows in the quiver? Cell Mol Immunol, 2015. 12(2): p. 139-53.

137. Alcami, A., Viral mimicry of cytokines, chemokines and their receptors. Nat Rev Immunol, 2003. 3(1): p. 36-50.

138. Cekinovic, D., V.J. Lisnic, and S. Jonjic, Rodent models of congenital cytomegalovirus infection. Methods Mol Biol, 2014. 1119: p. 289-310.

139. Brune, W., et al., Rapid identification of essential and nonessential herpesvirus genes by direct transposon mutagenesis. Nat Biotechnol, 1999. 17(4): p. 360-4.

140. Desai, P.J., A null mutation in the UL36 gene of herpes simplex virus type 1 results in accumulation of unenveloped DNA-filled capsids in the cytoplasm of infected cells. J Virol, 2000. 74(24): p. 11608-18.

141. Wang, J., et al., High-molecular-weight protein (pUL48) of human cytomegalovirus is a competent deubiquitinating protease: mutant viruses altered in its active-site cysteine or histidine are viable. J Virol, 2006. 80(12): p. 6003-12.

142. Upton, J.W., W.J. Kaiser, and E.S. Mocarski, DAI/ZBP1/DLM-1 complexes with RIP3 to mediate virus-induced programmed necrosis that is targeted by murine cytomegalovirus vIRA. Cell Host Microbe, 2012. 11(3): p. 290-7.

143. Noda, S., et al., Cytomegalovirus MCK-2 controls mobilization and recruitment of myeloid progenitor cells to facilitate dissemination. Blood, 2006. 107(1): p. 30-8.

144. Saederup, N., et al., Murine cytomegalovirus CC chemokine homolog MCK-2 (m131-129) is a determinant of dissemination that increases inflammation at initial sites of infection. J Virol, 2001. 75(20): p. 9966-76.

145. Saederup, N.L., Y.C.; Dairaghi, D.J.; Schall, T.J.; Mocarski, E.S., Cytomegalovirus-encoded β chemokine promotes monocyte-associated viremia in the host. Proc Natl Acad Sci U S A, 1999. 96: p. 10881-10886.

146. MacDonald, M.R., et al., Spliced mRNA encoding the murine cytomegalovirus chemokine homolog predicts a beta chemokine of novel structure. J Virol, 1999. 73(5): p. 3682-91.

147. Meyer, H., M. Bug, and S. Bremer, Emerging functions of the VCP/p97 AAA-ATPase in the ubiquitin system. Nat Cell Biol, 2012. 14(2): p. 117-23.

148. Byun, H., et al., Retroviral Rem protein requires processing by signal peptidase and retrotranslocation for nuclear function. Proc Natl Acad Sci U S A, 2010. 107(27): p. 12287-92.

149. Wagner, F.M., et al., The viral chemokine MCK-2 of murine cytomegalovirus promotes infection as part of a gH/gL/MCK-2 complex. PLoS Pathog, 2013. 9(7): p. e1003493.

150. Mach, M., et al., Complex formation by human cytomegalovirus glycoproteins M (gpUL100) and N (gpUL73). J Virol, 2000. 74(24): p. 11881-92.

151. Boone, D.L., et al., The ubiquitin-modifying enzyme A20 is required for termination of Toll-like receptor responses. Nat Immunol, 2004. 5(10): p. 1052-60.

152. Wertz, I.E., et al., De-ubiquitination and ubiquitin ligase domains of A20 downregulate NF-kappaB signalling. Nature, 2004. 430(7000): p. 694-9.

153. Jin, J., et al., Epigenetic regulation of the expression of Il12 and Il23 and autoimmune inflammation by the deubiquitinase Trabid. Nat Immunol, 2016. 17(3): p. 259-68.

154. Damgaard, R.B., et al., The Deubiquitinase OTULIN Is an Essential Negative Regulator of Inflammation and Autoimmunity. Cell, 2016. 166(5): p. 1215-1230 e20.

155. Wang, D., et al., Human cytomegalovirus uses two distinct pathways to enter retinal pigmented epithelial cells. Proc Natl Acad Sci U S A, 2007. 104(50): p. 20037-42.

156. Lemmermann, N.A., et al., Non-redundant and redundant roles of cytomegalovirus gH/gL complexes in host organ entry and intra-tissue spread. PLoS Pathog, 2015. 11(2): p. e1004640.

157. Daley-Bauer, L.P., et al., Cytomegalovirus hijacks CX3CR1(hi) patrolling monocytes as immune-privileged vehicles for dissemination in mice. Cell Host Microbe, 2014. 15(3): p. 351-62.

158. Daley-Bauer, L.P., G.M. Wynn, and E.S. Mocarski, Cytomegalovirus impairs antiviral CD8+ T cell immunity by recruiting inflammatory monocytes. Immunity, 2012. 37(1): p. 122-33.

159. Dogra, P., et al., A little cooperation helps murine cytomegalovirus (MCMV) go a long way: MCMV co-infection rescues a chemokine salivary gland defect. J Gen Virol, 2016. 97(11): p. 2957-2972.

160. Visalli, R.J., et al., Characterization of the murine cytomegalovirus 38 kDa m137 gene product. Virus Res, 2002. 84(1-2): p. 181-9.

161. Manning, W.C., et al., Cytomegalovirus determinant of replication in salivary glands. J Virol, 1992. 66(6): p. 3794-802.

162. Xiao, J., et al., In vitro and in vivo characterization of a murine cytomegalovirus with a transposon insertional mutation at open reading frame M43. J Virol, 2000. 74(20): p. 9488-97.

163. Lagenaur, L.A., et al., Structure and function of the murine cytomegalovirus sgg1 gene: a determinant of viral growth in salivary gland acinar cells. J Virol, 1994. 68(12): p. 7717-27.

164. Ogawa-Goto, K., et al., An endoplasmic reticulum protein, p180, is highly expressed in human cytomegalovirus-permissive cells and interacts with the tegument protein encoded by UL48. J Virol, 2002. 76(5): p. 2350-62.

165. Benyamini, P., P. Webster, and D.I. Meyer, Knockdown of p180 eliminates the terminal differentiation of a secretory cell line. Mol Biol Cell, 2009. 20(2): p. 732-44.

166. Ueno, T., et al., Enhancement of procollagen biosynthesis by p180 through augmented ribosome association on the endoplasmic reticulum in response to stimulated secretion. J Biol Chem, 2010. 285(39): p. 29941-50.

167. Spain, E., et al., Detection of prostate specific antigen based on electrocatalytic platinum nanoparticles conjugated to a recombinant scFv antibody. Biosens Bioelectron, 2016. 77: p. 759-66.

168. Zoski, C.G.W., M., Electrochemistry at Ultramicroelectrode Arrays and Nanoelectrode Ensembles of Macro- and Ultramicroelectrode Dimensions. Israel Journal of Chemistry, 2010. 50(3): p. 347-359.

169. Rackus, D.G., M.H. Shamsi, and A.R. Wheeler, Electrochemistry, biosensors and microfluidics: a convergence of fields. Chem Soc Rev, 2015. 44(15): p. 5320-40.

170. D'Arcy, P., X. Wang, and S. Linder, Deubiquitinase inhibition as a cancer therapeutic strategy. Pharmacol Ther, 2015. 147: p. 32-54.

171. Kelley, L.A., et al., The Phyre2 web portal for protein modeling, prediction and analysis. Nat Protoc, 2015. 10(6): p. 845-58.

172. Hansen, S.G., et al., Profound early control of highly pathogenic SIV by an effector memory T-cell vaccine. Nature, 2011. 473(7348): p. 523-7.

173. Hansen, S.G., et al., Immune clearance of highly pathogenic SIV infection. Nature, 2013. 502(7469): p. 100-4.

174. Hilterbrand, A.T., et al., Murine Cytomegalovirus Deubiquitinase Regulates Viral Chemokine Levels To Control Inflammation and Pathogenesis. MBio, 2017. 8(1).

175. Demaille, C.F., F-R.F., The preparation of tips for scanning electrochemical microscopy. Second ed. Scanning Electrochemical Microscopy. 2001.

176. Redwood, A.J., et al., Use of a murine cytomegalovirus K181-derived bacterial artificial chromosome as a vaccine vector for immunocontraception. J Virol, 2005. 79(5): p. 2998-3008.

177. Clambey, E.T., H.W.t. Virgin, and S.H. Speck, Disruption of the murine gammaherpesvirus 68 M1 open reading frame leads to enhanced reactivation from latency. J Virol, 2000. 74(4): p. 1973-84.

178. Britt, W.J., Human cytomegalovirus: propagation, quantification, and storage. Curr Protoc Microbiol, 2010. Chapter 14: p. Unit 14E 3.

179. MacLean, B., et al., Skyline: an open source document editor for creating and analyzing targeted proteomics experiments. Bioinformatics, 2010. 26(7): p. 966-8.

180. Upton, J.W., W.J. Kaiser, and E.S. Mocarski, Virus Inhibition of RIP3-Dependent Necrosis. Cell host & microbe, 2010. 7(4): p. 302-313.

181. Jmol: an open-source Java viewer for chemical structures in 3D. Available from: http://www.jmol.org/.

182. Spear, P.G. and R. Longnecker, *Herpesvirus entry: an update.* J Virol, 2003. **77**(19): p. 10179-85.